

Jacob Berg Lofthus

Snow Avalanches on Svalbard: Investigating changes in depositional patterns and their palaeoclimatic significance

Master's thesis in Geography

Supervisor: Chantel Nixon and Lena Rubensdotter

June 2020



Jacob Berg Lofthus

Snow Avalanches on Svalbard: Investigating changes in depositional patterns and their palaeoclimatic significance

Master's thesis in Geography
Supervisor: Chantel Nixon and Lena Rubensdotter
June 2020

Norwegian University of Science and Technology
Faculty of Social and Educational Sciences
Department of Geography

Snow Avalanches on Svalbard:

Investigating changes in depositional patterns and their palaeoclimatic significance



Jacob Berg Lofthus

Master's thesis in Geography

Department of Geography

Norwegian University of Science and Technology

Supervisors: Francis Chantel Nixon & Lena Rubensdotter

June 2020

Master diktet

Jeg sitter her med mine mange år

Og slikker mine nye sår

En masteroppgave er en strevsom prosess

Som har gitt mye unødvendig stress

I starten var entusiasmen lik hundre

Men nå er den lik null

Lange dager på kontoret

Skulle heller vært i felten

Jeg søkte om penger så mange

Håpet at jeg skulle få alt i fanget

Men forskningsrådet sa nei

Og jeg måtte låne 50.000 til scooter for felten

Jeg hadde så mange planer store

Feltarbeid to ganger i uka med scooter

Men det kom jo faen ikke snø

Og da måtte jeg bare gå å trø

Forskning blir aldri som du håper på

Du har så mange ideer

Store og små

Men flesteparten går likevel att skogen

Men på en måte er det fint

Livet går aldri som du hadde tenkt

Men kaffe har jeg drukket

Og youtube videoer har jeg sett

10.000 timer med master

Er mer 20.000 timer med bortkastet tid

Med kabal på mobilen

Akk, jeg skulle brukt tiden bedre

Likevel skulle jeg løse en gåte

Om snøskred og klima

Interessant nok det

Ja, på en måte

Så på PCen jeg satt

Til langt ut på natt

Bare frokost var nok

For magefett til lunsj og middag er topp

Men UNIS ble stengt

Og jeg følte meg hengt

For til hjem til Tromsø ble jeg sendt

Av jævla korona

Nå sitter jeg her

Og ber på mine knær

På gutterommet

Mens pappa kommer med kaffe og boller

Snøskred og småstein

Er det jeg kan tilby

Om det ikke er nok

Så ikke les min master

Abstract

Snow avalanches are important geomorphological agents in the High Arctic, and snow avalanche fans are striking landforms that occurs below the mountain plateau margins of central Svalbard. Earlier studies of avalanche fans in the Longyearbyen area noted that light-coloured, recent avalanche debris is commonly draped on the surface of darker, more extensive and thus older avalanche fans (Eckerstorfer, 2013; De Haas et al., 2015), but no explanation for this observation nor follow-up studies were performed. This apparent changes in avalanche size and runout length during the Holocene, is reflected in the surface colour of the avalanche fans today, was investigated in this thesis. Geomorphological mapping conducted in September 2019 is compared to remote sensing data to quantify changes in fan size and runout lengths between the older and more recent avalanche deposits. Results show that the older deposits has on average 33% longer runout lengths. Avalanche runouts were then reconstructed using the two-dimensional numerical avalanche model RAMMS, with the overall aim of elucidating what climatic and meteorological conditions were necessary to produce the larger avalanches in the past. The findings from this study suggest that the larger avalanches of the past were most likely caused by an increase in precipitation, possibly in a combination with a shift in prevailing wind direction. Another contributing factor may be that there were fewer winter warming events in the past compared to today's climate in central Svalbard. Today, avalanche release is restricted to the upper part of the snowpack due internal ice layers. Lack of warming events would result in a more homogeneous snow pack with fewer shallow failure surfaces, which would allow the entire snowpack to fail, resulting in much larger avalanches than are common today. The results of this study also suggest that cornice fall avalanches are not necessarily a requirement for avalanche fan development in central Svalbard, as a large avalanche fan in Adventdalen is interpreted to have been developed by full-depth wet slab avalanches under a different climatic setting than today.

Sammendrag på Norsk

Snøskred er en viktig geomorfologisk prosess i Arktisk, og snøskredvifter er en påfallende landform som forekommer under fjellplatåene i sentrale Svalbard. Tidligere studier av snøskredvifter i områdene rundt Longyearbyen har bemerket seg de lyse, nylige snøskredavsetningene som er avsatt over eldre, mørkere og mer omfattende skredvifter (Eckerstorfer, 2013; De Haas et al., 2015), men ingen forklaring på denne observasjonen eller oppfølgingsstudier vært utført. De tilsynelatende endringene i skredstørrelse og utløpslengde gjennom Holocen, som er gjenspeilet i fargen på overflateavsetningene til dagens skredvifter, ble undersøkt i denne masteroppgaven. Geomorfologisk kartlegging ble gjennomført i september 2019 og sammenlignet med fjernmålinger for å kvantifisere endringer i størrelse av avsetningslengde mellom de eldre og nyere skredavsetningene. Resultatene viser at de eldre avsetningene hadde i gjennomsnitt 33% lengre utløpslengde. Utløpslengden til snøskredene ble rekonstruert i det to-dimensjonale numeriske snøskredmodellen RAMMS, med det overordnende målet å belyse hvilke klimatiske og meteorologiske forhold som var nødvendige for å gjenskape de historiske skredene. Resultatene fra denne masteroppgaven antyder at de større snøskredene fra tidligere tid, mest sannsynlig var forårsaket av en økning i nedbør, muligens i kombinasjon med en endring i dominerende vindretning. En annen medvirkende faktor kan være en reduksjon av milde perioder i løpet av vinteren i tidligere tid, sammenlignet med dagens klima i sentrale Svalbard. Mangelen på milde perioder vil resultere i mer homogent snølag med færre svake lag i øvre del av snølaget, kan føre til veldig store skred som løsner hele snølaget. I dag løsner skred i den øvre delen av snølaget på grunn av islag. Resultatet fra denne studien antyder også at skred forårsaket av skavler ikke er nødvendig for dannelsen av snøskredvifter i sentrale Svalbard, ettersom en stor skredvifte i Adventdalen tolkes til å ha blitt utviklet av våte flakskred som har løsnet store deler av snølaget, under andre klimatiske forutsetninger.

Acknowledgements

Huge thanks to my two supervisors Chantel Nixon (NTNU) and Lena Rubensdotter (NGU) for the guidance and good talks. I know that I have you called you at all inappropriate times: when you have been making dinner, taken your kids to bed etc., for questions I probably could have waited with, or just sent as an email. But at least I take self-criticism, and, in the end, I actually started sending emails and text messages before I called. It's been a pleasure every time we talked, even though when you asked me to call tomorrow. I hope it wasn't too bad.

All things come to an end, and after 6 years in university there are too many people how deserve a thanks. From my geography buddies Marte, Emil "The Eternal Looser of Mattis", Anders and Martin; it's been amazing drinking coffee and playing "Mattis" more than actually writing the thesis. I will miss the GIS lab, GEOLF-kontoret and all the stupid fun we had when I start in a job with semi-retired people.

To all my UNIS friends how wanted to participate in fieldwork that never happened, I hope it never happens to you! Feeling like a maniac on the snow scooter, and skiing the mountains on Svalbard is something that I will always miss. A special thanks to PhD student Holt Hancock who provided me with much needed data, and answered all my questions when I too frequently came to your office.

Thanks to my parents who accepted a 26-year-old corona-refugee back home. Being home has never been this good, you brought me bread and a glass of milk every night when I worked to 04-07 every morning for 2 months, and without complaints notice me steal chocolate and milk from the basement.

Last but not least, I want to thank by girlfriend Marianne who has put up with me for so many years, and seen me take off to the opposite side of the globe so many times. Amazing.

Table of contents

CHAPTER 1. INTRDUCTION.....	1
1.1 THESIS AIM AND RESEARCH QUESTION	4
CHAPTER 2. THEORY	5
2.1 SNOW PROCESSES AND FORMATION	5
2.1.1 Snow Crystal Formation.....	5
2.1.2 Snow Metamorphism.....	6
2.1.3 Equi-temperature metamorphism.....	7
2.1.4 Kinetic growth metamorphism.....	8
2.1.5 Snow stratigraphy.....	9
2.2 SNOW AVALANCHES	10
2.2.1 Slab avalanche.....	13
2.2.2 Cornice fall avalanches.....	16
2.3 FAN-SHAPED LANDFORMS	17
2.4 SNOW AVALANCHE FANS AND GEOMORPHIC EFFECT OF AVALANCHES.....	19
2.5 SNOWDRIFT PROCESSES.....	24
2.6 SNOW AVALANCHE RESEARCH ON SVALBARD.....	26
CHAPTER 3. STUDY AREA	32
3.1 CLIMATE AND METEOROLOGY	33
3.2 CLIMATE FLUCTUATIONS ON SVALBARD SINCE THE LAST ICE AGE AND THE IMPLICATION FOR THE AVALANCHE ENVIRONMENT	37
3.3 SNOW AND AVALANCHE CLIMATE ON SVALBARD.....	40
3.4 GEOLOGY AND PHYSICAL GEOGRAPHY.....	42
3.4.1 Longyeardalen.....	44
3.4.2 Todalen	44
3.4.3 Adventdalen	45
CHAPTER 4. FIELDWORK AND METHODS.....	46
4.1 WORKFLOW.....	46

4.2 GEOMORPHOLOGICAL MAPPING.....	47
4.3 AVALANCHE FAN MAPPING.....	49
4.4 TERRESTRIAL LASER SCANNING (TLS).....	50
4.4.1 TLS data processing	50
4.4.2 DEM calculations	51
4.5 DYNAMICAL AVALANCHE MODELLING	53
4.5.1 Physical friction model.....	53
4.5.2 Topographic data.....	55
4.5.3 Release information and orthophotos.....	55
4.5.4 Friction parameters.....	56
4.5.5 Snow density and cohesion.....	58
4.5.6 Simulation output	58
4.6 EXTREME PRECIPITATION ANALYSIS AND AUTOMATED SNOW AND WEATHER DATA	59
CHAPTER 5. RESULTS.....	61
5.1 GEOMORPHOLOGICAL AND AVALANCHE FAN MAPPING	61
5.1.1 Todalen	61
5.1.2 Adventdalen	66
5.1.3 Longyeardalen.....	67
5.2 SNOW DEPTH CALCULATIONS	68
5.2.1 Gruvefjellet	68
5.2.2 Platåberget	70
5.3 AUTOMATED SNOW AND WEATHER DATA.....	71
5.4 EXTREME PRECIPITATION ANALYSIS	75
5.5 AVALANCHE CYCLES AND THE RELEASE PROPERTIES.....	77
5.6 BACK CALCULATION IN RAMMS	80
5.7 RECONSTRUCTION OF RECENT AND HISTORICAL AVALANCHE RUNOUTS	83
5.7.1 Adventdalen	83
5.7.2 Todalen	88
CHAPTER 6. DISCUSSION.....	94
6.1 GEOMORPHOLOGICAL MAPPING OF AVALANCHE FANS.....	94

6.2 RAMMS MODELLING	96
6.3 COMPARING MODELLED FRACTURE HEIGHTS WITH SNOW DEPTH AND EXTREME PRECIPITATION ANALYSIS	101
6.4 COMPARISON BETWEEN FACTORS DETERMINING AVALANCHE RELEASE AND FAN SEDIMENTATION IN TODALEN, LONGYEARDALEN AND ADVENTDALEN.....	104
6.4.1 The effect of snow depths, snow distribution and meteorological variables.....	104
6.4.2 The enigmatic Adventdalen fan; proposed mechanism to explain observed results ..	107
6.5 THE PALAEOCLIMATIC SIGNIFICANCE OF AVALANCHE FANS	110
CHAPTER 7. CONCLUSION	115
7.1 FUTURE STUDIES	117
REFERENCES:	118

List of figures

FIGURE 1. THE MAP WAS CREATED BY THE AUTHOR FOR A UNIVERSITY TERM PROJECT (GEOG3523 – GIS DATA CAPTURE AND MAPPING), INVESTIGATING THE SPATIAL DISTRIBUTION OF SNOW AVALANCHE FANS AROUND LONGYEARBYEN, BEFORE THE INITIATION OF THIS MASTER PROJECT	3
FIGURE 2. THE SNOW CRYSTAL MORPHOLOGY DIAGRAM. SNOW CRYSTALS GROW DIFFERENTLY AS A FUNCTION OF TEMPERATURE AND VAPOR SUPERSATURATION IN THE ATMOSPHERE (FROM LIBBRECHT, 2005).	5
FIGURE 3. SKETCH OF EQUI-TEMPERATURE METAMORPHISM AFTER BALDER (1939) BY CURVATURE EFFECTS FROM A COLD LABORATORY. THE NUMBERS GIVEN TIME IN DAYS. IN FIELD CONDITIONS, THE TIME WILL ONLY BE A FEW DAYS (FROM MCCLUNG & SCHAERER, 2006).	7
FIGURE 4. (A) ROUNDED GRAINS DUE TO EQUI-TEMPERATURE METAMORPHISM, THAT BONDS WELL WITH NEIGHBORING GRAINS, (B) FACETS WHICH DEVELOP THROUGH KINETIC GROWTH METAMORPHISM. RECOGNIZE THE ANGULAR SHAPE WHICH MAKES THE GRAINS BONDING CAPABILITIES WORSE, AND (C) DEPTH HOAR WHICH ARE LARGE STRIATED CUPS AND HAS POOR BONDING WITH ADJACENT GRAINS (FROM FIERZ ET AL., 2009).	9
FIGURE 5. TYPES OF AVALANCHES. A) SLAB AVALANCHE. B) LOOSE SNOW AVALANCHE. C) SLUSH AVALANCHE. D) CORNICE FALL AVALANCHE (FROM ECKERSTORFER, 2013)	12
FIGURE 6. CONCEPTUAL MODEL OF DRY SNOW AVALANCHE RELEASE THROUGH FOUR STAGES: (1) FAILURE INITIATION IN A WEAK LAYER UNDERLYING A COHESIVE SLAB, (2) THE ONSET OF CRACK PROPAGATION, (3) DYNAMIC CRACK PROPAGATION THROUGH THE WEAK LAYER ACROSS THE SLOPE, (4) TENSILE SLAB FAILURE FOLLOWED BY SLIDING OF THE SLAB. THE RED ARROWS INDICATE MIXED-MODE LOADING (FROM SCHWEIZER ET AL., 2016).....	13
FIGURE 7. COHESIVE SLAB ON TOP OF A WEAK LAYER AND A BED SURFACE (FROM SCHWEIZER ET AL., 2003).....	14
FIGURE 8. SHOWS A COMPARISON BETWEEN COLLUVIAL FANS AND ALLUVIAL FANS (FROM BLIKRA & NEMEC, 1998).	17
FIGURE 9. SHOWS THE DIFFERENT DEPOSITIONAL PROCESSES AND THEIR SEDIMENTARY FEATURES (FROM BLIKRA & NEMEC, 1998)	19

FIGURE 10. SCHEMATIC FIGURE OF HOW PERCHED BOULDER/COBBLES ARE DEPOSITED. THE DEPOSITS GET STACKED ON TOP OF EACH OTHER WHEN THE AVALANCHE MELTS OUT IN SPRING	21
FIGURE 11: SKETCH OF A "DEBRIS TAIL/SHADOW" WHICH OCCURS ON MANY SURFACES OF AVALANCHE TRACKS (FROM RAPP, 1959)	22
FIGURE 12: FIGURE FROM DE HAAS ET AL. (2015), SHOWING AVALANCHE DOMINATED FANS AND TYPICAL PROPERTIES. (A) TONGUE-SHAPED FAN, NOTE THAT THE SEDIMENTS TURN GRAYER (OLDER) TOWARDS THE DISTAL DOMAIN. (B) AVALANCHE FAN SHOWING TYPICAL BASAL CONCAVITY WITH A STEEP TOE. (C) CONE-SHAPED AVALANCHE FANS IN LONGYEARDALEN. (D) DEBRIS TAIL, WITH BLACK ARROW SHOWING FLOW DIRECTION. (E) AVALANCHE EROSION ON THE PROXIMAL DOMAIN LEADS TO A MORE FINE-GRAINED TEXTURE. (F) DEBRIS HORN, SHOWN BY THE WHITE ARROW, AND BLACK ARROW FLOW DIRECTION. (G) ACCUMULATION OF COARSE-GRAINED SEDIMENTS AT THE DISTAL DOMAIN. (H) PERCHED BOULDER – A VERY TYPICAL, EASY TO IDENTIFY AVALANCHE FEATURE.....	23
FIGURE 13: SNOW IS ERODED DUE TO WIND ACCELERATING AND DEPOSITS ON THE LEE SIDE, WHERE SNOW DECELERATES. A) AND B) SHOWS SNOW ACCUMULATION ON THE LEE SIDE. C) AND D) SHOWS ACCUMULATION IN A GULLY (FROM MCCLUNG & SCHAERER, 2006).	24
FIGURE 14. THE THREE DIFFERENT MODES OF SNOW TRANSPORTATION BY WIND (FROM MCCLUNG & SCHAERER, 2006).....	25
FIGURE 15. OVERVIEW MAP OF LONGYEARBYEN IN CENTRAL SPITSBERGEN, SVALBARD AND THE SURROUNDING AREA (FROM ECKERSTORFER & CHRISTIANSEN, 2011C).....	32
FIGURE 16. SVALBARD'S LOCATION IN THE NORTH-WEST CORNER OF THE BARENTS SEA AND OCEAN CURRENTS INFLUENCING THE REGION. THE WEST SPITSBERGEN CURRENT (WSC) BRINGS WARM WATER TO THE WEST COAST, MAKING THE REGION RELATIVELY MILD COMPARED TO OTHER REGIONS AT THE SAME LATITUDE. EAST COAST IS INFLUENCED BY THE PERSEY CURRENT, BRINGING COLD POLAR WATER. AS A RESULT, EAST COAST OF SVALBARD IS SIGNIFICANTLY COLDER AND HAS MORE SEA ICE THAN THE WEST COAST (FROM DALLMANN, 2015).....	33
FIGURE 17. MEAN ANNUAL AIR TEMPERATURE AND PRECIPITATION AT LONGYEARBYEN SINCE 1912. POINTS ARE ANNUAL OBSERVATION, AND THE LINES ARE 5-YEAR AVERAGE (FROM CHRISTIANSEN ET AL., 2013).	35
FIGURE 18. TIMELINE OF LATE PLEISTOCENE AND HOLOCENE FLUCTUATIONS (FROM FARNSWORTH ET AL., OCT. 2019 SUBMITTED).....	38

FIGURE 19. THE HIGH ARCTIC MARITIME SNOW CLIMATE PRESENTED BY ECKERSTORFER & CHRISTIANSEN (2011A), BASED AND MODIFIED FROM STURM ET AL. (1995). THE BLACK BOXES INDICATE THE AMOUNT OF THE CERTAIN SNOWPACK CHARACTERISTICS IN THE STUDY AREA, COMPARED TO DIFFERENT SNOW CLIMATES.....	41
FIGURE 20. OVERVIEW MAP OF THE STUDY AREAS IN (A) ADVENTDALEN, (B) LONGYEARDALEN AND (C) TODALEN. METEOROLOGICAL STATIONS USED IN THIS THESIS IS MARKED WITH A RED STAR, AND SNOW DEPTH SENSORS PLACED AT GRUVEFJELLET AND PLATÅBERGET ARE MARKED WITH YELLOW CIRCLE.	43
FIGURE 21. LANDFORM AND SEDIMENT MAP OF TODALEN. BLACK BOX INDICATES THE STUDY AREA IN THIS THESIS (MODIFIED FROM RUBENSDOTTER ET AL., 2015).....	45
FIGURE 22. CONCEPTUAL WORKFLOW FOR DATA PROCESSING AND COLLECTION LEADING UP TO THE RECONSTRUCTION OF MODERN AND HISTORICAL AVALANCHE RUNOUTS IN RAMMS...	47
FIGURE 23. GEOPROCESSING MODEL IN ARCGIS PRO TO ITERATE THROUGH TLS DATA FROM GRUVEFJELLET AND PLATÅBERGET. OUTPUT OF THE MODEL IS A XY POINT FILE, NATURAL NEIGHBOR INTERPOLATION AND HILLSHADE FOR EACH SCAN.	51
FIGURE 24: RASTER MINUS CALCULATION AND HILLSHADE OF THE SAME RELEASE AREA SHOWS SCAN SHADOWS IN THE DATASET. YELLOW ARROWS INDICATE THREE EXAMPLES OF SCAN SHADOWS IN THE DATASET.....	52
FIGURE 25: EXAMPLE OF FRICTION VALUES AT DIFFERENT ALTITUDES IN RAMMS BASED ON LARGE VOLUME AND RETURN PERIOD OF 30 YEARS (BARTELT ET AL., 2017).....	56
FIGURE 26: OVERVIEW OF GLOBAL PARAMETERS. VOLUME WAS AUTOMATICALLY CLASSIFIED BASED ON VOLUME IN THE RELEASE AREA. RETURN PERIOD FOR ALL AVALANCHES WAS SET TO 10 YEARS (FIGURE FROM BARTELT ET AL., 2017)	57
FIGURE 27. SNOW DEPTH SENSORS AT (A) GRUVEFJELLET AND (B) PLATÅBERGET (PHOTO: PROKOP ET AL., 2018).....	60
FIGURE 28: HILLSHADE (A) AND ORTHOPHOTO (B) REPRESENTATION OF THE STUDY AREA IN EASTERN TODALEN. THE RIVER TODALSELVA FLOWS THROUGH THE VALLEY BOTTOM, ERODING INTO SOME OF THE FANS IN THE INNER PART OF THE VALLEY. GPS POINTS WERE COLLECTED DURING THE FIELD CAMPAIGN IN SEPTEMBER 2019, AND THE EXTENT WAS MAPPED IN ARCGIS.....	62

FIGURE 29: A, C AND D SHOW TYPICAL PERCHED COBBLES DEPOSITS. B SHOW PERCHED BOULDER. PERCHED COBBLES AND BOULDERS WERE THE MOST COMMON DEPOSITIONAL SIGNATURE OF RECENT AVALANCHE DEPOSITS. DEPOSITS WERE INTERPRETED AS RECENT IF NO LICHEN WAS GROWING ON THE SURFACE AND NO IMPRINT WAS LEFT ON THE UNDERLYING ROCK. GPS RECEIVER FOR SCALE. 63

FIGURE 30: PERCHED COBBLES INTERPRETED AS HISTORICAL DEPOSITS BECAUSE OF EXTENSIVE LICHEN GROWTH ON THEIR SURFACE, AND IMPRINT ON THE UNDERLYING ROCK. GPS FOR SCALE. PERCHED BOULDERS WERE FOUND FAR AWAY FROM THE SOURCE AREA, RULING OUT ROCKFALL AS A POTENTIAL TRANSPORT AGENT. 63

FIGURE 31: A, B AND E SHOW THE DIFFERENCE BETWEEN RECENT AND HISTORICAL AVALANCHE FAN DEPOSITS WHICH HAD LEFT AN IMPRINT ON THE UNDERLYING SURFACE. RED OUTLINE IS THE ORIGINAL POSITION. AFTER MOVING THE ROCK, B SHOWS NO IMPRINT WHILE E SHOWS A PARTLY SHIELDED SURFACE. C: SHOWS THE SCATTERED AVALANCHE DEPOSITS WITH HIGH FREQUENCY OF PERCHED BOULDERS. D: DEBRIS HORN WHERE DEBRIS HAS ACCUMULATED ON THE UPWARD SIDE OF A LARGER OBSTACLE. F: FRAGMENT HAS BROKEN OFF WITH A FRESH EXPOSED SURFACE, IMPLYING RE-DEPOSITION. 64

FIGURE 32. HILLSHADE (A) AND ORTHOPHOTO (B) OF THE SW FACING AVALANCHE FAN IN ADVENTDALEN WITH THE MAPPED EXTENT OF RECENT AND OLD DEPOSITS. 66

FIGURE 33. HILLSHADE (A) AND ORTHOPHOTO (B) OF THE ESE FACING AVALANCHE FANS IN LONGYEARDALEN WITH MAPPED EXTENT OF RECENT AND OLD DEPOSITS 67

FIGURE 34. SNOW DEPTH MAPS OF THE RELEASE AREAS AT GRUVEFJELLET IN LONGYEARDALEN. THE 2016-2017 SNOW SEASON (A) HAS ACCUMULATED MORE SNOW COMPARED TO THE 2017-2018 (B) SEASON IN THE RELEASE AREAS. THE FIGURE ILLUSTRATES THE IMPORTANCE OF SNOW ACCUMULATION BY WIND, AS OVER 3 TIMES THE SNOW DEPTH IS MEASURED COMPARED TO THE OBSERVED PRECIPITATION. THE YELLOW ARROWS INDICATE EVIDENCE OF CROSS LOADING. 69

FIGURE 35. SNOW DEPTH MAPS OF THE RELEASE AREAS AT PLATÅBERGET. THE 2016-2017 (A) SNOW SEASON HAS MORE ACCUMULATED SNOW THAN THE 2017-2018 (B) SEASON. CROSS-LOADING IS PRONOUNCED, WHERE OVER 3 METERS HAVE ACCUMULATED. THE SNOWPACK IS HIGHLY VARIABLE, BUT DATA HOLES ARE EXTENSIVE, AND THE MAP MUST BE INTERPRETED WITH CARE. THE YELLOW ARROWS SOME AREAS WITH CROSS LOADING 70

FIGURE 36. SUMMARY OF SNOW DEPTH AND WEATHER DATA FOR THE 2017-2018 WINTER SEASON. PRECIPITATION IS MEASURED AT LONGYEARBYEN AIRPORT (28 M A.S.L). SNOW DEPTH VALUES ARE FROM SNOW SENSORS AT GRUVEFJELLET (350 M A.S.L) AND PLATÅBERGET (450 M A.S.L). WIND AND TEMPERATURE DATA WERE COLLECTED FROM GRUVEFJELLET AWS (464 M A.S.L). TEMPERATURES ARE DAILY AVERAGE VALUES, WIND

SPEED IS ARITHMETICAL AVERAGE, WIND DIRECTION IS VECTOR AVERAGED, AND MAXIMUM WIND SPEED IS THE DAILY MEASURED MAXIMUM. THE HIGHLIGHTED BARS IN GREY REPRESENT PRECIPITATION PERIODS WHERE SNOW DEPTHS SIGNIFICANTLY INCREASED AT ONE OR BOTH SNOW SENSORS. YELLOW BAR REPRESENTS PRECIPITATION PERIOD WHEN NO SNOW DEPTH INCREASE WAS REGISTERED. 71

FIGURE 37. FREQUENCY ANALYSIS OF WINDSPEED AND DIRECTION AT GRUVEFJELLET AWS FOR THE 2017/2018 SNOW SEASON. THE SNOW SEASON IS DEFINED AS NOVEMBER-MAY. 74

FIGURE 38. EXTREME PRECIPITATION ANALYSIS OF 1-DAY PRECIPITATION. X-AXIS REPRESENTS THE PRECIPITATION VALUES, WHICH TRANSLATES INTO SNOW DEPTH IN CM. Y-AXIS IS RETURN PERIODS IN YEARS. 75

FIGURE 39. EXTREME PRECIPITATION ANALYSIS OF 3-DAY PRECIPITATION. X-AXIS REPRESENTS THE PRECIPITATION VALUES, WHICH TRANSLATES INTO SNOW DEPTH IN CM. Y-AXIS IS RETURN PERIODS IN YEARS. 75

FIGURE 40. MAP SHOWING THE AVALANCHE DEPOSITS FROM MULTIPLE AVALANCHES RELEASED DURING TWO AVALANCHE CYCLES AT PLATÅBERGET DURING THE 2016/2017 WINTER SEASON. THE YELLOW ARROWS INDICATE IMPACT CRATERS FROM CORNICE FALL AVALANCHE, AND DOTTED OUTLINE SHOWS THE EXTENT OF THE RELEASE AREA WHICH WAS CLEARLY VISIBLE IN THE SCAN. 78

FIGURE 41. MAP SHOWING THE AVALANCHE DEPOSITS FROM MULTIPLE AVALANCHES RELEASED DURING TWO AVALANCHE CYCLES AT GRUVEFJELLET DURING THE 2016/2017 (B) 2017/2018 (A) WINTER SEASON. THE YELLOW ARROWS INDICATE IMPACT CRATERS FROM CORNICE FALL AVALANCHE, AND DOTTED OUTLINE SHOWS THE EXTENT OF THE RELEASE AREA WHICH WAS CLEARLY VISIBLE IN THE SCAN. 79

FIGURE 42. VISUALIZATION OF RAMMS MODELLING RESULTS FROM ADVENTDALEN WITH SMALL RELEASE AREA. A AND C SHOW THE HISTORICAL RUNOUT RESULT. B AND D SHOW THE RECENT RUNOUT. A AND B REPRESENTS MODELING OF DRY SLAB AVALANCHES WITH A COHESION OF 100, COMPARED TO C AND D WHICH REPRESENTS WET SLAB AVALANCHES WITH A COHESION OF 200. 84

FIGURE 43. VISUALIZATION OF RAMMS MODELLING RESULTS FROM ADVENTDALEN WITH LARGE RELEASE AREA. A AND C SHOW THE HISTORICAL RUNOUT RESULT. B AND D SHOW THE RECENT RUNOUT. A AND B REPRESENTS MODELING OF DRY SLAB AVALANCHES WITH A COHESION OF 100, COMPARED TO C AND D WHICH REPRESENTS WET SLAB AVALANCHES WITH A COHESION OF 200. LARGER RELEASE AREA RESULTED IN LOWER VOLUME AND FRACTURE HEIGHT COMPARED TO SMALLER RELEASE AREA. 85

FIGURE 44. VISUALIZATION OF THE RESULTS FROM MODELLING DRY SLAB AVALANCHES IN TODALEN. (A) SHOW THE MODELLED AVALANCHES REACHING THE RECENT DEPOSITS, AND (B) SHOW THE MODELLED AVALANCHES REACHING THE HISTORICAL DEPOSITS. **89**

FIGURE 45. VISUALIZATION OF THE RESULTS FROM MODELLING WET SLAB AVALANCHES IN TODALEN. (A) SHOW THE MODELLED AVALANCHES REACHING THE RECENT DEPOSITS, AND (B) SHOW THE MODELLED AVALANCHES REACHING THE HISTORICAL DEPOSITS. **90**

FIGURE 46. OVERVIEW OF THE AVALANCHE FAN IN ADVENTDALEN. MAIN SOURCE AREA FOR ROCK FALL FEEDING THE AVALANCHE FAN IS MARKED WITH BLUE CIRCLE. THE PREVAILING WIND DIRECTION FROM THE SOUTHEAST IS MARKED WITH YELLOW ARROW. THE TOTAL LENGTH IS APPROX. 1.5 KM AND A VERTICAL DROP OF 650 M FROM 850 M A.S.L TO 200 M A.S.L **109**

FIGURE 47. THE DOTTED GREEN LINE INDICATES THE LOCATION OF THE RELICT NIVATION HOLLOW, WHICH DURING MELTING SEASON FED THE STREAM (YELLOW ARROW) WHICH CREATED THE V-SHAPED GORGE UNDERNEATH..... **112**

FIGURE 48. (A) YELLOW ARROWS INDICATE WHERE WAVE ACTION POSSIBLY HAS ERODED INTO THE FAN DEPOSITS. **113**

LIST OF TABLES

TABLE 1: SHOWS STUDIES FROM SVALBARD FOCUSING THE GEOMORPHIC SIGNIFICANCE OF AVALANCHES, FAN DEVELOPMENT, ROCKWALL RETREAT AND ITS KEY FINDINGS 29

TABLE 2. MORPHOLOGICAL FEATURES WHICH ARE CAUSED BY AVALANCHES. 48

TABLE 3. SNOW COHESION PARAMETERS FOR DRY AND WET SNOW AVALANCHES, AS PROPOSED BY BÜHLER ET AL. (2014)..... 54

TABLE 4. SUMMARY OF FAN STATISTICS FOR THE AVALANCHE FANS IN TODALEN 65

TABLE 5. SUMMARY OF FAN STATISTICS FOR THE AVALANCHE FAN IN ADVENTDALEN..... 66

TABLE 6. SUMMARY OF FAN STATISTICS FOR AVALANCHE FANS IN LONGYEARDALEN..... 68

TABLE 7. SUMMARY OF MAJOR SNOW DEPTH CHANGES AT GRUVEFJELLET IN LONGYEARDALEN DURING THE 2017-2018 SNOW SEASON. SIGNIFICANT ACCUMULATION OCCURRED WITHIN A SINGLE TO A FEW DAYS DUE TO SUBSTANTIAL SNOWDRIFT, OFTEN IN COMBINATION WITH PRECIPITATION. REGOBS OBSERVATIONS HAVE BEEN INSPECTED UP TO 3 DAYS BEFORE AND AFTER THE EVENT, INCLUDING THE DAY(S) OF THE EVENT. PRECIPITATION IS MEASURED AT SVALBARD AIRPORT AWS, SNOW DEPTH DATA ARE FROM THE SNOW SENSOR INSTALLED AT GRUVEFJELLET, WINDSPEEDS AND TEMPERATURE ARE FROM GRUVEFJELLET AWS. THE INVESTIGATED DATA HAS BEEN RECORDED HOURLY EXCEPT FOR PRECIPITATION. 72

TABLE 8. SUMMARY OF MAJOR SNOW DEPTH CHANGES AT PLATÅBERGET IN LONGYEARDALEN DURING THE 2017-2018 SNOW SEASON. SIGNIFICANT ACCUMULATION OCCURRED WITHIN A SINGLE TO A FEW DAYS DUE TO SUBSTANTIAL SNOWDRIFT, OFTEN IN COMBINATION WITH PRECIPITATION. REGOBS OBSERVATIONS HAVE BEEN INSPECTED UP TO 3 DAYS BEFORE AND AFTER THE EVENT, INCLUDING THE DAY(S) OF THE EVENT. PRECIPITATION IS MEASURED AT SVALBARD AIRPORT AWS, SNOW DEPTH DATA ARE FROM THE SNOW SENSOR INSTALLED AT PLATÅBERGET, WINDSPEEDS AND TEMPERATURE ARE FROM GRUVEFJELLET AWS. THE INVESTIGATED DATA HAS BEEN RECORDED HOURLY EXCEPT FOR PRECIPITATION. 73

TABLE 9. ESTIMATED FRACTURE HEIGHT VALUES BASED ON EXTREME PRECIPITATION ANALYSIS FOR RELEASE AREAS IN TODALEN AND LONGYEARDALEN. THREE DIFFERENT FRACTURE HEIGHTS ARE PRESENTED BASED ON CORRECTION FOR THE VERTICAL GRADIENT AND UPWARDS CORRECTION OF MEASURED PRECIPITATION IN ADDITION TO THE VERTICAL GRADIENT 76

TABLE 10. ESTIMATED FRACTURE HEIGHT VALUES BASED ON EXTREME PRECIPITATION ANALYSIS FOR RELEASE AREA IN ADVENTDALEN. THREE DIFFERENT FRACTURE HEIGHTS ARE PRESENTED BASED ON CORRECTION FOR THE VERTICAL GRADIENT AND UPWARDS CORRECTION OF MEASURED PRECIPITATION IN ADDITION TO THE VERTICAL GRADIENT. ...	76
TABLE 11. SUMMARY OF AVALANCHE CYCLES WITH WEATHER HISTORY BETWEEN THE TWO SCANS.....	77
TABLE 12. SUMMARY OF PARAMETERS IN RAMMS WHICH GAVE THE BEST FIT IN BACK-CALCULATION OBSERVED AVALANCHES WHICH RELEASED DURING 4 AVALANCHE CYCLES BETWEEN THE 2016-2017 AND 2017-2018 WINTER SEASON.	82
TABLE 13. SUMMARY OF MODELLING STATISTICS AND STATISTICAL COMPARISON HIGHLIGHTING THE PERCENTAGE DIFFERENCE BETWEEN MODELLING WITH SMALL AND LARGE RELEASE AREA FOR THE SAME RUNOUT.....	86
TABLE 14. SUMMARY OF MODELLING STATISTICS HIGHLIGHTING THE VOLUME AND FRACTURE HEIGHT INCREASE NECESSARY TO REACH THE HISTORICAL DEPOSITS FOR THE SAME AVALANCHE TYPE.	87
TABLE 15. SUMMARY OF MODELLING STATISTICS HIGHLIGHTING THE VOLUME AND FRACTURE HEIGHT DIFFERENCE BETWEEN THE TWO AVALANCHE TYPES, WHEN THE SAME RUNOUT WAS COMPARED.....	88
TABLE 16. SUMMARY OF FAN STATISTICS FROM THE AVALANCHE MODELLING IN TODALEN, HIGHLIGHTING THE AVERAGE FRACTURE HEIGHT AMONG ALL AVALANCHES FOR EACH RUNOUT AND AVALANCHE TYPE. THE TWO FANS (ID 5 AND 6) MARKED IN RED IS NOT INCLUDED IN THE AVERAGE FRACTURE HEIGHT CALCULATION.....	91
TABLE 17. SUMMARY OF FAN STATISTICS FROM THE AVALANCHE MODELLING IN TODALEN, HIGHLIGHTING THE INCREASE IN FRACTURE HEIGHT AND VOLUME NECESSARY TO REACH THE HISTORICAL RUNOUTS. THE TWO FANS (ID 5 AND 6) MARKED IN RED IS NOT INCLUDED IN THE AVERAGE FRACTURE HEIGHT AND VOLUME CALCULATION.....	92
TABLE 18. SUMMARY OF FAN STATISTICS FROM THE AVALANCHE MODELLING IN TODALEN, HIGHLIGHTING THE VOLUME AND FRACTURE HEIGHT DIFFERENCE BETWEEN THE TWO AVALANCHE TYPES, WHEN THE SAME RUNOUT WAS COMPARED.....	93
TABLE 19. THE COMBINED RESULTS SHOWING THE FRACTURE HEIGHT AND THE CORRESPONDING RETURN PERIODS, USING THE 3-DAY SUM. EMPHASIS IS PLACED ON THE GEV +V. GRADIENT RATHER THAN THE GEV ANALYSIS WITH UPWARDS CORRECTION.	102

Chapter 1. Introduction

Snow avalanches are a significant hazard in mountainous regions with seasonal snow cover throughout the world, causing major damage to infrastructure and loss of life (Schweizer et al., 2003). The study of avalanches is interdisciplinary, requiring knowledge of meteorology, physical geography, engineering, hydrology, geophysics and geomorphology. Avalanches are a great threat to alpine societies; therefore, much focus has been placed on the hazard research. Yet, much about the release process remains unknown. Predicting a single avalanche in time and space is difficult because the interaction between the snow (a highly unstable and variable material), terrain, and changing meteorological conditions is complex and not fully understood (Schweizer et al., 2003).

Snow avalanches have been identified as a significant geomorphological agent for sediment transport, erosion and deposition. Numerous studies have recognized the geomorphological importance of avalanches as a sediment transport agent (Rapp, 1960a, 1960b; Luckman, 1977, 1988; Bell et al., 1990; Humlum et al., 2007; Eckerstorfer et al., 2013a, 2013b; de Haas et al., 2015). Snow avalanches are also known as an important factor in rock glacier development (Humlum et al., 2007), and a significant contributor to periglacial landscape development (Eckerstorfer, 2013). When snow avalanche deposits containing rocks and other debris melt out in spring and leave a geomorphological trace, an avalanche fan will develop if avalanches containing debris occur in the same location year after year (Luckman, 1977). Such fans have a specific depositional signature, and by studying avalanche deposits, one can identify where avalanches have occurred in the past. Recently deposited particles can be recognized by an absence of lichen, and their lighter colour, as lichen growth on the rock over time makes the rock surface darker (De Haas et al., 2015). As climate changes over decades or millennia, mountain areas can experience a change in avalanche activity. Thus, avalanche fans serve as archives for past and present processes leading to fan development, which is found in the fan morphology and internal structure (Blikra & Nemeč, 1998; Iturrizaga, 2012; Tomczyk et al., 2019).

Svalbard, an archipelago in the High Arctic, has snow cover persisting for 10 months of the year, and thus avalanches are a natural phenomenon throughout the winter season (Eckerstorfer & Christiansen, 2011a). The archipelago is underlain by continuous permafrost and has sparse

vegetation with no trees (Humlum et al., 2003), making it an ideal location to study avalanches and avalanche deposits. Longyearbyen, the only permanent Norwegian settlement, is located on Spitsbergen, the largest island on Svalbard. The topography is dominated by plateau mountains and U-shaped valleys with steep valley sides carved out by glaciers (Major, 2001). On Svalbard, snow is highly variable due to low total precipitation and wind transportation is the dominant factor for snow accumulation (Christiansen et al., 2013). For avalanche release, this means that some aspects are more prone than others. Today, the dominant wind direction is from the southeast, which favours cornice formation and snow accumulation on slopes with westerly aspects (Eckerstorfer & Christiansen, 2011a). The geomorphic effect of snow avalanches is pronounced around Longyearbyen (Fig. 1). Tomczyk & Ewertowski (2017) studied the surface morphology and spatial distribution of fan-shaped landforms in Petuniabukta, 60 km north of Longyearbyen. They suggested that the lack of plateau mountains in this area explained the absence of avalanche dominated fans compared to the numerous fan-shaped landforms around Longyearbyen (De Haas et al. 2015), which is surrounded by plateau mountains. Thus, on the regional scale, the plateau landscape seems to be a critical factor controlling avalanche release and fan sedimentation (Eckerstorfer et al., 2013a). Large cornices develop on the plateau margins, causing frequent avalanches which deposit sediments onto the fan. Compared to other mountainous regions in the world, central Svalbard is unique having cornice fall avalanches as the most important factor for bedrock weathering, rockwall retreat and fan sedimentation (Eckerstorfer et al., 2013a, 2013b). The climatic factors, interacting with the static topography determines the snowpack characteristics, which in turn determine avalanche type, frequency and erosional potential of the avalanche (Luckman, 1977). Therefore, understanding the processes determining avalanche sedimentation can in effect give clues about previous climatic conditions.

As part of a master student project prior to the initiation of this thesis, 224 avalanche fans were mapped around Longyearbyen, primarily on east-southeast and west-northwest facing slopes (Fig. 1). The east-south-easterly and west-south-westerly slopes correspond to valleys cutting into the plateau landscape. However, avalanche fans were mapped in most aspects, even those which lie against the dominant wind direction. Approximately 90% were found to have their top slope topography as plateau, and over 80 avalanche fans had recently deposited sediments which do not reach the terminus of the fan. This simplistic mapping of avalanche fans on aerial imagery of the Longyearbyen area demonstrated that the spatial distribution of avalanche fans on

Svalbard is not determined by the present prevailing wind direction, because avalanche deposits are found on slopes with different aspects. Additionally, recent deposits do not reach the terminus of the fan in all aspects. These observations were acknowledged by De Haas et al. (2015) and Eckerstorfer (2012), who briefly mention the occurrence of recent light-coloured sediments being draped on top of an old body of avalanche deposits. To develop the avalanche fans, large debris-rich avalanches must occur frequently, but judging by the deposits, these large avalanches have decreased in frequency. If avalanches were bigger in the past, what conditions had to be present for the larger avalanches to release?

Most studies of avalanche fans on Svalbard have focused on the morphological description, avalanche sedimentation and rockwall retreat rates (Humlum et al., 2007; Siewert et al., 2012; Eckerstorfer et al., 2013a, 2013b; De Haas et al., 2015). This study aims to move beyond these research questions, and use dynamical avalanche modelling to investigate the observed spatial and temporal differences in fan deposition and relate them to climate conditions. Understanding the processes leading to different runout regimes on Svalbard can help the community with avalanche mitigation planning and risk assessment, in a changing climate.

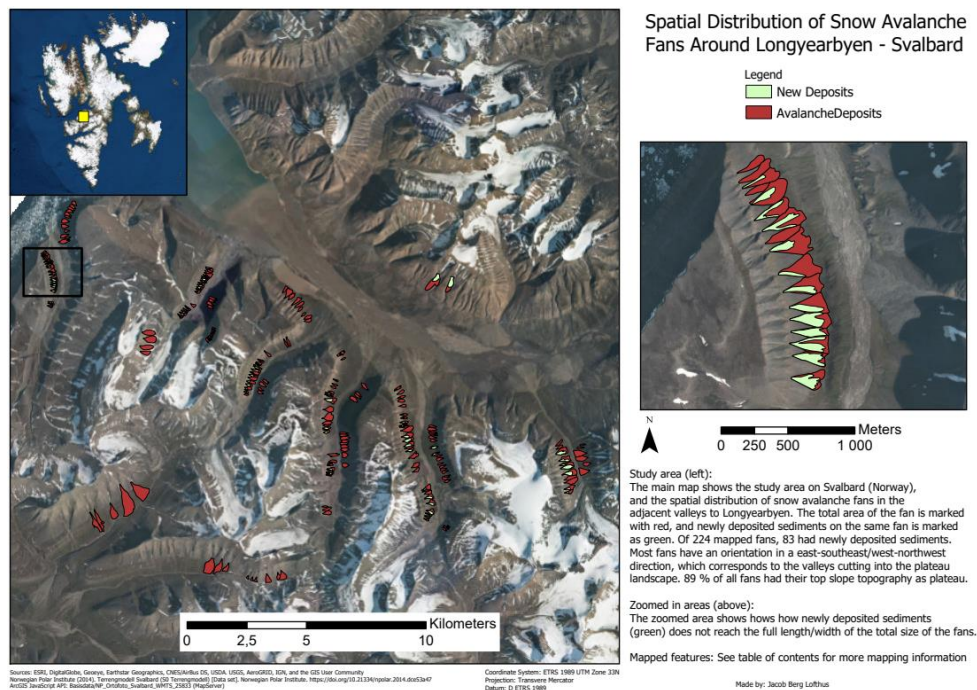


Figure 1. The map was created by the author for a university term project (GEOG3523 – GIS Data Capture and Mapping), investigating the spatial distribution of snow avalanche fans around Longyearbyen, before the initiation of this master project

1.1 Thesis Aim and Research Question

This thesis investigates the recent and historical snow avalanche deposits around Longyearbyen in central Spitsbergen, Svalbard. The study aim is to use a combination of dynamical avalanche modelling, remote sensing, geomorphological mapping, meteorological and snow distribution analysis to provide new insights into observed changes in depositional patterns of avalanche debris fans. Can the study of avalanche fans and past runout lengths be used a proxy for past climate and meteorological conditions on Svalbard? Research questions and aims include:

- *To map recent and historical avalanche deposits and geomorphology in the field and extend to larger relevant areas using remote sensing data.*
- *To reconstruct recent and historical avalanches using dynamical numerical modelling tools calibrated to modern avalanche observations and present day understanding of release mechanisms*
- *To evaluate and suggest what types of differences in release parameters that are required to accurately reconstruct the historical avalanches runout*
- *Give an estimate of what type of meteorological and climatic changes in precipitation, temperature, wind direction etc. that have influenced past avalanche runout, and the timing of the events*

Chapter 2. Theory

2.1 Snow Processes and Formation

2.1.1 Snow Crystal Formation

Snow crystals have large surface areas due to the granular structure of snow, and exhibit a variety of forms and growth rates that are dependent on temperature, supersaturation, and other external parameters (Libbrecht, 2005; Colbeck, 1982). Because of the varieties of grain sizes, shapes and assemblies that result from such external parameters, snow also has wide ranging material properties and develops typical patterns of layering for specific climatic zones (Colbeck, 1987; Sturm et al., 1995).

Snow starts to form when water droplets in the clouds condense onto small particles called condensation nuclei (salt, dust, or soil). When the temperature goes below 0°C, the water droplets can freeze into ice crystals by crystallizing on freezing nuclei. These freezing nuclei are less abundant than condensation nuclei, and have a different molecular structure that promotes freezing (McClung & Schaerer, 2006). As the temperature in the cloud continues to decrease, ice crystal growth becomes easier as the number of freezing nuclei increases (McClung & Schaerer, 2006).

Further growth is decided by two mechanisms: direct transfer of molecules from droplets, and riming resulting from collision when crystals move in the atmosphere (Libbrecht, 2005).

Whether snow crystals form as plates or columns depend on the temperature, while increasing supersaturation increase the complexity of the structure (Fig. 2). Therefore, the shape is also a function of time, as growth behavior changes with varying temperature and humidity in the atmosphere.

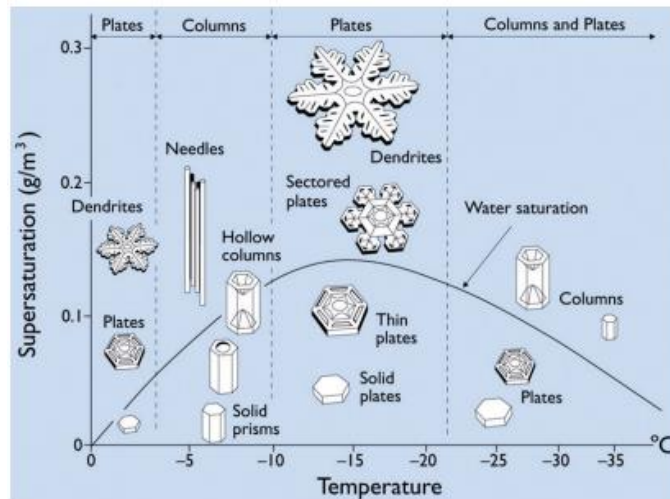


Figure 2. The snow crystal morphology diagram. Snow crystals grow differently as a function of temperature and vapor supersaturation in the atmosphere (from Libbrecht, 2005).

2.1.2 Snow Metamorphism

The large specific surface area of snow is close to the melting point, and from the moment snow touches the ground, the crystals will constantly undergo changes in physical properties due to external influences (Yosida et al., 1956; Sommerfeld & LaChapelle, 1970; Colbeck 1982, 1983; Pielmeier & Scbeebeli, 2003). This transformation process of snow crystals in the snowpack is called metamorphism, and describes how snow undergoes change in size, shape and cohesion over time (Colbeck, 1982). Metamorphism is therefore an important mechanism for understanding avalanche release (Colbeck, 1980).

Initial change to snow crystals is caused by aeolian degradation, which breaks down the snow structure and decrease the surface area of the crystal (Sommerfeld & LaChapelle, 1970; Cabanes et al., 2003). On the ground, the environment and external driving forces leads to differences in crystal transformation, resulting in significant spatial and temporal variations within the snowpack (Colbeck, 1991; Armstrong & Brun, 2008). The main external driving forces are air temperature, wind and solar radiation which influence the temperature gradient in the snowpack (McClung & Schaerer, 2006). The temperature gradient controls the water vapor flux, and thereby how water vapor moves within the snowpack. The water vapor moves from warmer areas to colder areas within the snowpack, and deposits onto snow crystals once reaching the colder area (Colbeck, 1982). Thereby, the water vapor flux along the temperature gradient controls the rate of recrystallization of snow grains. Even though the movement of water vapor along the temperature gradient is not fully understood (Pinzer at al., 2012), water vapor moves either by (1) diffusion in the pore space between snow crystals, and (2) conduction from crystal to crystal (McClung & Schaerer, 2006).

Snow can be divided into wet or dry snow depending on whether it is at or below the melting temperature. They are in literature treated as different materials and have very different appearance. Dry snow can be subdivided into either equilibrium form (rounding) or kinetic growth form (faceting), and wet snow is subdivided depending on its liquid water content (Colbeck, 1982, 1986). The metamorphism of dry snow will be considered here, because dry snow metamorphism leads to development of either well rounded or faceted crystals. Whether dry snow metamorphism leads to equilibrium forms or kinetic growth forms depends on

pressure, temperature and vapor gradients in the snowpack, as the snow crystals try to reach a state of equilibrium (Sommerfeld & LaChapelle, 1970).

2.1.3 Equi-temperature metamorphism

Destructive metamorphism, also known as “equi-temperature” metamorphism is the process which causes rounding of the grains (Fig. 3) (Sommerfeld & LaChapelle, 1970). A newly deposited snow crystal needs a high amount of energy to sustain its crystal shape and is in disequilibrium with the surroundings (McClung & Schaerer, 2006). In order to reach equilibrium, the crystals transform by sublimation of the branches on the crystal and deposits in the concave areas – effectively causing rounding of the crystals (Colbeck, 1980). This is known as the curvature effect (La Chapelle, 1969). The rounded shape is more energy efficient and the shape has a smaller surface area to volume ratio (LaChapelle, 1969). The initial rounding from the curvature effect strengthens the snowpack due to bonding between the grains (Colbeck, 1980). In the absence of imposed temperature gradient, this process is slow in a seasonal snow cover, and does not control metamorphism except for a short period in fresh snow (Colbeck, 1980).

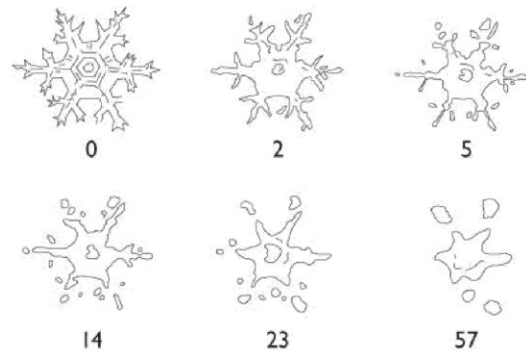


Figure 3. Sketch of equi-temperature metamorphism after Balder (1939) by curvature effects from a cold laboratory. The numbers given time in days. In field conditions, the time will only be a few days (From McClung & Schaerer, 2006).

The temperature gradient is what largely controls equi-temperature metamorphism, which is much faster than the curvature effect (McClung & Schaerer, 2006). Equi-temperature metamorphism occurs when the temperature gradient is less than $10^{\circ}\text{C}/\text{m}$. The growth rate of rounded grains is very rapid near 0°C , and decreases with lower temperatures (Perla & Martinelli, 1976). The imposed effect of the temperature gradient causes low water vapor flux and sublimation of the branches of the crystal. The sublimation and water vapor movement enhance larger grains to grow on the account of smaller grains, because water vapor tends to condense on larger particles where water vapor pressure is lower (McClung & Schaerer, 2006). Therefore, will the average particle size increase in a snowpack with a variety of grain sizes. In many cases, the bonding (or sintering) often forms hard dense slabs (Colbeck, 1991).

2.1.4 Kinetic growth metamorphism

Constructive metamorphism, temperature-gradient metamorphism (Sommerfeld & LaChapelle, 1970), or kinetic growth form as defined by Colbeck (1982) occurs when the snowpack has a temperature gradient of 10° C/m or more (Fig. 4b, c) (LaChapelle & Armstrong 1977; Armstrong, 1980). When a snowpack is subject to the high temperature gradient, there is a high vapor flux and excess water vapor in the pore space. The strong temperature gradient forces water vapor to migrate upwards and condenses on the surface of the colder grains (Akitaya, 1974). This causes crystal growth, and subsequently angular/faceted crystals and depth hoar (Sommerfeld & LaChapelle, 1970). However, if a cold period persists over a longer period, the snowpack will turn isothermal and only slow metamorphism will take place (Eckerstorfer & Christiansen, 2011a).

Development of angular crystals is most prominent in the beginning of the season when the snowpack is thin. A thin snowpack will increase the temperature gradient and vapor will move in a shorter period of time (Sturm & Benson, 1997; Marbouty, 1980). Sturm & Benson's (1997) observations indicate that during the transformation into depth hoar, the mean grain-size increases by a factor of 2-3 while the number of grains decreases by a factor of 10. The subsequent growth of the crystals has fewer bonds per grain, and fewer bonds per unit volume. This causes a layer of lower strength (Schweizer et al., 2003). A weak and unstable snowpack develops, and the poor bonding with adjacent layers and brittle behavior of the crystals promotes avalanche danger (McClung & Schaerer, 2006).

Even with a strong enough temperature gradient, the density plays a significant role in kinetic growth. As the density decreases, vapor transport becomes easier allowing large faceted crystals to grow (Miller et al., 2003). High density on the other hand decreases the ability to grow large crystals because of the lack of pore space, and has been referred to as "hard" depth hoar by Akitaya (1974). Another factor which influences the temperature gradient is aspect. In north-facing slopes and in shaded gullies the temperature is lower due to radiation loss. The lower temperature allows for stronger temperature gradients, causing an increase in avalanche danger (Pela & Martinelli, 1976). Typically, the development of facets and depth hoar comes early in the season after a storm followed by a longer period of cold, clear weather – promoting a high temperature gradient (Hägeli & McClung, 2003).

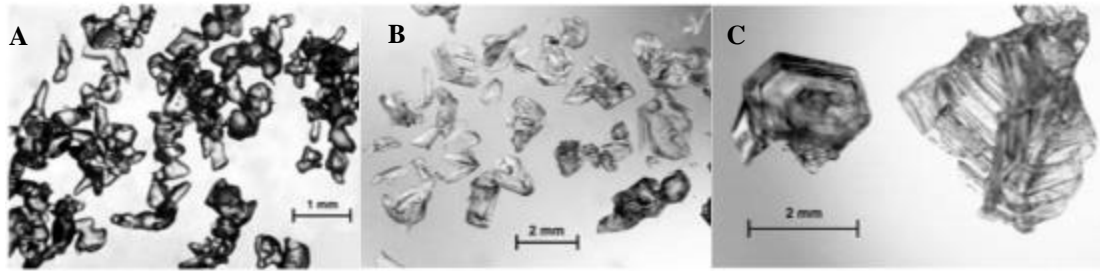


Figure 4. (A) rounded grains due to equi-temperature metamorphism, that bonds well with neighboring grains, (B) facets which develop through kinetic growth metamorphism. Recognize the angular shape which makes the grains bonding capabilities worse, and (C) depth hoar which are large striated cups and has poor bonding with adjacent grains (from Fierz et al., 2009).

2.1.5 Snow stratigraphy

The seasonal snowpack consists of distinct layers with various grain sizes, hardness and thickness (Colbeck, 1991). Due to the interaction between precipitation, wind and the continuous metamorphism of snow, distinct layers of snow build up the snowpack. As a result, each layer is different from the adjacent layer above and below (Fierz et al., 2009). The evolution of the snowpack is complicated, not only because it is discontinuous and highly irregular at different scales, but also from season to season, within climatic zones and the fact that it changes as the season progresses (Colbeck, 1991; Schweizer et al., 2008). The existence of snow layering and the exact sequence of layers is a crucial understanding in avalanche science, since avalanches release due to instabilities in the layered snowpack (Schweizer, 1999). The main interest for avalanche release is the development of weak layers such as hoar layers, wind slabs and ice layers which can cause avalanching (Colbeck, 1991). Weak layers form due to kinetic growth and have weak intercrystalline bonding, which makes them more likely to collapse (McClung & Schaerer, 2006).

Surface hoar is a kinetic growth form known as a weak layer which frequently forms slab avalanches (Föhn, 2001; Schweizer & Jamieson, 2001), and can cause snow instability for several weeks over entire mountain ranges (Hägeli & McClung, 2003; Schweizer & Kronholm, 2007). Surface hoar forms during clear, cold nights with gentle wind when water vapor deposits on the snow surface (Breyfolge, 1987; Hachikubo & Akitaya, 1997). Depth hoar on the other hand, typically develops deep in the snowpack due to very high temperature gradients and can cause very large avalanches (Mock & Birkeland, 2000). They can be looked as the “end product” in kinetic growth metamorphism, since they have developed significantly since initial growth

took place. Since strong temperature gradients are necessary, they are most common in environments where the snowpack is thin and cold (Eckerstorfer & Christiansen, 2011a), or at the beginning of the season when the snow cover is thin (Mock & Birkeland, 2000). However, in alpine terrain with complex topography, depth hoar is commonly found around rocky outcrops or terrain features where the snowpack is thin, locally increasing the avalanche danger (Birkeland et al., 1998; Arons et al., 1998). Depth hoar also acts as a persistent weak layer, which in some cases can survive almost the entire season (Mock & Birkeland, 2000; Eckerstorfer & Christiansen, 2011a).

Ice crusts within the snowpack can in effect block upward migration of water vapor, and faceted crystals or depth hoar can develop around them (Stethem & Perla, 1980; Colbeck, 1991; Schweizer & Jamieson, 2001). Ice layers develop under rain-on-snow events or with sufficient energy input from warm air or radiation. The melted snow will percolate into the snowpack and refreeze into crusts both vertically and horizontally (Albert & Perron, 2000). Several studies (Armstrong, 1985; Fukuzawa & Akitaya, 1993; Birkeland, 1998; Jamieson et al., 2001; Colbeck & Jamieson, 2001; Jamieson & Herwijnen, 2002) also showed that wet snow beneath a subsequent fall of cold snow provides a large enough heat source to create strong temperature gradients which enables near-wet-layer faceting within hours to a few days. Birkeland (1998) termed this melt-layer recrystallization. Glude (2008) points out that not only can facets develop above and underneath frozen melt layers, but within as well, terming it faceted melt forms. These structures can develop in any climate where colder weather is followed by large increase in temperature or rain events and are highly unpredictable and not fully understood.

2.2 Snow Avalanches

Snow avalanches (hereby referred to as avalanches) are masses of snow that move downslope under the influence of gravity, and can contain rocks, soil, vegetation or ice (Schweizer et al., 2003). Avalanche release is a complex interaction between the topography, snowpack and meteorological conditions (Schweizer et al., 2003).

Avalanche activity over multiple temporal scales has been explored by several researchers. For long timescales, Holocene snow avalanche activity has been reconstructed from lake sediments (Seierstad et al., 2001; Nesje et al., 2007; Vasskog et al., 2011) and depositional facies and

pollen studies (Blikra & Selvik, 1998; Blikra & Nemec, 1998) in Norway, showing several periods with high avalanche frequency. Late Holocene avalanche activity was reconstructed from lichenometry studies in southern Norway (McCarroll, 1993; McCarroll et al., 1995) and the French alps (Jomelli & Pech, 2004), while tree rings has been used to reconstruct historic avalanche frequency in the USA (Reardon et al., 2008), Canada (Dubé et al., 2004) and the Swiss alps (Stoffel et al., 2006). Some studies focusing on avalanche trends during the 20th century in France have shown an overall reduction in the number of snow avalanche since 1977 in response to climate fluctuations (e.g. Eckert et al., 2010), although Jomelli et al. (2007) found no correlation between fluctuations in avalanche activity in Vallée de la Maruennce, France, and large-scale atmospheric patterns between 1978 and 2003. Laternser & Schneebeli (2002) did not find any evidence of changing avalanche activity during the between 1950-2000 period in Switzerland. However, increased climate variability since 1980 has been invoked as the cause of increasingly larger avalanches in eastern Canada (Germain et al., 2009). Together, these studies indicate that understanding the impact of climate change on avalanche frequency and magnitude, is important for understanding the potentially changing hazards for mountain communities.

Depending on the snowpack characteristics and metamorphic processes, different kinds of avalanche types exists (Mock & Birkeland, 2000). How avalanches are triggered is separated into either natural or artificial. Naturally triggered avalanches are due to increased loading from snowfall and windblown snow or change in temperature, whereas artificial avalanches are triggered by humans, for example, a skier, snowmobile or explosives (van Herwijnen & Jamieson, 2005; Thumlert & Jamieson, 2014; Jamieson & Stethem, 2002). Schweizer et al (2003) divided avalanches into two types: loose snow avalanche and slab avalanche, and both can occur in a wet or dry snowpack. Loose snow avalanches are triggered from a point on the surface of cohesionless snow (wet or dry) and typically spread out in a triangular shape (Fig. 5b). Initial volume is typically less than 1m³. Slab avalanches release as a cohesive slab due to failure in an underlying weak layer, which propagate through the snowpack, making a characteristic crown in the release area (Fig. 5a). Slab avalanches are the most dangerous avalanche type to human lives and infrastructure, as they involve more snow, long runout distances, and are difficult to forecast (Mock & Birkeland, 2000; Marienthal et al., 2012).

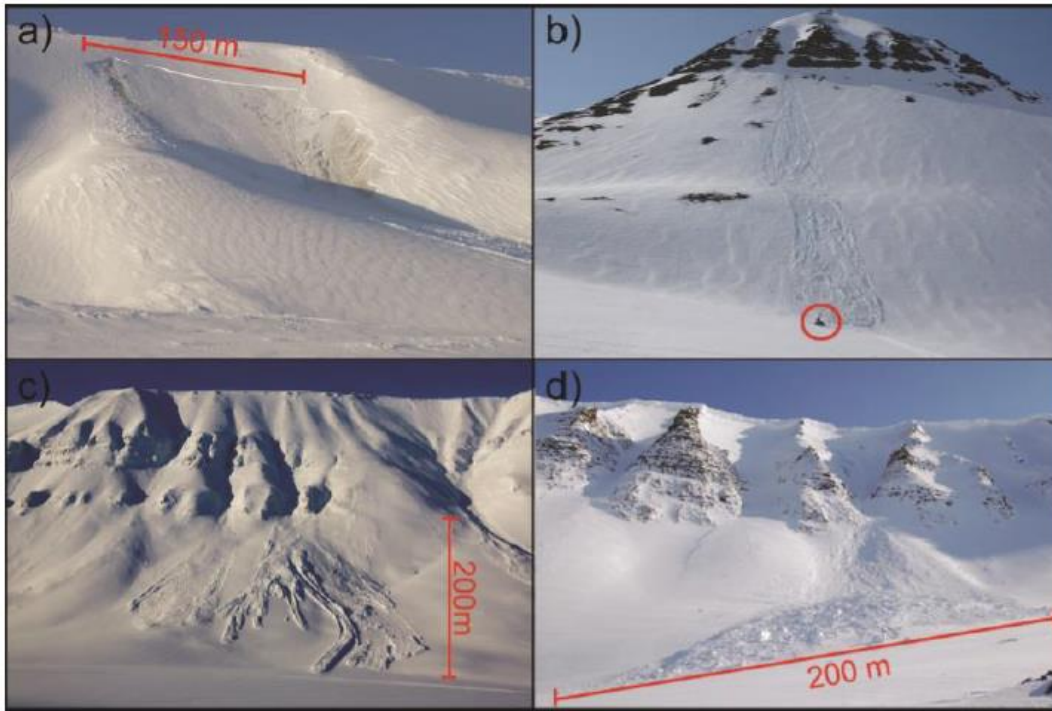


Figure 5. Types of avalanches. a) Slab avalanche. b) Loose snow avalanche. c) Slush avalanche. d) Cornice fall avalanche (From Eckerstorfer, 2013)

Slush avalanches and cornice fall avalanche are two additional types of avalanches. Slush avalanches are typically found in northern latitudes, like northern Scandinavia or Svalbard, and are a type of wet snow avalanche where the snowpack is partly or fully water saturated (Hestnes, 1985; Scherer et al., 1998) (Fig. 5c). They release either during intensive melting of snow or rain on snow events and can transport a considerable amount of debris (André, 1995; Hestnes, 1998; Scherer et al., 1998). Slush avalanches typically develop on gentle slopes, in gullies or channels where water is concentrated (Hestnes, 1998). Due to very high density they are considered very dangerous to human infrastructure (Hestnes, 1985). Cornices are wedge like projections of snow which usually form on the lee sides of ridges due to snowdrift (Montagne et al., 1968; Seligman, 1936; Eckerstorfer et al., 2013b). If the cornice deforms and collapses, it is considered a cornice fall avalanche (Vogel et al., 2012) (Fig. 5d). Cornice falls can trigger loose snow avalanches or slab avalanches as a secondary avalanche (Eckerstorfer & Christiansen, 2011c; Vogel et al., 2012).

Around Longyearbyen on Svalbard, Eckerstorfer & Christiansen (2011c) reported cornice fall avalanches as the most common type with 45.2% of all observed avalanches. In 16.2% of the cornice fall avalanches a secondary slab avalanche occurred, and in 12.1% a loose snow avalanche occurred as secondary avalanche. The second most reported avalanche type was slab avalanches (32.6%) (Eckerstorfer & Christiansen, 2011c). As dry and wet slab avalanches are the type that are required for avalanche fan development, they are the focus in this thesis. Even though slush avalanches are known to transport significant amounts of debris, and are certainly a contributing factor in fan development and the periglacial landscape in general (André, 1990). They do not occur often and are not the dominant factor the widespread distribution of avalanche fans. Most avalanche fans are located in relation to the plateau landscape where cornices develop. As cornice falls erode sediments and trigger slab avalanches, they are also an important control on the avalanche fan distribution (Vogel et al., 2012; Eckerstorfer et al., 2013a; 2013b).

2.2.1 Slab avalanche

Dry snow avalanches release through four stages: (1) failure initiation in a weak layer underlying a cohesive slab, (2) the onset of crack propagation, (3) dynamic crack propagation through the weak layer across the slope, and (4) tensile failure followed by sliding of the slab (Fig. 6). The release of a slab avalanche leaves a prominent crown perpendicular to the slope and flanks representing the boundaries for the release area (McClung & Schaerer, 2006). The slab glides over a bed surface on which the weak layer collapses, being the ground or a snow layer (Fig. 7). They range in size from a few meters to several kilometres. The depth of the weak layer and the failure propagation determines the size of the avalanche, which in turn is controlled by the size of the starting zone and snow depth (McClung & Schaerer, 2006).

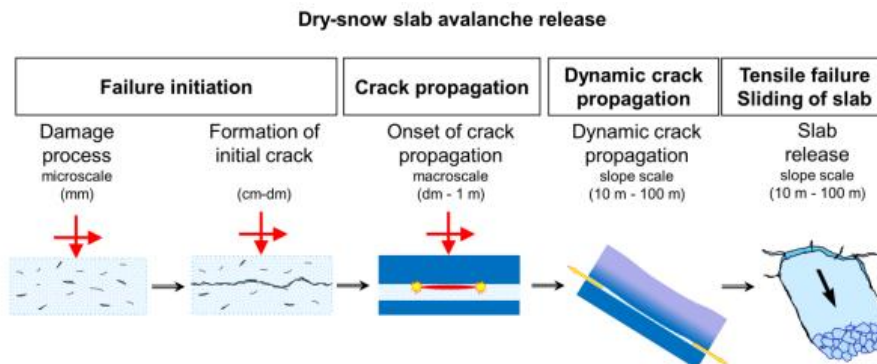


Figure 6. Conceptual model of dry snow avalanche release through four stages: (1) failure initiation in a weak layer underlying a cohesive slab, (2) the onset of crack propagation, (3) dynamic crack propagation through the weak layer across the slope, (4) tensile slab failure followed by sliding of the slab. The red arrows indicate mixed-mode loading (From Schweizer et al., 2016).

In their simplest form, dry slab avalanches release when the shear stress of the overlying slab and additional load exceeds the shear strength of the weak layer (McClung, 1979). However, Heierli et al. (2008) launched a new theory called the anticrack model, sparking a debate about whether weak layer failure and slab avalanche release is due to shear or collapse (Schweizer, 2017).

Topography is the most important factor in determining slab avalanche release. Slab avalanches commonly release between 28 and 55° (Perla, 1977; Schweizer & Lütschg, 2001). The greatest probability for release is between 35-45°, but larger avalanches tend to release on slopes less than 35°. Above 45° avalanche probability decrease due to increased sluffing (Veitinger et al., 2016). Direct solar radiation and meteorological factors such as wind speed and direction, precipitation and air temperature cause favorable conditions for avalanche release, all influenced by topography (McClung & Schaerer, 2006).

Schweizer et al (2003) describes three different triggering mechanisms for slab avalanche release: (1) a localized rapid near-surface loading by people or explosives, (2) gradual uniform loading due to precipitation and/or wind loading, or (3) a no-loading situation that changes snowpack properties, like surface warming (spontaneous release). Slab avalanche release is mostly associated with storms. They release naturally during or shortly after the storm from increased loading from new snow and additional wind transported snow, termed direct-action avalanches (Schweizer et al., 2003). New snow influences the stress and strength in the snowpack, and the weak layer might not respond quick enough to support the rapid loading. For large natural avalanches, when the 3-day sum of new snow depth exceeds 30 cm, it can cause instability and increase the avalanche danger (Schweizer et al., 2003). When the loading of new snow is slow, the strengthening rate of the weak layer can prevent release (Schweizer et al., 2003). Instabilities in the old snowpack due to constructive metamorphism (buried surface hoar, facets and depth

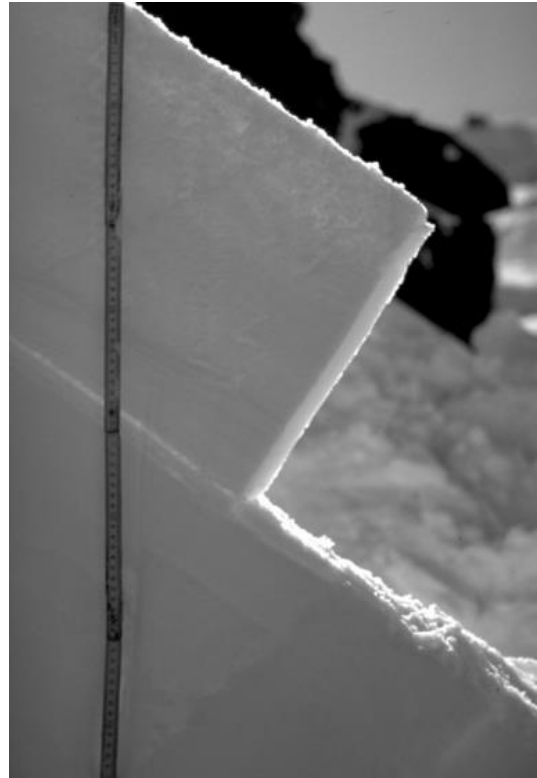


Figure 7. Cohesive slab on top of a weak layer and a bed surface (From Schweizer et al., 2003).

hoar) are persistent weak layers which can trigger large climax avalanches and cause instabilities throughout the winter season (Birkeland et al., 1998). The different trigger mechanisms also cause two periods with different avalanche regimes. During the winter phase, direct or delayed action avalanches releases (dry slab avalanches), and spring phase when wet slab avalanches releases (Luckman, 1977).

Wet snow avalanches have received little attention compared to dry snow avalanches (Baggi & Schweizer, 2009). Wet slab avalanches occur when liquid water is introduced into the snowpack from melting and/or rain-on-snow events (Heywood, 1988; Conway & Raymond, 1993).

Compared to dry slab avalanches, which release due to increased shear stress, wet slab avalanches release due to decrease in shear strength (Kattelmann, 1984). Baggi & Schweizer (2009) suggested three different trigger mechanisms which might also act in combination: (1) loss of strength due to water infiltration and storage at capillary barrier, (2) overloading of partially wet and weakened snowpack due to precipitation and (3) gradual weakening of (basal) snowpack due to warming of the snowpack to 0°C and eventual failure of basal layer.

Slope stability decreases when water percolates into the snowpack, causing additional load, melting and disintegration of bonds between crystals (Conway & Raymond, 1993). The liquid water spreads laterally along impermeable boundaries, increasing water content in the upper layer, lubricating and weakening the basal or weak layer (Heywood, 1988). Increasing temperatures, solar radiation and rain is the primary causes for wet slab avalanche release (Baggi & Schweizer, 2009). In warm maritime climates, this can happen at any time. In cold climates, it is generally a late spring phenomenon (Kattelmann, 1984). However, wet slab avalanches can release due to mid-winter rain-on-snow events even in cold maritime climates (Eckerstorfer & Christiansen, 2012). When wet slab avalanches release due to melting by solar radiation, the spatial distribution is controlled by aspect. Rain-on-snow events affect every aspect, however elevation and temperature controls where precipitation falls as rain. While wet slab avalanches are less frequent than dry slab avalanches, they can be very destructive and are an important morphological agent in mountain environments (Luckman, 1977; Kattelmann, 1984; Jomelli & Bertran, 2001).

2.2.2 Cornice fall avalanches

Cornices are overhanging masses of snow which generally form on lee side of ridges and plateaus due to snowdrift (Montagne et al., 1968; Seligman, 1936, Vogel et al., 2012). Cornices become a hazard when the entire cornice or a partial failure of the cornice collapses. The falling cornice move down the slope as a single or multiple blocks and can trigger a secondary slab avalanche (Eckerstorfer & Christiansen, 2011c). Research has focused on cornice fall avalanches as a geomorphic agent in the High Arctic (Humlum et al., 2007; Eckerstorfer, 2013), but the main interest has been investigating the hazard potential of cornice fall avalanches (Montagne et al., 1968; Seligman, 1936; Vogel et al., 2012; Hancock et al., 2020). Cornice growth is caused by accumulation of snow when a sharp change in topography causes eddies due to flow separation (McClung & Schaerer, 2006). Therefore, will the location and size of cornices give direct indication on snowdrift processes and dominant wind direction (van Herwijnen & Fierz, 2014). Cornice growth requires a minimum windspeed of about 5 m/s if temperature and snow conditions are favorable (McClung & Schaerer, 2006). Vogel et al (2012) found that on Svalbard, cornice accretion was related to storms with wind speeds in excess of 10 m/s. On the other hand, windspeeds exceeding 27 m/s will lead to cornice scouring (Montagne et al., 1968). While gravity and creep is the primary reason for deformation and tension crack formation (Montagne et al., 1968; Vogel, 2010), Burrows & McClung (2006) listed three meteorological factors which causes or induces cornice failure: (1) snow loading of the cornice during a storm or wind event, (2) abrupt temperature change at the surface due to waring/cooling of air temperature, rain-on-snow event and solar radiation, and (3) seasonal warming or warm periods midwinter. Even though there is sparse scientific research on the timing and release mechanism of cornice falls (Eckerstorfer & Christiansen, 2011c), Vogel et al (2010) found a temporal pattern with cornice failure increasing towards the end of the season. Nevertheless, he argued that meteorological conditions presented by Burrows & McClung (2006) where less important than the length of time since crack initiation, and tilting related to temperature variations associated to storms. In contrast, Hancock et al. (2020) found that cornice failure from the same location was related to high accretion rates ($>10\text{mm hr}^{-1}$) during storms and mid-winter rain, thereby supporting the conceptual models that cornice failure responds to specific meteorological events.

2.3 Fan-shaped landforms

Fan-shaped landforms are found in every climatic region on earth and are typically referred to as landforms that develop where a channel emerges from a mountainous catchment to an adjoining valley (De Haas et al., 2015). Many human settlements are located on top of fans and understanding fan-related processes is important to evaluate potential geohazards. This is particularly important in densely populated mountainous areas, but also in low populated areas like Svalbard (Tomczyk et al., 2019).



TYPICAL CHARACTERISTICS	colluvial fan	alluvial fan
Geomorphic setting:	mountain slope and its base (slope fan)	mountain footplain or broad valley floor (footplain fan)
Catchment:	mountain-slope ravine	intramontane valley or canyon
Apex location:	high on the mountain slope (at the base of ravine)	at the base of mountain slope (valley/canyon mouth)
Depositional slope:	35-45° near the apex, to 15-20° near the toe	seldom more than 10-15° near the apex, often less than 1-5° near the toe
Plan-view radius:	less than 0.5 km, rarely up to 1-1.5 km	commonly up to 10 km, occasionally more than 100 km
Sediment:	mainly gravel, typically very immature	gravel and/or sand, immature to mature
Grain-size trend:	coarsest debris in the lower/toe zone	coarsest debris in the upper/apical zone
Depositional processes:	avalanches, including rockfall, debrisflow and snowflow; minor waterflow, with streamflow chiefly in gullies	debrisflow and/or waterflow (braided streams)
EXAMPLES	 <p>The Brotofonna colluvial fan, Trollvegen near Romsdal, Norway; one of the world's largest colluvial fans, with a height of 830 m and a plan-view radius of 1.5 km.</p>	 <p>The Badwater alluvial fan, eastern side of Death Valley, California; a modest fan, with a radius of c. 6 km.</p>

Figure 8. Shows a comparison between colluvial fans and alluvial fans (from Blikra & Nemeč, 1998).

Fans are formed by different processes and can be roughly divided into two main categories: colluvial fans and alluvial fans (Fig. 8). Colluvial fans are a product of gravity driven processes e.g. avalanche/rock fall, while alluvial fans are a formed by fluid-gravity flow (Blikra & Nemeč, 1998; Blair & McPherson, 2009). In the literature, colluvium is also referred to as “talus”, “scree” and “debris slope” among others (Blikra & Nemeč, 1998). Colluvial fans mainly consists of angular stones and boulders. Smaller particles lie at the top and larger stones and boulders at the base of the talus by fall sorting (Rapp, 1960b; Blikra & Nemeč, 1998). Within the category of colluvial fans, there are a number of different processes that lead to fan development (Fig. 8).

These processes can act together, resulting in fans with complex morphology and internal structure. Processes acting in isolation develop fans with specific signatures, which can be differentiated into, for example avalanche-dominated fans and rock fall dominated fans (De Haas et al., 2015).

While fans have been studied extensively in many environments, knowledge about fans in periglacial environments is limited (De Haas et al., 2015; Tomczyk & Ewertowski, 2017; Tomczyk et al., 2019). Climate as a driver for fan development and morphology has been debated, with some studies suggesting that it is not an important driver (Blair & McPherson, 1994, 2009). Meanwhile, others support the idea that climate change leads to differences in fan morphology for both alluvial (Nemec & Postma, 1993; Dorn, 1994; Ritter et al., 1995) and colluvial fans (Whittecar & Ryter, 1992). Some studies suggest that the processes leading to fan formation vary little no matter the environment (Kesel, 1985; Brierley et al., 1993; Harvey et al., 2005). However, De Haas et al. (2015) points out that large-scale morphometry (e.g. catchment, fan area and slope) might be similar between most environments. In the case of periglacial environments, the interaction between regular processes (e.g. debris flow and fluvial flow) and periglacial processes (e.g. snow avalanches, solifluction) leads to a unique fan morphology. Fan development will therefore depend on local and regional environmental settings, and the corresponding processes typical for that specific environment (Senderak et al., 2017)

2.4 Snow avalanche fans and geomorphic effect of avalanches

Sass et al. (2010) stated that the geomorphological importance of avalanches as sediment erosion, transportation and accumulation agent is often underrated, but in favorable climatic and lithological settings, avalanches are a pronounced geomorphological agent (Luckman, 1977, Decaulne & Saemundsson, 2006). The geomorphic significance of avalanches on mountain slopes and development of avalanche fans has previously been described in Swedish Lapland (Rapp, 1959, 1960a, 1995) Canada (Gardner, 1970; Luckman, 1977, 1978), Norway (Bikra & Nemeč, 1998), Iceland (Decaulne & Saemundsson, 2006), the French Alps (Jomelli & Francou, 2000; Jomelli & Pech, 2004), Scotland (Luckman, 1992) and Svalbard (Rapp, 1960b; Humlum et al., 2007; Siewert et al., 2012; Eckerstorfer et al., 2013a; 2013b; de Haas et al., 2015). Avalanche fans are often referred to as “avalanche boulder tongues” and “road-bank tongue” (Rapp, 1959; Luckman, 1977), but will only be referred to as “avalanche fans” in this thesis.

SEDIMENTARY FEATURES	DEPOSITIONAL PROCESSES				
	rockfall/debrisfall	debrisflow		snowflow	waterflow
TYPE/GEOMETRY OF DEPOSITS	Fresh rock debris Resedimented gravel Upslope fining Scattered clasts Lobate or "patchy" accumulations of debris; scattered large "outrunners"	AVALANCHES Relatively broad lobes Highly elongate, tongue-shaped lobes (upslope fining) Levées Spill-over lobes		Toolmark grooves "Debris horn" Longitudinal grooves, debris ridges & clast-thick levées One clast-thick levée Small "digitated" lobe with frontal wash-out sand "Patchy" lobes Scattered clasts Drier snowflows Slushflow	Levées of bypassing debrisflows Overbank sand Narrow, gully-type channels; or shallow channels with braid-bars
three-dimensional view					
vertical cross-section	Upward fining Openwork Infilled by "tail"	Tabular beds Large "floating" clasts	"Imbricate" beds Lenticular beds with "imbricate" or more complex stacking	Indistinct boundaries Melt-out clasts in precarious positions Stratified waterlain infill of larger interstices Redeposited humic soil Waterlain infill	Remnant debrisflow deposits Tractional infill Isolated channel-fills (up to 1.5 m thick)
TEXTURE AND STRUCTURE	Highly immature debris; mainly angular clasts Boulder to sand size grade. Clast-supported and commonly openwork, with pebbly to sandy infill at the top. Deposits often infilled with waterlain sand and/or redeposited soil material.	Mature debris; subrounded to rounded clasts Matrix rich to clast-supported. Sandy/muddy matrix. Common "coarse-tail" inverse grading and outsized cobbles or boulders.	Clast-supported, bouldery to cobbly "heads" and clast- to matrix-supported, pebbly upslope "tails". Common normal grading.	Unsorted, scattered clasts and gravel "patches" infilled with waterlain sand or pebbly sand. The sand in large interstices shows stratification, but is massive, very fine/silty and possibly shell-bearing in submarine deposits.	Clast-supported, pebbly to cobbly gravel interlayered with poorly sorted/stratified sand. Matrix-supported gravel occurs as debrisflow remnants.
CLAST FABRIC	Boulders and large cobbles often show "rolling" fabric, a(t) or a(t)l(b)l, when emplaced frontally in isolation. Many large clasts upslope show "sliding" fabric a(p), but a disorderly "adjustment" fabric predominates; "shear" fabric a(p) often typifies the avalanche's overriding tail, when evolved into a grainflow.	Large clasts mainly aligned downflow, a(p) or a(p)l(l), but showing a(l) orientation along the lobe front.	Common "rolling" fabric a(t) in the frontal and top part of the debrisflow head; common "shear" fabric a(p) or a(p)l(a)l in the flow's tail.	Mainly disorderly (chaotic "melt-out" fabric). Boulders and cobbles deposited from turbulent snowflows may have "rolling" fabric a(t), but the scattered debris is vulnerable to rotation by subsequent avalanches. Dense snowflows and slushflows may create "shear" fabric a(p), but this loses order during the melt-out.	Common tractional fabric; poorly developed in gullies due to clast pivoting and adjustment to banks. Many large clasts are rotated in situ to a(p) position by less competent waterflow.
DEBRIS SOURCE	Weathered bedrock.	Glacial till and valley-side kame terraces.	Glacial till, kame terraces and upper-slope colluvium.	Glacial till and upper-slope colluvium, including fresh bedrock. Common slope-soil erosion.	Upper slope colluvium and glacial till.

Figure 9. Shows the different depositional processes and their sedimentary features (from Bikra & Nemeč, 1998)

Topography largely determines the distribution of starting zones and tracks, and thereby the geomorphic effect of avalanches, since they limit the distribution of avalanche activity (Luckman, 1977). Landforms associated with avalanches develop because avalanches can carry significant amounts of debris that has accumulated on the snowpack due to rockfall, windblown fines, entrainment along the track and erosion of the underlying surface (Blikra & Nemeč, 1998). Avalanches are sometimes termed “dirty avalanches” when the debris content is particularly high (Rapp, 1960b; Eckerstorfer et al., 2013a). Four controls on the debris content in avalanches determines the distribution of avalanche fans (Luckman, 1977): (1) Type of avalanche and snow cover, (2) vegetation cover, (3) debris availability and (4) magnitude-frequency considerations. Vegetation protects the underlying debris, and erosion potential thereby increases with less vegetation cover and limited snow (Luckman, 1977). Since this thesis focuses on Svalbard where trees are non-existent, vegetation won’t be elaborated further.

Avalanche erosion only occurs when avalanches involve the whole snow cover or runs over bare ground. Observations show that avalanche erosion mainly involves wet slab avalanches (Rapp, 1959; 1960a; Luckman, 1977; 1988; Bell et al., 1990; Decaulne & Saemundsson, 2006; Jomelli & Bertran, 2001; Eckerstorfer et al., 2013a, 2013b). Dry slab avalanches often have limited geomorphic impact. As failure occurs along a persistent weak layer or due to new snow instabilities, the underlying snow cover protects the ground from erosion (Decaulne & Saemundsson, 2006). Nevertheless, dry slab avalanches can transport material downslope which accumulates on the snowpack due to rockfall and contribute to avalanche fan sedimentation mid-winter (Eckerstorfer et al., 2013a). This happens often in association with cornice fall avalanches, which are also a pronounced sediment transport agent (Montagne et al, 1968; Humlum et al., 2007; Eckerstorfer et al., 2013b). Cornices can erode large quantities of sediments by plucking, and when the cornice collapses and falls downhill or trigger a secondary avalanche, the plucked sediments will add to the accumulation on the fan (Eckerstorfer et al., 2013a; 2013b).

Whether large fans develop is controlled by the debris availability and the avalanche sedimentation rate. Loose, unconsolidated debris in the avalanche track provides the best conditions for debris entrainment by avalanches (Luckman, 1977). The avalanche sedimentation rate is the most direct measurement of the geomorphological effect of avalanches (Eckerstorfer

et al., 2013a). From the sedimentation rate, rockwall retreat can be calculated as the backward erosion capacity by avalanches on a slope (Krautblatter & Dikau, 2007). In periglacial or paraglacial environments, avalanche landforms are considered short lived if conditions become less favourable for development (André, 2003, Ballantyne & Benn, 1994). Therefore, for large fans to develop, enough debris needs to be available for transport, frequent enough avalanches to transport the debris downhill, and favourable climate for erosional avalanches. Lithology and climate are thereby a controlling factor. For example, hard bedrock is less subject to weathering, and thus limits the sediment supply compared to weak and highly fractured rocks (André, 1997). On Svalbard, rockwall weathering rates are among the highest in the Arctic, for example in the weak sedimentary rocks in the Adventdalen

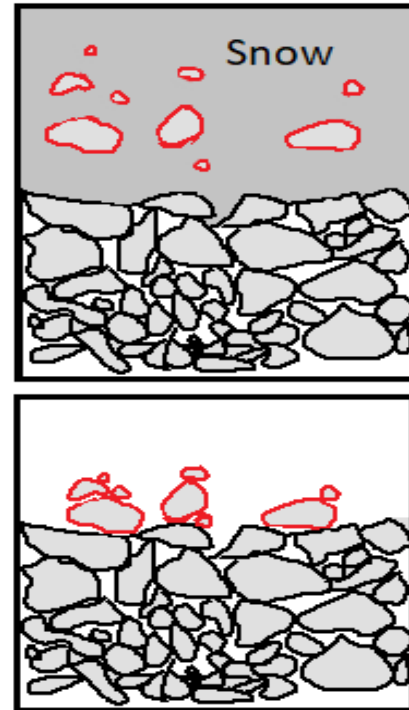


Figure 10. Schematic figure of how perched boulder/cobbles are deposited. The deposits get stacked on top of each other when the avalanche melts out in spring

region where topographical and climatological conditions also allow for cornice plucking on the rock face (Siewert et al., 2012; Eckerstorfer et al., 2013a; 2013b). The constant removal of debris by avalanches and cornices also exposes fresh rock to the weathering process (Rapp, 1959). The magnitude and frequency of avalanches is not directly proportional with size of the avalanche fan, since the factors mentioned above control the debris content transported by the avalanches (Luckman, 1977). Luckman (1977) argues that there is no simple relationship between snowfall and frequency of avalanches, except from where direct-action avalanches are most dominant. Thus, avalanche erosion and deposition are impossible to determine from snowfall or avalanche frequency alone (Luckman, 1977).

Avalanche deposits and morphology differs from the regular talus slope because avalanches don't sort material in size fractions, producing a chaotic avalanche deposit (Gardner 1970; Luckman, 1977). Important morphological indicators are perched boulders and cobbles, typically found anywhere on the fan where small rocks resting on top of larger rocks, implying that there has been a melt-out process from an avalanche (Fig. 10) (Rapp, 1960a; Luckman, 1977; De Haas et al., 2015). From now on, they will only be referred to as perched boulders. Perched boulders

give the deposits a unique signature, which is not found in other colluvial fan environments where avalanches don't exist (De Haas et al., 2015). Debris horns (Fig. 11) and debris tails (Fig. 11) are characteristic of avalanche activity. Debris horns occur upslope of large obstacles due to plastic freezing of avalanche rich sediments, while debris tails are found on the lee side of obstacles where erosion is preserved (Blikra & Nemec, 1998; De Haas et al., 2015). Avalanches re-distribute debris from the proximal towards the distal zone of the fan, developing a large basal concavity (Luckman, 1977; Jomelli & Francou, 2000) The proximal part can therefore often be dominated by finer grained sediments (Fig. 12) (De Haas et al., 2015). Fan profiles are commonly concave, while the cross profile is plano-convex with a flat top due to avalanche erosion (De Haas et al., 2015). Avalanche fans are pronounced features in the terrain, as they have a lower mean angle than other types of talus and typically develops under well-developed couloirs. Above the fans, the rockwall is often stripped of loose debris (Luckman, 1977).

Given the depositional nature of avalanches, the individual boundaries from successive avalanches are hard to recognize in an outcrop section. Large clasts within a thicker section of fine material often represents separate avalanches, but the actual number of events is uncertain because not all avalanches carry debris. Implying that a thin sedimentary unit might represent 5-15 avalanche events (Blikra & Nemec, 1998). However, the sharp transitions in sediment color from light to grey and increased lichen growth on the fan surface can indicate the limit for previous avalanche activity (De Haas et al., 2015). As the description of avalanche fans deposits have been established in literature, the focus of research has shifted towards quantifying sedimentation, fan accretion and rockwall retreat rates in order to discuss avalanches as a geomorphic agent for landscape evolution.

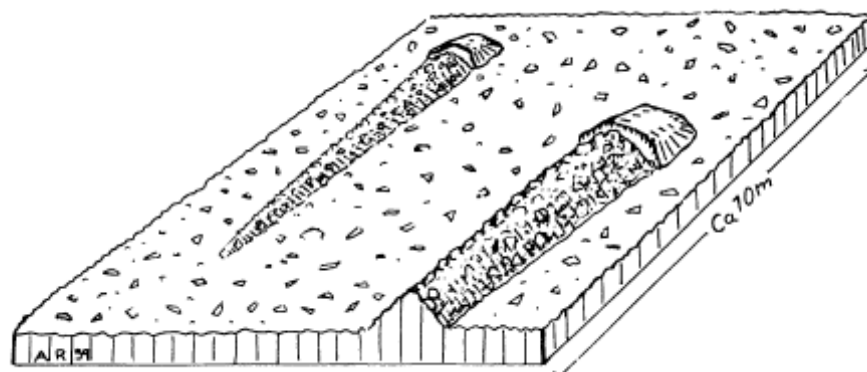


Figure 11: sketch of a "debris tail/shadow" which occurs on many surfaces of avalanche tracks (from Rapp, 1959)

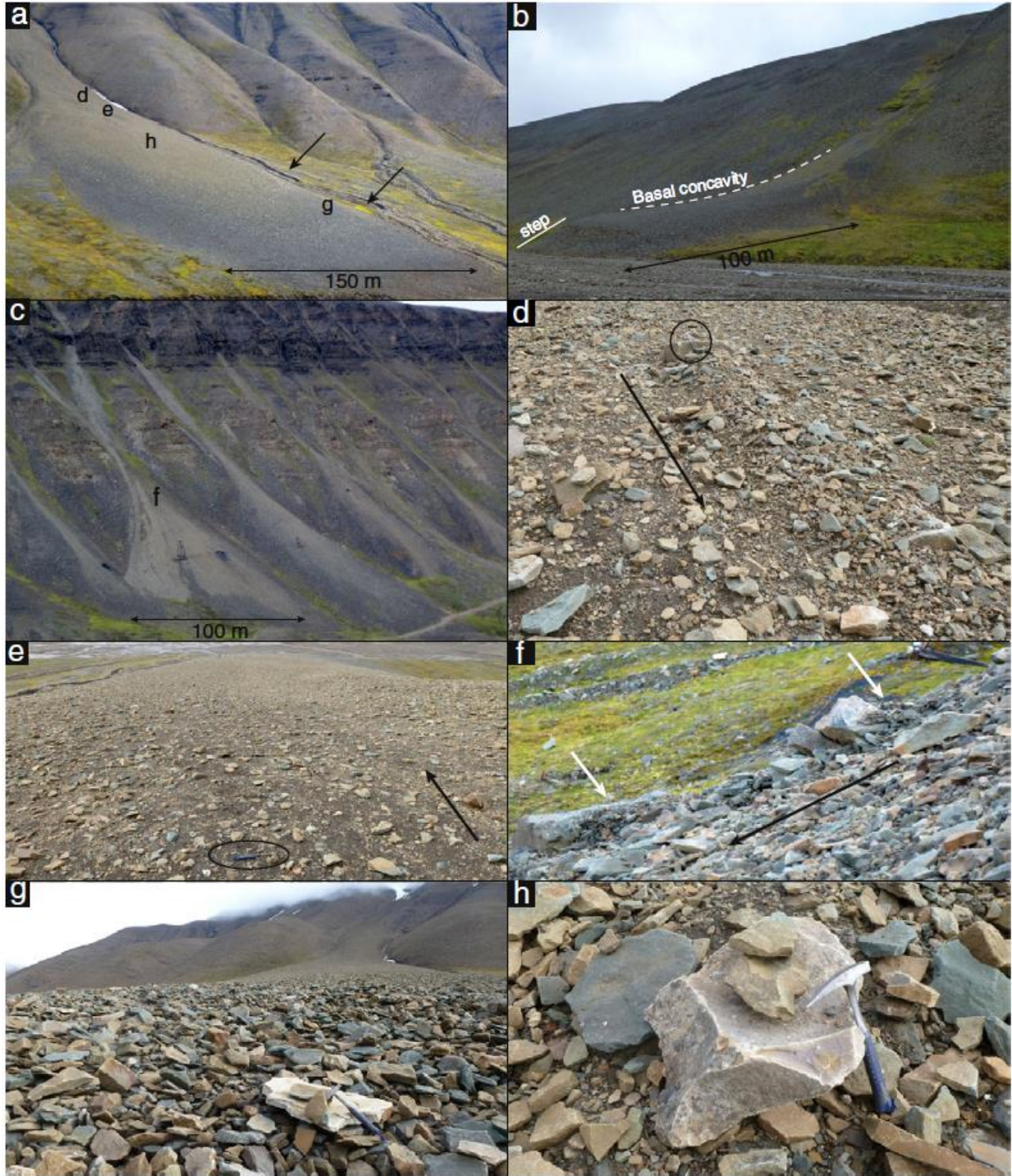


Figure 12: Figure from De Haas et al. (2015), showing avalanche dominated fans and typical properties. (a) Tongue-shaped fan, note that the sediments turn grayer (older) towards the distal domain. (b) Avalanche fan showing typical basal concavity with a steep toe. (c) Cone-shaped avalanche fans in Longyeardalen. (d) Debris tail, with black arrow showing flow direction. (e) Avalanche erosion on the proximal domain leads to a more fine-grained texture. (f) Debris horn, shown by the white arrow, and black arrow flow direction. (g) Accumulation of coarse-grained sediments at the distal domain. (h) Perched boulder – a very typical, easy to identify avalanche feature

2.5 Snowdrift processes

The spatial distribution of snow is heavily influenced by wind in arctic and alpine regions, and snow is redistributed by a complex interaction between terrain and meteorology (Pomeroy et al., 1997). Snow deposits on lee sides where the terrain causes wind speed deceleration, and snow erosion occurs where wind speed is accelerating (McClung & Schaerer, 2006) (Fig. 13). Several meters of snow can accumulate in certain aspects, while other aspects can be snow-free (Jaedicke & Sandvik, 2002). Avalanche activity is thus heavily linked to snow drift processes such as windspeed, dominant winter wind direction and wind direction of storms (Schweizer et al., 2003). Snowdrift can even trigger avalanches in clear weather (McClung & Schaerer, 2006).

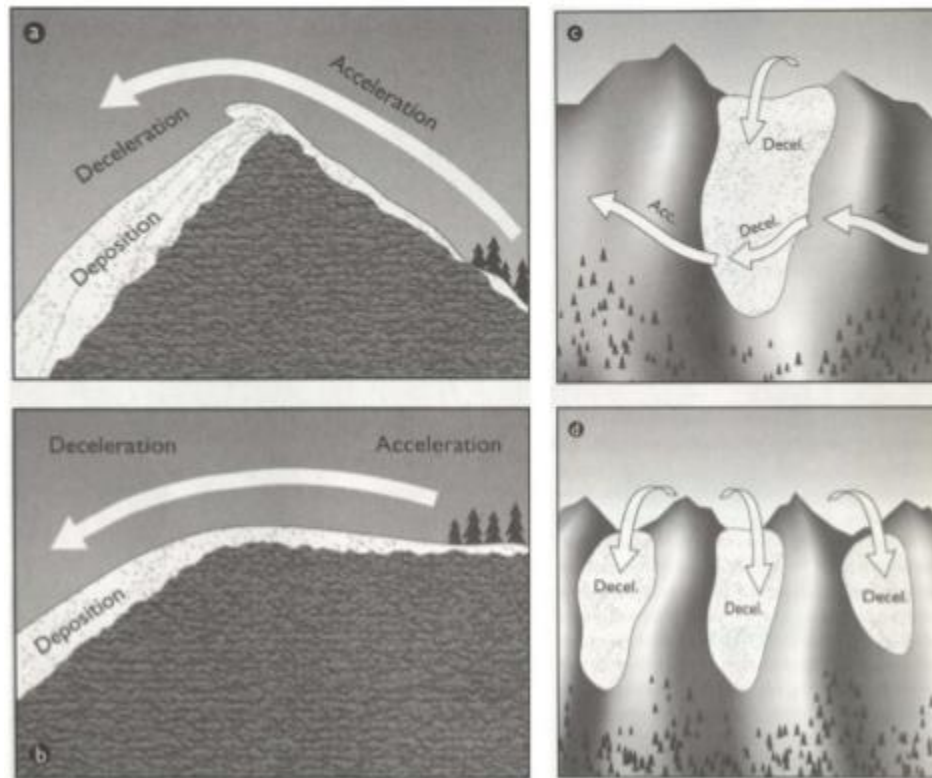


Figure 13: Snow is eroded due to wind accelerating and deposits on the lee side, where snow decelerates. A) and B) shows snow accumulation on the lee side. C) and D) shows accumulation in a gully (From McClung & Schaerer, 2006).

There are three different types of snow movement: creep (rolling), saltation and turbulent suspension (Fig. 14) (Lehning et al., 2008). Creep is the gravitational deformation or settlement of snow, and accounts for only 10% of total mass transport (McClung & Schaerer, 2006). The process is negligible compared to saltation and turbulent suspension and is not considered in

most snow drift models (Jaedicke, 2001; Lehning et al., 2008). Saltation occurs when airspeeds at a certain threshold lifts the snow particle from the surface. Saltation is limited to the first 10cm above the surface and causes small rounded particles and dense wind slabs (Jaedicke, 2001). The total snow transport by saltation is <50% when wind speeds are lower than 10 m/s (Pomeroy & Gray, 1990). Threshold wind speeds for initiation or sustaining saltation depends on surface snowpack properties such as snow particle bonding, cohesion and kinetic friction (Li & Pomeroy, 1997). Threshold winds for wet snow range from 7 to 14 m/s with an of average of 9.9 m/s, while dry snow ranges from 4 to 11 m/s and average 7.7 m/s (Li & Pomeroy, 1997). Suspension starts when turbulent eddies form due to high wind speeds. Suspension can account for over 90% of the total snow transport with wind speeds exceeding 15 m/s (Pomeroy, 1989). With increasing wind speeds, snow drift rates increase proportional to the fourth power (Pomeroy, 1989). Thus, total snow mass transported by wind can be high and loading can be very rapid (Schweizer et al., 2003). For snow transport to be effective, a long fetch (distance), upwind where snow can be entrained by the wind is needed. With a fetch of 300-350 m, snow transport will increase significantly (Takeuchi, 1980; Pomeroy et al., 1993).

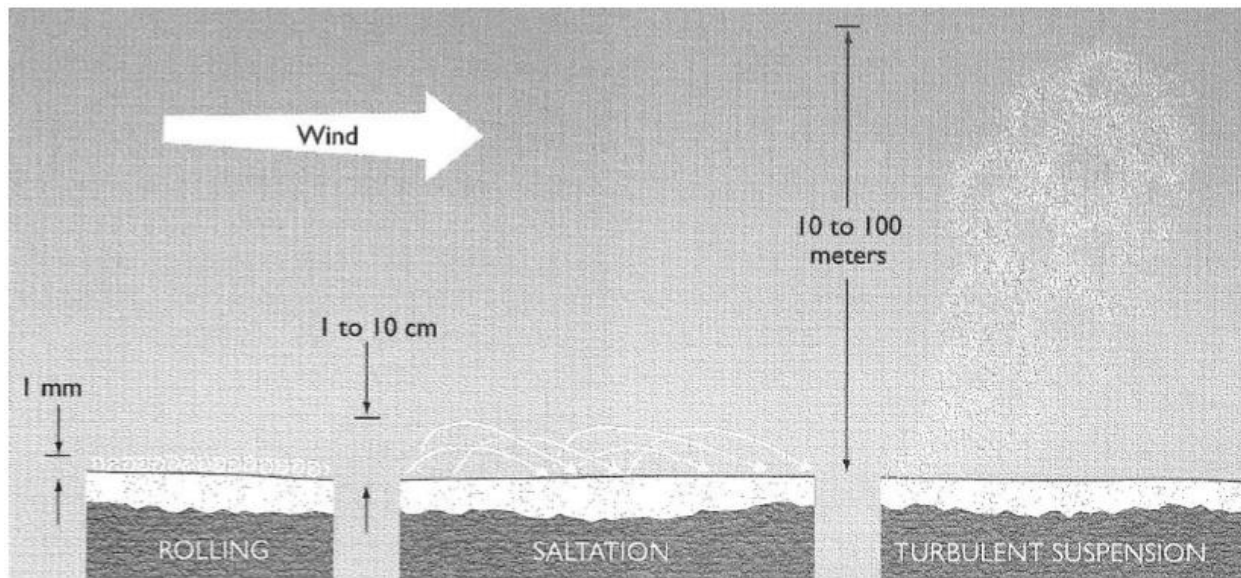


Figure 14. The three different modes of snow transportation by wind (From McClung & Schaerer, 2006)

2.6 Snow avalanche research on Svalbard

Avalanches were mentioned as early as 1956 by Balstad (1956), who reported a slush flow avalanche that destroyed the hospital in Longyearbyen in 1953. Early avalanche research focused mainly on the geomorphological significance of avalanches in combination with slope processes re-shaping the landscape (Rapp, 1960a, 1960b; Jahn, 1967; Åkerman, 1984). Avalanches are a contributing factor on talus morphology, and Åkerman (1984) noted that the highest frequency of dirty avalanches occurred during spring. Jahn (1976) assigned only minor importance to avalanches for slope denudation in Longyeardalen, and while André (1990; 1996) acknowledged the potential for spring avalanches as a geomorphological agent in reshaping the talus.

Slush avalanches caught the attention of several researchers due to their high frequency in an Arctic climate (Thiedig & Kresling, 1973; Thiedig & Lehmann, 1973; Jahn, 1976; Rapp, 1985; André, 1990; André, 1995; Hestnes, 1998; Scherer et al., 1998). Large slush avalanches could transport enormous amounts of debris and develop avalanche boulder tongues (André, 1990). However, André (1995) argued from the geomorphological evidence, slush avalanches are rare events with recurrence interval between 80 and 500 years. Later, André (1996) concluded that geological rather than climatic factors controlled the geomorphic activity of the avalanches in Northwest Spitsbergen.

Hestnes (2000) summarized previous work conducted by the Norwegian Geotechnical Institute (NGI) and identified the hazards in Longyearbyen related to snowdrift and avalanches. He highlighted the need to better understand avalanche processes on Svalbard, especially around Longyearbyen. A study of snowdrift patterns in complex Arctic terrain was conducted by Jaedicke (2001) in his PhD thesis. He identified snow accumulation patterns and prevailing wind direction, and in effect the spatial distribution of avalanche activity. The first winter and spring avalanche monitoring program was established by Ellehauge (2003), out of which came the Cryoslope project, and the beginning of a multi-year avalanche monitoring program conducted by PhD student Markus Eckerstorfer at the University Center in Svalbard (UNIS) (Eckerstorfer, 2013). Eckerstorfer laid the groundwork for further avalanche research on Svalbard. A number of MSc projects have since investigated cornice development (Vogel, 2010), the spatial variability of Svalbard's snow cover (Farnsworth, 2013; Kristiansen, 2014), hazard prediction and warning procedures (Kaufmann, 2014), avalanche climatology (Hancock, 2016) and

dynamic avalanche modelling (Pellaud, 2014; Eiken, 2017). Mechanical properties of spontaneous avalanche release in the Arctic snowpack was the focus of another PhD, who discussed how climate change could have implications for the present avalanche climate on Svalbard (Delmas, 2013). Eckerstorfer & Christiansen (2011a) identified the regional snow avalanche climate on Svalbard (presented in section X), and the topographical and meteorological controls on all types of avalanches typical to the High Arctic snowpack on Svalbard (Eckerstorfer & Christiansen, 2011b). Weather patterns for natural slab avalanches release showed that snowdrift was the best indicator for slab release (Eckerstorfer & Christiansen, 2011c). Mid-winter slush avalanches and wet slab avalanche releases were, on the other hand, caused by extreme mid-winter rain-on-snow events (Eckerstorfer & Christiansen, 2012).

Humlum et al. (2007) first introduced cornice fall avalanches as an important agent on Svalbard while studying how rock glaciers develop from dirty avalanches. Rock debris accumulation rates ranged from 0 to 50.4 kg/ m²/yr, and averaged 13 kg/m²/yr. Since the first mention of cornice fall avalanches (Humlum et al, 2007), more research has focused on cornice fall development, dynamics, geomorphological significance and hazard potential on Svalbard (Vogel et al., 2012; Eckerstorfer et al., 2013a, 2013b; Hancock et al., 2020). Eckerstorfer et al. (2013a, 2013b) argued that seasonal snow cornice dynamics are an important control on the bedrock weathering and erosion rates. Furthermore, a shift in prevailing wind direction could lead to a change in sedimentation by changing the avalanche activity. Sedimentation by cornice fall avalanches happens in a two-step fashion: (1) Cornice plucking in the headwall and subsequent collapse mid-winter will transport rock downslope. (2) At the end of spring, full-depth cornice fall avalanches will release and entrain debris of different origin along the track (Eckerstorfer et al., 2013a).

Siewert et al. (2012) studied rockwall retreat rates for both sides of the valley in Longyeardalen. They found that rockwall retreat rates varied from 0.52 mm yr⁻¹ on the SE facing slope and 0.83-1.17 mm yr⁻¹ on the opposite NW facing slope. Rockwall retreat rates were also calculated on the west facing slopes at Larsbreen (0.9mm yr⁻¹) and Nybyen (0.9mm yr⁻¹). They were considerably higher than on the opposite SE facing slope, studied by Siewert et al. (2012) (Eckerstorfer et al., 2013b). Siewert et al. (2012) and Eckerstorfer et al. (2013a, 2013b) attributed the difference to

more frequent cornice fall avalanching on the NW facing slopes. Both Siewert et al. (2012) and Rapp (1960b) acknowledged that the slope landscape is relatively old based on the calculated rockwall retreat rates. Christiansen et al. (2013) argued that, in addition to avalanche fan sedimentation, rock glacier development is primary controlled by meteorology. The result of Siewert et al. (2012), Eckerstorfer et al. (2013a, 2013b) and Christiansen et al. (2013) results contradicts André's (1996) assertion that bedrock is the primary control on geomorphic activity related to avalanches.

De Haas et al. (2015) described the surface morphology of fans around Longyearbyen. Three types of fans were listed: (1) colluvial fans, mainly formed by snow avalanches and additional rock falls, but with snow avalanche dominated morphology, (2) alluvial fans dominated by debris flows and (3) alluvial fans dominantly formed by fluvial flows. In total, 50% of the fans were considered to be snow avalanche dominated. De Haas et al. (2015) argued that avalanche activity on colluvial fans are mainly dominated by shifts in dominant winter wind direction.

Recently the SASM (Svalbard Automated Snow Monitoring) program has been established in Longyearbyen (Prokop et al., 2018). Prokop et al. (2018) presented the first continuously collected data on snow depth, snow surface temperature and snow temperatures on slopes in Svalbard. Data from one winter season (2017/2018) showed that over 30 cm of new snow can accumulate on lee slopes due to extensive wind drift during precipitation events. Prokop et al. (2018) identified wind slabs and cornice fall as the main avalanche problem on Svalbard, whereas storm slabs are non-existent around Longyearbyen. Due to continuous solar radiation and rain-on-snow events in spring, wet snow avalanches were also considered a very important avalanche problem around Longyearbyen.

As this thesis focus on avalanche fan development, table 1 shows a summary of the geomorphic impact of avalanches, fan development and rockwall retreat described in literature on Svalbard.

Table 1: Shows studies from Svalbard focusing the geomorphic significance of avalanches, fan development, rockwall retreat and its key findings

Reference	Location	Focus	Method	Key findings
Rapp, 1960	Tempelfjorden, Svalbard	Reconstruction of the morphological development of talus formation and the corresponding mountain wall.	Field measurements and mapping	Talus cones probably started forming after deglaciation. Rockwall retreat in modern times calculated to 0.02-0.2 mm per year. Lack of agreement between present-day supply and size of the cones.
Jahn, 1967	Hornsund, Svalbard	Mass movement on slopes	Field investigations	Important morphologic process connected with the action of wet snow mixed up with water recorded on Svalbard. Slush avalanches contributor to fan development.
Åkerman, 1984	Kapp Linné, Svalbard	Describe morphology, morphometry and active processes in talus slopes in two different aspects	Meteorological data, geomorphological mapping and aerial photos	Aspect influences solar radiation, precipitation and temperature change, which may explain differences in morphology and morphometry, and the presence of dirty avalanches.
André, 1990	Northwest Spitsbergen, Svalbard	Investigating the geomorphic impact of spring avalanches	Field investigations	Accretion rates from 0.04 mm/yr to 8.13 mm/yr. Geomorphic impact of snow avalanching is at least twenty times higher on dissected mica schist walls than on steep and smooth gneissic walls. No significant avalanche sediment erosion, only slight reshaping of the talus in schist and gneissic rock
André, 1995	Northwest and central Spitsbergen, Svalbard	Geomorphic impacts of extreme avalanche events	Geomorphological mapping and	Recurrence interval for extreme slush streams of 500 years. Results show that mobilization and deposition from slush events can be up to 1300 to

			lichenometry as dating mechanism	7000 m ³ . Life expectancy of avalanche boulder tongues more than 2000 years
André, 1996	Northwest Spitsbergen, Svalbard	Geological control of slope processes	Field investigations	Geological rather than climatic conditions should be regarded as the predominant controlling factors of avalanche geomorphic efficiency – controlled by tectonic networks. Observed only 3% dirty avalanches from gneissic walls compared to 40% from fractured mica schist walls.
Humlum et al., 2007	Longyeardalen, central Spitsbergen, Svalbard	Avalanche sedimentation	18m ² of durable plastic used to quantify rock debris accumulation in the runout zone at the end of each summer	Avalanches can be driving the formation of rock glaciers, and the amount of fresh rock debris recorded on each sediment trap ranged from 0 to 917 kg, corresponding to rock debris accumulation rate of 0 to 50.4 kg/m ² /yr. Average value for all traps was 13 kg/m ² /yr
Siewert et al., 2012	Longyeardalen, central Spitsbergen, Svalbard	Rockwall retreat and fan thickness	Combine ERT profiles with TLS data and GIS to calculate talus volume.	Calculated Holocene rockwall retreat from 0.33 to 1.96 mm per year. Retreat rates for debris flow and avalanche influenced fans are higher than those dominated by single rockfall. Slope landscape on Svalbard relatively old. Rock wall retreat rates from NW facing slopes in Longyeardalen where significantly larger than rates on the opposite SE facing side of the valley
Eckerstorfer et al., 2013a	Longyeardalen, central Spitsbergen, Svalbard	Avalanche sedimentation	Combining monitoring of cornice fall activity with automatic time-laps photography and	Rockwall retreat rates high due to cornice plucking. Avalanches the primary rock debris transport agent. Avalanche sedimentation rates between several thousands to hundreds of thousands of kilos per year

			direct field measurements to calculate avalanche sedimentation, accretion and rockwall retreat rates	for Nybyen and Larsbreen. Fan surface accretion rates up to 13.9mm per yr ⁻¹ . Climate-induced changes in the dominant winter wind direction can lead to significant changes in rockslope sedimentation from avalanches
Eckerstorfer et al., 2013b	Longyeardalen, central Spitsbergen, Svalbard	Cornices as agent for rockwall erosion	Air, snow and ground temperature sensors, automatic time-lapse cameras to study seasonal cornice dynamics	During cornice accretion, snow accumulates around loose weathered rocks on the plateau edge, being incorporated in the cornice mass. Debris is plucked away during cornice collapse. Contributes to avalanche fan development
De Haas et al, 2015	Adventdalen region, central Spitsbergen, Svalbard	Effects of periglacial conditions on morphology of snow avalanches	High resolution imagery and geomorphological fieldwork	Avalanches found to dominate surface morphology and morphometry on colluvial fans. 50% of all mapped fans where avalanche dominated
Tomczyk & Ewertowski, 2017	Petuniabukta, central Spitsbergen	Surface morphology and spatial distribution of fan-shaped landforms	Aerial photography, satellite images, geomorphological fieldwork	Colluvial fans the most common fan-shaped landform, but little influence from avalanches. Most likely due to the lack of plateau mountains and little precipitation.

Chapter 3. Study area

Svalbard is an archipelago located at 74° – 81° N and 10° – 35° E in the High Arctic, and is placed between the Arctic ocean, Fram Strait, Barents Sea and the Norwegian sea (Fig. 16). Longyearbyen (78°13'N), the main settlement on Svalbard is located in Nordenskiöld land on central Spitsbergen, the largest island on the archipelago (Fig. 15). The study areas are located in Adventdalen, Longyeardalen and Todalen (Fig. 20), which deglaciated around 10 ka BP (Mangerud et al., 1992).

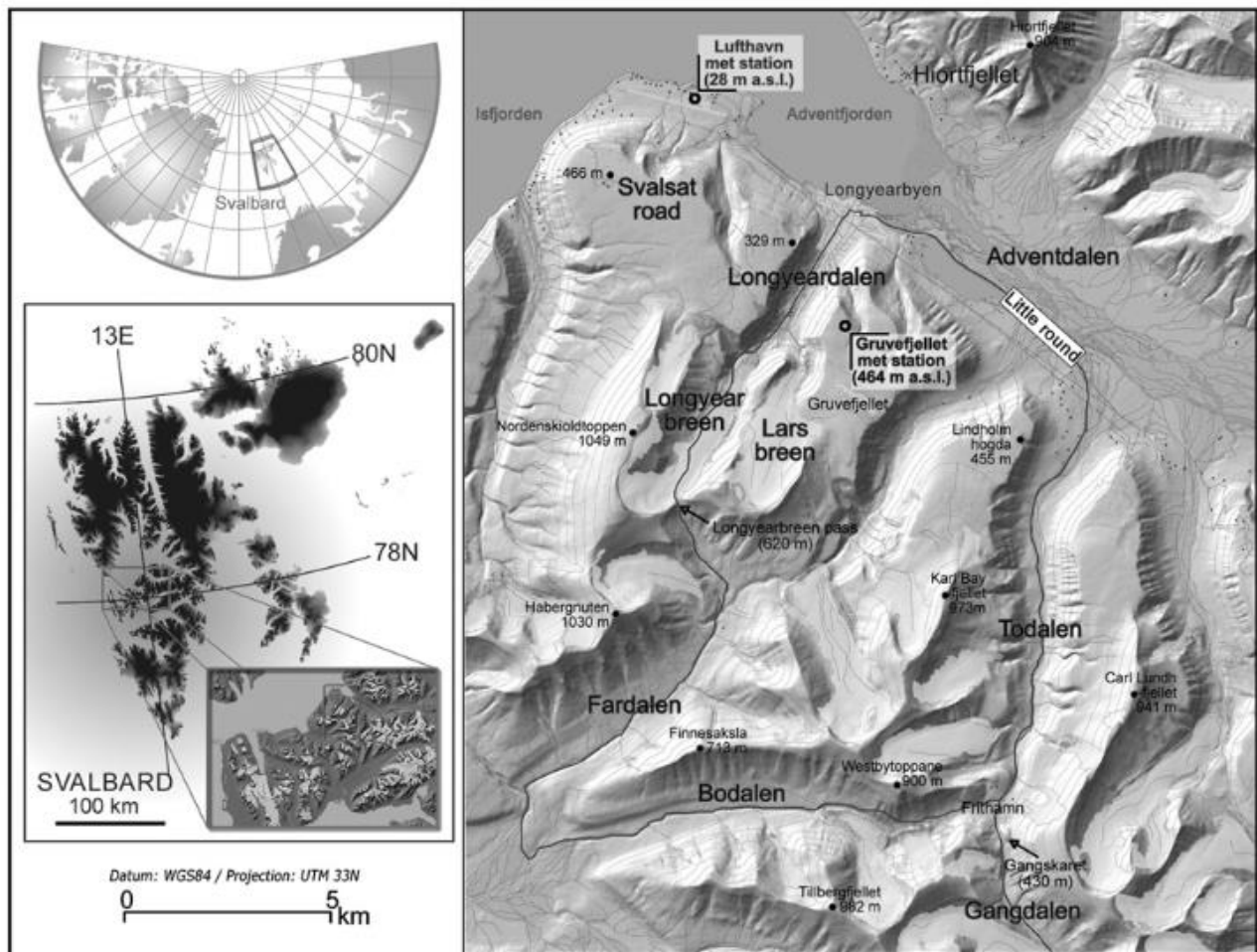


Figure 15. Overview map of Longyearbyen in central Spitsbergen, Svalbard and the surrounding area (from Eckerstorfer & Christiansen, 2011c).

3.1 Climate and Meteorology

The climate on Svalbard is classified as polar tundra according to the Koeppen-Geiger climate classification (Kottek et al., 2006). Compared to other regions at the same latitude, Svalbard has a relatively mild climate (Førland et al., 1997), and is considered one of the most climate sensitive places on earth (Rogers et al., 2005). Svalbard is snow covered between 8-10 months each year and temperatures above freezing only lasts for 2-3 months (Eckerstorfer & Christiansen, 2011a).



Figure 16. Svalbard's location in the north-west corner of the Barents Sea and ocean currents influencing the region. The West Spitsbergen Current (WSC) brings warm water to the west coast, making the region relatively mild compared to other regions at the same latitude. East coast is influenced by the Persey Current, bringing cold polar water. As a result, east coast of Svalbard is significantly colder and has more sea ice than the west coast (From Dallmann, 2015).

Situated between the Arctic Basin and the North-Atlantic (Fig. 16), Svalbard is climate sensitive due to the influence from ocean currents, air masses with different thermal character and variations in sea ice extent (Humlum, 2002). The combined effect of the atmospheric and oceanic changes has the potential to cause significant climatic variability on Svalbard, even if the changes are small (Humlum et al., 2007). Warm water from the West Spitsbergen current flows up the west coast of Svalbard, while cold polar water flows on the east (Fig. 16) (Hanssen-Bauer, 2019). This circulation pattern becomes visible in Svalbard's regional sea ice extent, because the

west coast has much less sea ice compared to the east coast (Humlum et al., 2007; Walczowski & Piechura, 2011). Sea ice blocks ocean-to-atmosphere heat flux, and thereby reduces moisture availability and air temperature (Gjelten et al., 2016; Kopec et al., 2016). The ice-free conditions on the west coast and central Svalbard thus create a milder and more maritime climate (Christiansen et al., 2013). The general loss in sea ice in the Arctic is believed to be influencing the arctic amplification and arctic land warming (Kumar et al., 2010; Lawrence et al., 2008).

Two pressure systems mainly determine the air flows on Svalbard. The low-pressure system near Iceland and the high-pressure system over Greenland and the Arctic Ocean (Førland et al., 1997). The North Atlantic Cyclone track brings mild and moist air towards Svalbard, leading to west and south-westerly winds and higher temperatures, especially in winter (Hanssen-Bauer et al., 1990; Dickson et al., 2000). Cold anticyclonic airflows prevailing from the east and northeast alternate with the moist cyclonic air masses, which turns the weather cold and clear. The result is large air temperature variations during winter (Eckerstorfer, 2013). Large-scale weather phenomenon's, such as the Siberian High influences winter temperature and precipitation, particularly during winter (Humlum et al., 2003; Hanssen-Bauer et al., 2019). When cold anticyclonic air forms over eastern Siberia and the air masses extend over Europe, airflow over the Nordic Sea is strong and southerly. Advection of warm air moves towards Svalbard, causing heavy precipitation either as snow or rain. Periods of snowmelt in the middle of the winter are therefore a possible scenario (Humlum et al., 2003). Rogers et al. (2005) found that mild winters were connected to increased cyclone frequency over the Fram Strait, whereas cold winters were associated with increased cyclone frequency over the Barents Sea.

Wind patterns on Svalbard are strongly affected by the topography and the pressure systems mentioned above (Christiansen et al., 2013). The most common wind direction is along fjords and valleys, from inland towards the coast. The general wind direction is mainly from the south east, but often changes to westerly or south-westerly during winter storms (Christiansen et al., 2013). Channelling through the valleys explains why average wind speed is 1 m/s higher than on the plateaus (Christiansen et al., 2013). Average hourly wind speeds on the plateaus are lower in summer (1-8 m/s) compared to the winter (5-20 m/s), and the highest wind speeds are usually recorded from November to February (Humlum et al., 2007; Christiansen et al., 2013). Annual average wind speed is around 5 m/s (Eckerstorfer, 2013), and the lack of vegetation enhances the

effect of wind across the landscape; making wind the dominant factor influencing snow accumulation (Jaedicke & Sandvik, 2002). The combination of wind and low precipitation makes some parts completely snow free, while the lee side can have meters of snow (Jaedicke et al., 2000; Eckerstorfer, 2013).

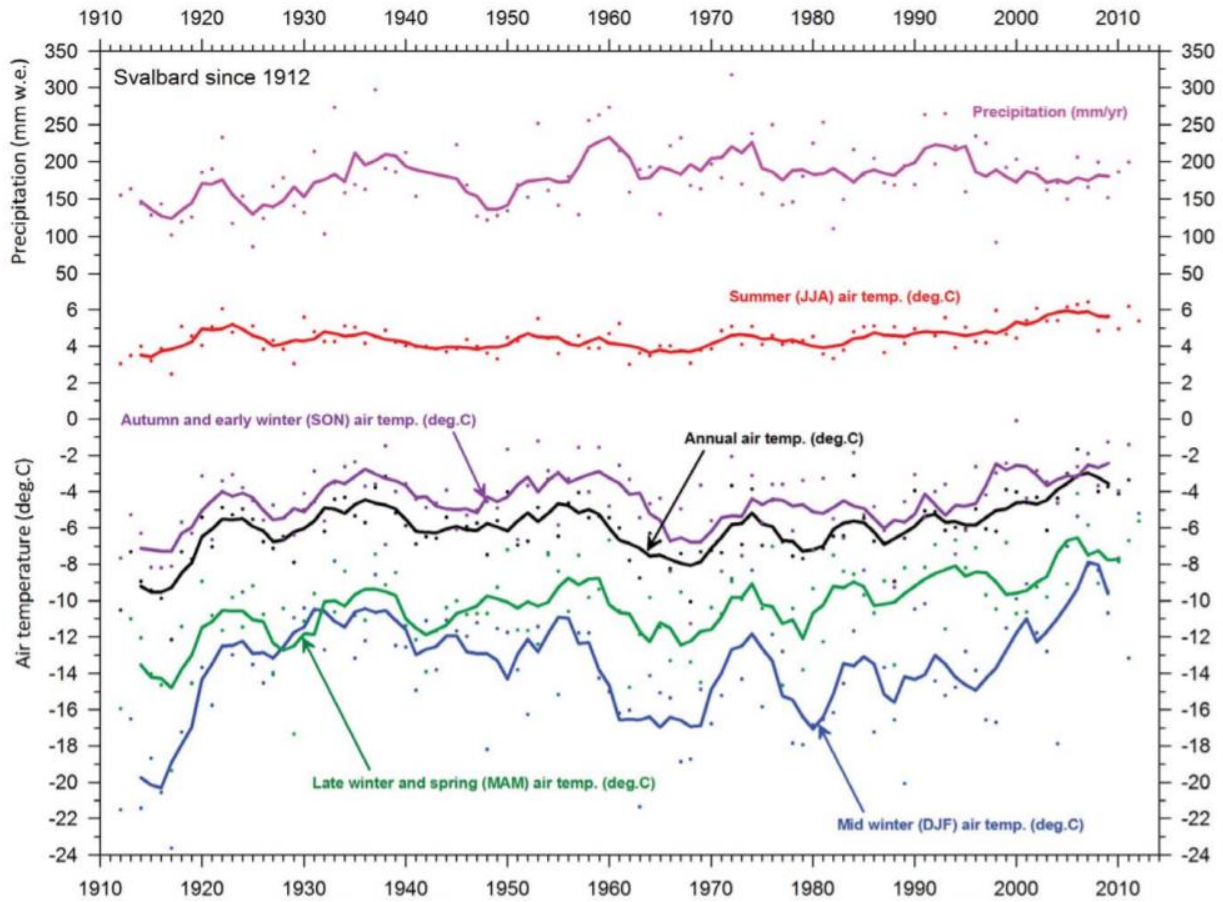


Figure 17. Mean annual air temperature and precipitation at Longyearbyen since 1912. Points are annual observation, and the lines are 5-year average (from Christiansen et al., 2013).

Meteorological stations have been able to record data since 1911 on Svalbard, making it the longest meteorological time series in the Arctic (Fig. 17) (Førland et al., 1997; Humlum et al., 2011). Temperature measurements at Longyearbyen Airport have been recorded since 1975, but by combining several series, composite time series for Longyearbyen reach back to 1898 (Nordli et al., 2014). The temperature record on Svalbard shows a rapid warming from 1917-1922 and lasting until 1955, before a cold period initiated and lasted until 1980-1990 (Fig. 17). Since then, renewed warming has taken place and the temperature on Svalbard has increased by 3-4°

(Humlum et al., 2011; Nordli et al., 2014). Summer average temperatures have only increased slightly (0.5-1°C), while winters have experienced a 3.5°C increase in average temperature at Longyearbyen Airport (Førland et al., 2011). The linear trend in air temperature from 1912-2010 increased by 0.23°-0.25° per decade, or 2.5°C during the last 100 years (Humlum et al., 2011; Førland et al., 2011). Since 2010, the MAAT has continued to increase at Longyearbyen Airport, and in 2016 the MAAT reached -0.1°C, the highest ever recorded (seklima.met.no, 2020). Both Førland et al. (2011) and Humlum et al. (2011) did future projections of annual temperature on Svalbard. However, they reach different conclusions. Førland et al. (2011) used downscaled global climate models forced with observed greenhouse gas emissions to suggest that the MAAT will continue to increase, and the warming rate up to year 2100 will be three times stronger than observed during the last 100 years. The warming from 1971-1990 to 2071-2100 equals 0.6°C per decade for annual temperatures, and 0.9°C per decade for the winter season. Humlum et al. (2011) used Fourier and wavelet analysis and suggested on the other hand that temperatures will be variable the next 20-25 years, but temperature will not generally increase.

In 2019, the annual precipitation at Longyearbyen airport was 167mm, which is below the recorded average of around 190mm (Førland et al., 2011). Compared to other meteorological stations, Longyearbyen receives significantly less precipitation, and represents the driest region on Svalbard (Humlum, 2002; Førland et al., 1997, 2011). Data from the surrounding meteorological stations suggests a significant vertical and horizontal precipitation gradient. The difficulty of measuring precipitation, especially solid precipitation, is already known (Legates & Willmott, 1990; Førland & Hanssen-Bauer, 2000; Humlum, 2002). Humlum (2002) compensated therefore the undercatch by using a 100% upward correction in modelling the late 20th century precipitation in central Svalbard. Humlum (2002) also accounted for a vertical precipitation gradient corrected by the upward correction of 15-20% per 100m along the coast and 5-10% in the central part. Large inter-annual differences in precipitation are common, and snow can fall even during summer (Dickson et al., 2000; Humlum, 2002). Changes in precipitation does not have the same trend as temperature the last decades. For the 1971-2017 period observations show a slight increase in precipitation, while modelled precipitation show a slight decrease. However, the changes are so small that it is statistically insignificant (Vikhamar-Schuler, 2019; Hanssen-Bauer et al., 2019). Rain-on-snow events has on the other hand increased in the winter months (October-April) in Longyearbyen the last decades (Vikhamar-Schuler et al., 2016).

3.2 Climate fluctuations on Svalbard since the last Ice Age and the implication for the avalanche environment

Younger Dryas marked the end of the Pleistocene period, and transitioned into the warmer Holocene period around 11.7 ka BP (Dansgaard et al., 1993). The Holocene is divided into three periods: Early (11.7-8.2 ka BP), Mid (8.2-4.2 ka BP) and Late (4.2 ka BP to present) Holocene (Fig. 18) (Wanner et al., 2011). During the Early and Mid-Holocene, glaciers on Svalbard retreated to, or beyond the extension we observe today, before re-advancing in Late Holocene (Fig. 18) (Svendsen & Mangerud, 1997; Ingólfsson & Landvik, 2013). However, the Holocene has been regarded as relatively stable (Steffensen et al., 2008; Rockström et al., 2009), but this view has been challenged (Bond et al., 2001; Wanner et al., 2011, Farnsworth, 2018). Glacial re-advances during Early and Late Holocene indicates that significant changes in climate have taken place.

Early Holocene marks the period with maximum summer insolation during the entire Holocene (Fig. 18) (Laskar et al., 2004), and the Svalbard-Barents Sea Ice Shelf (SBIS) had collapsed and retreated to the inner fjords (Mangerud et al., 1992). Radiocarbon dating of warm water shells suggests that sea temperatures were 2° -6° C warmer than today (Salvigsen et al., 1992; Blake, 2006; Mangerud & Svendsen, 2017). This continued into the Mid Holocene, to around 6.2 ka BP, only separated by a slight cooling event between 10.5-8.5 ka BP (van der Bilt et al, 2018). Present day ocean temperatures were not reached until the end of Mid Holocene (Mangerud & Svendsen, 2017). The high insolation is believed to be the main climatic forcing which caused a warmer climate (Zhang et al., 2016). The input of warm Atlantic water caused a further heating of the oceans (Mangerud & Svendsen, 2017). As the warmer climate caused glacial retreat during Early and Mid-Holocene, it is believed that the Holocene glacial minimum occurred during early-Mid Holocene, although little evidence constrains the spatial extent (Farnsworth, 2018). MAAT during Early and Mid-Holocene presumably ranged from 0 to -3°C at sea level, limiting permafrost (Humlum, 2005). Humlum (2005) suggested that permafrost during this period was absent or highly discontinuous near sea level, but continuous above 300-500 m a.s.l. From Mid Holocene, ocean temperature decreased along with summer insolation (Laskar et al., 2004; Skirbekk et al., 2010; Lacka et al., 2014). In the same period sea ice cover presumably increased (Müller & Stein, 2014).

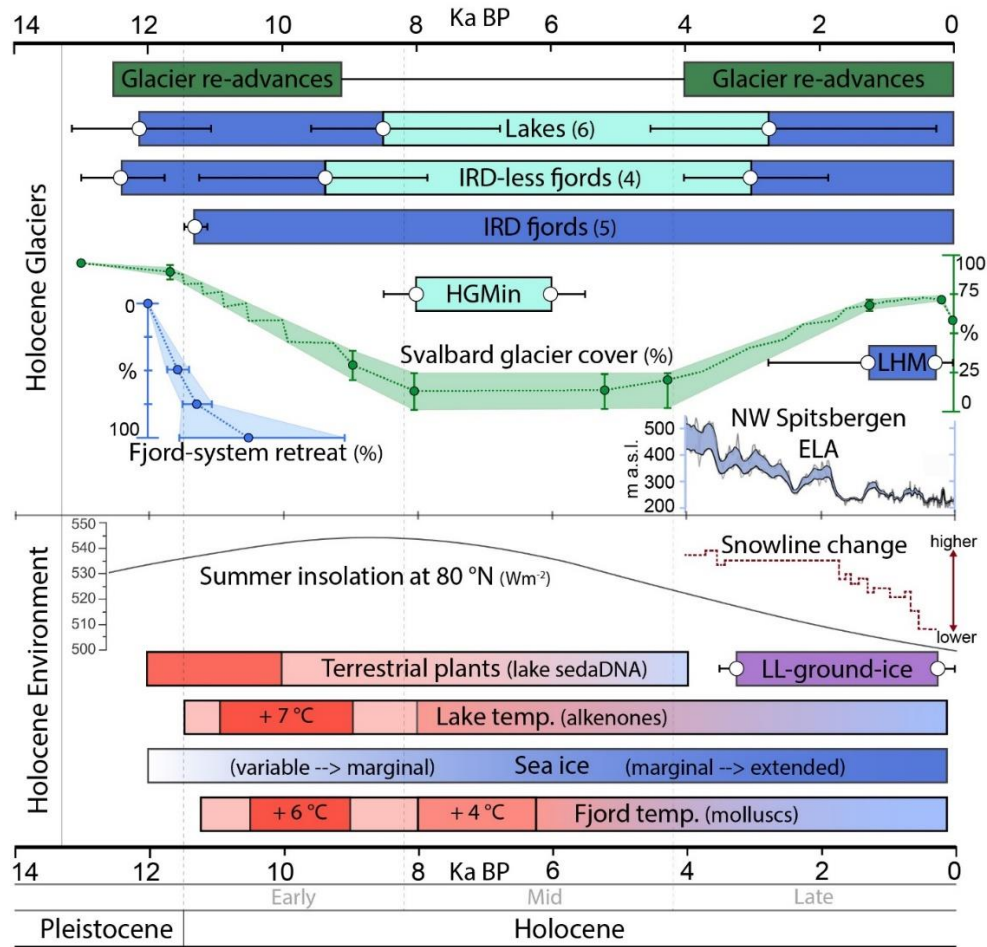


Figure 18. Timeline of Late Pleistocene and Holocene fluctuations (From Farnsworth et al., Oct. 2019 submitted).

Further cooling trend marks the onset of Late Holocene and decrease in ocean temperature (Werner et al., 2013) due to low summer insolation (Laskar et al., 2004) and volcanic activity (Miller et al., 2012). Simultaneous driftwood decrease has been interpreted as a result from persistent to semi-permanent land-fast ice. From 2.0 ka BP until present day driftwood occurrence started variably to increase, suggesting small spells of oceanic warming (Müller et al., 2012). Lichenometry studies of from Northwest Spitsbergen suggests that rock glacier formation started 3500 ka BP, at the beginning of Late Holocene (André, 1994). Glaciers re-advanced during the entire Late Holocene (Fig. 18) (Larsen et al., 2018, Farnsworth et al., 2017). D’Andrea et al. (2013) suggested that precipitation contributed to regional glacial advance during the Little Ice Age (LIA) (1250-1920) and that LIA was mild. Røthe et al. (2018) supports the idea of increased winter precipitation, and that the shift from cold and arid environment changed around 1750 years ago. While precipitation increase is argued as a greater contributor

than previously acknowledged, evidence shows that air and ocean temperatures also were cold and favoured glacial advancing during Late Holocene (Divine et al., 2011; van der Bilt et al., 2018). It is however unknown if climate (e.g. precipitation patterns) or glacier dynamics are the main factor of Holocene ice-front fluctuations (Farnsworth et al., 2018).

Precise precipitation changes during the Holocene remains largely unknown, as very few studies exist on the topic (Farnsworth, 2018). However, an interconnection between increasing temperatures, decreasing sea ice extent and increased precipitation is suggested from modern studies (Nowak & Hodson, 2013; Isaksen et al., 2016; Kopec et al., 2016). Leaf wax hydrogen isotopes from Hakluyvatnet in north western Svalbard indicated that warmer and wetter climate occurred from 12.8-7.5 ka BP. Between 7.5 – 5.0 ka BP a potential decrease in precipitation and desiccation of the lake explains the observed hiatus. While after 5.0 ka BP until 0.18 ka a progressive increase in polar air masses and colder temperatures occurred (Balascio et al., 2018). Farnsworth (2018) therefore argues that precipitation, at least during Early Holocene, likely had a large, but unquantifiable influence on regional hydroclimate and glacier mass balance. André (1995) related Holocene climate fluctuations and geomorphic impact of extreme events on Svalbard. Even though a link between frequency of extreme activity and climate fluctuations appeared difficult, André (1995) concluded that mass movements such as slush flows and debris flows were triggered by heavy rainfall during Late Holocene.

Palaeo-wind direction has received little attention by researchers, as only a handful of studies have touched upon the issue. Sessford et al (2015) reconstructed wind direction from beach ridges at Fredheim in Sassendalen, indicating that prevailing wind came from the southeast during the Holocene. Although not fully explained, Balascio et al. (2018) discussed that higher precipitation rates in north western Spitsbergen reflected mild air masses from the south and southwest. The study of avalanche-derived rock glaciers on the other hand could give an indication on palaeo-wind direction during the Holocene. Humlum et al (2007) argues that avalanche-derived rock glaciers are expected to exhibit a regional downwind preferred orientation during winter months. Applying the High Arctic nivation process-form-sediment model by Christiansen (1998) could additionally be used to reconstruct palaeo-wind direction and periods of snowdrift activity on Svalbard (Eckerstorfer, 2013).

3.3 Snow and Avalanche Climate on Svalbard

Snow climate describes the combination between meteorology and snowpack properties, e.g. snow depth, type of weak layer, ice content etc., which determines the frequency and nature of a regions avalanche activity (Armstrong & Armstrong, 1987; Mock & Birkeland, 2000). Three main snow climates have been identified: maritime, continental and transitional from work in the Rocky Mountains in western North America (Roch, 1949; LaChapelle, 1966; Hægeli & McClung, 2003; McClung & Schaerer, 2006). In addition, Sturm et al. (1995) proposed another classification system, including six classes: tundra, taiga, alpine, maritime, prairie and ephemeral.

However, in Svalbard's unique climatic setting none of these classifications fit. Eckerstorfer & Christiansen (2011a) expanded the snow climate classification, terming Svalbard's snow climate "The High Arctic maritime snow climate". On Svalbard, the snowpack lasts between 8-10 months and is relatively thin, hard, cold and underlain by continuous permafrost (Eckerstorfer & Christiansen, 2011a). Since precipitation is low, the dominant factor influencing snow distribution is wind. Slopes in certain aspects can even be snowless, while the opposite facing slope has an abundance of snow (Jaedicke, 2001). The thin snowpack allows for a strong temperature gradient, which is reflected by Eckerstorfer & Christiansen's (2011a) findings that over 80% of all snow pits contained depth hoar. This persistent weak layer last almost the entire season. The maritime influence comes from the West Spitsbergen Current. Warm water flows on the western side of Spitsbergen, making the region more temperate than other regions on the same latitude, causing less sea ice and higher MAAT (Førland et al., 1997). At the same time, Svalbard lies in the main North Atlantic cyclone track (Hanssen-Bauer et al., 1990), leading to high temperatures and rain-on-snow events or heavy snowfall, with occasional snow melting in mid-winter (Humlum et al., 2003). The combination between the two phenomena's makes air temperatures to fluctuate on a daily or weekly basis (Humlum, 2002). In effect, the maritime influence causes significant amounts of ice layers in the snowpack (Eckerstorfer & Christiansen, 2011a). Due to the large climatic variations on Svalbard (Førland et al., 1997), the classification only fits the mountain area around Longyearbyen (Eckerstorfer & Christiansen, 2011a).

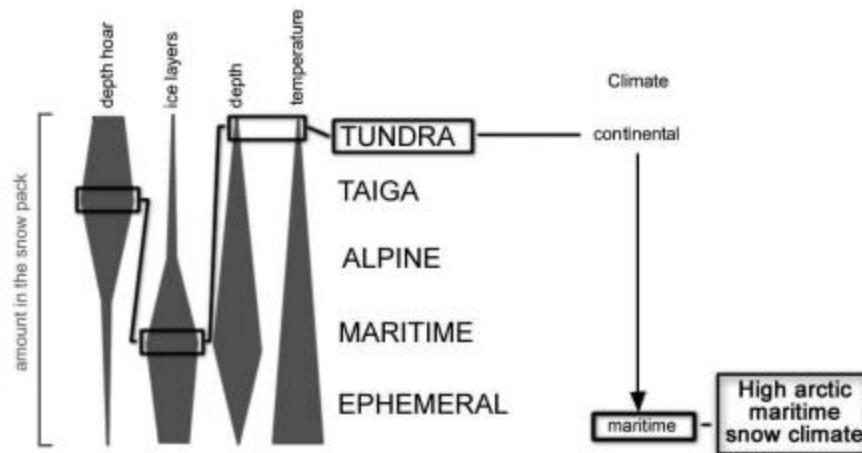


Figure 19. The High Arctic maritime snow climate presented by Eckerstorfer & Christiansen (2011a), based and modified from Sturm et al. (1995). The black boxes indicate the amount of the certain snowpack characteristics in the study area, compared to different snow climates.

The combination between topographical, meteorological and snowpack characteristics around Longyearbyen defines the avalanche activity (Eckerstorfer & Christiansen, 2011c). The prevailing south-easterly wind promotes snow accumulation and cornice accretion on west-north-westerly slopes and plateau edges. However, the channelling effect from topography somewhat disrupts this picture (Humlum, 2002). As a result, cornice fall avalanches are the most observed avalanche type, and slab avalanches the second most observed avalanche type (Eckerstorfer & Christiansen, 2011c). Hard wind slabs develop from the significant snowdrift in the region, which is typical for the snowpack on Svalbard. At the same time, ice lenses favour faceting around the crust and can serve as bed surface for slab avalanches (Eckerstorfer & Christiansen, 2011a). Mid-winter rain-on-snow events and spring melt also causes wet slab avalanche and slush avalanche release (Hestnes, 2000; Eckerstorfer & Christiansen 2012). Most avalanches releases during avalanche cycles, and Eckerstorfer & Christiansen (2011c) found that 80% of all observed avalanches released during these cycles between 2006 and 2009.

3.4 Geology and Physical Geography

The study areas lie inside the tertiary basin with predominantly flat oriented sedimentary rocks of Early Permian to Eocene age (Dallmann, 2015). The Tertiary bedrock mainly consists of the Van Mijenfjorden group of interchanging sandstone and shalestone beds, with some coal-bearing seams (Dallmann, 2015). The release areas for avalanches mainly consist of dark sandstones of the Grumantbyen and Hollendardalen formations and shales of the Basilika formation (Major et al., 2001). More resistant sandstones of the Firkanten formation underneath are responsible for the cliff noses which separate the different avalanche tracks. The weak sedimentary rocks are more exposed to weathering, and therefore erode more easily, increasing the sediment supply (Siewert et al., 2012; De Haas et al, 2015).

The topography is dominated by the characteristic plateau mountains and glacially eroded U-shaped valleys (Major, 2001). Most valleys in the study area are stretching north/northeast, making the dominant slope aspect east/northeast and west/southwest. The plateau mountains are generally around 450 m a.s.l. (Gruvefjellet meteorological station is at 465 m a.s.l.), but surrounding peaks reach above 800-1000 m a.s.l. (Nordenskiöldfjellet the highest at 1051 m a.s.l.). Although glaciers cover 60% of Svalbard (Hagen et al., 2003), the Nordenskiöld land has significant lesser glacial extent due to drier climate (Humlum 2002). Mostly small circle glaciers remain since deglaciation of the area around 10ka BP (Svendsen & Mangerud, 1997). The landscape is periglacial, and Svalbard is underlain by continuous permafrost, ranging from less than 100m near to coast to 500m in alpine area, and high vegetation is non-existent (Humlum et al., 2003). The landscape is characterized by steep concave slopes up to 55°, fluvially eroded gorges and river plains leading into the U-shaped valleys (Christiansen et al., 2013). Mountain slopes mainly consists of weathered material (Sorbel et al., 2001). Slope processes such as debris flows, solifluction, avalanches and rockfalls dominate the landscape and transport the weathered material downslope (Larsson, 1982; Humlum et al., 2007; Harris et al., 2011; Eckerstorfer et al., 2013a). The impact of avalanches is profound on the landscape as slopes beneath the plateau mountains has extensive spatial distribution of avalanche fans. Some of which has evolved into a rock glacier (Humlum et al., 2007).

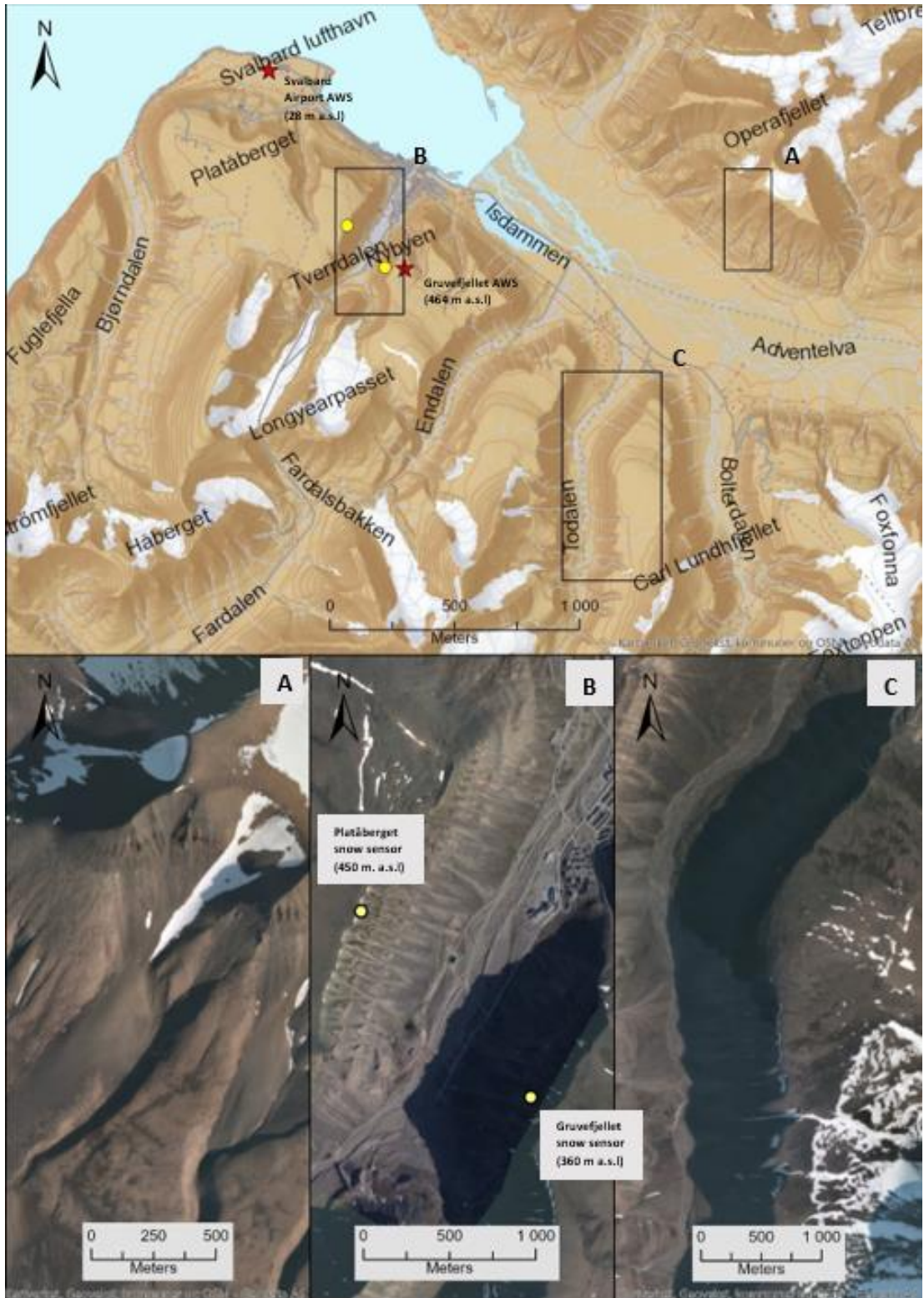


Figure 20. Overview map of the study areas in (A) Adventdalen, (B) Longyeardalen and (C) Todalen. Meteorological stations used in this thesis is marked with a red star, and snow depth sensors placed at Gruvefjellet and Platåberget are marked with yellow circle.

3.4.1 Longyeardalen

Longyeardalen is a glaciated U-shaped valley where the main settlement Longyearbyen is located (Fig. 20b). The valley is 4 km long and SSW-NNE oriented with plateau mountains of Gruvefjellet on the east and Platåberget on the west side. Release areas for avalanches lie between 300 – 470 m a.s.l. Avalanche fans are located on both sides of the valley from roughly 280 – 70 m a.s.l. Gruvefjellet slope consist of a 50-70m vertical drop from the plateau margin down to a 40-50° slope which acts as release area for slab avalanches. The release areas lead into couloirs between the rock noses and opens on the avalanche fans further down (Eckerstorfer et al., 2013a). Platåberget has similar morphology but lacks the vertical cliff. From the plateau, a 45-55° release area leads into the couloirs (Hancock et al., 2020). Large cornices develop on the plateau edges during winter and annually trigger avalanches when they collapse (Hancock et al., 2020). Debris flows and solifluction are active processes reshaping the avalanche fans (De Haas et al., 2015), while mining activity has modified parts of the slope systems on both sides of the valley.

3.4.2 Todalen

Todalen is located 7 km SE of Longyearbyen and is a U-shaped tributary valley to Adventdalen (Fig. 20c, Fig. 21). The inner part of Todalen has a N-S orientation, while the outer part is NE-SW oriented. Todalen has extensive avalanche fan distribution on both sides of the valley (Fig. 21) (Rubensdotter et al., 2015b). On the east side, glacially fed river has partly eroded some avalanche fans. Release areas for avalanches on the eastern side lie between roughly 300-400 m a.s.l for outer Todalen, and 400-500 m a.s.l for inner Todalen. Mean slope angle in the release areas are between 30-50°. Except for a large coal mine at the entrance of Todalen, only four locations have anthropogenic material from mining activity on the eastern slope (Fig. 21). Two rock glaciers are located on the western slope, and one rock glacier is located on the eastern slope in Todalen (Fig. 21). Todalen is known to release multiple avalanches every year and is a common snow mobile route during the winter (Eckerstorfer, 2012).

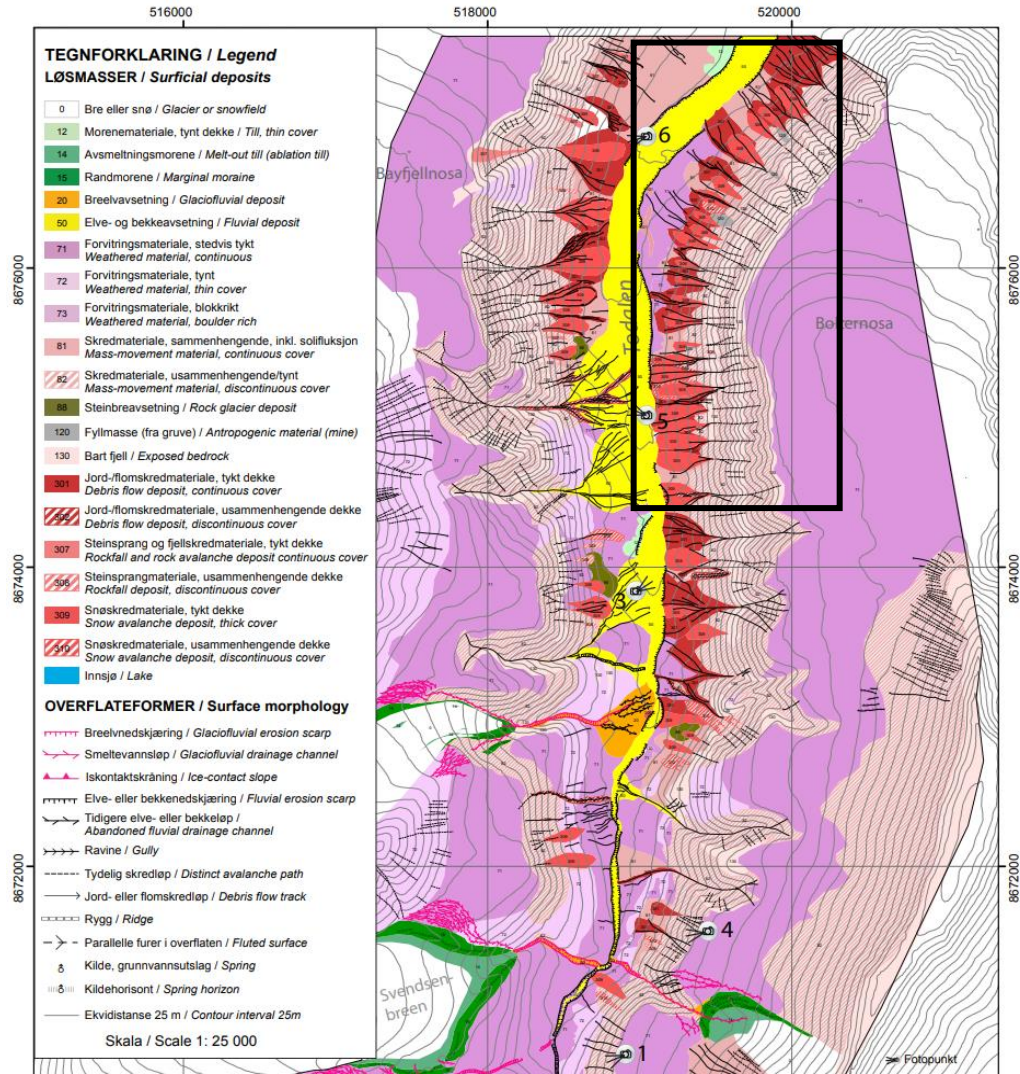


Figure 21. Landform and sediment map of Adventdalen. Black box indicates the study area in this thesis (modified from Rubensdotter et al., 2015b)

3.4.3 Adventdalen

Adventdalen is oriented NE-SW and is a large U-shaped valley which drains into Adventfjorden (Fig 20a). Adventdalen has less avalanche fan distribution compared to opposite valleys with large plateau mountains. The avalanche fan of interest in Adventdalen is located 7 km from Longyearbyen, facing towards the SSW. The release area has a slope angle between 30-45° and lie between 650-850 m a.s.l, while the avalanche fan reaches from 400 m a.s.l down to roughly 175 m a.s.l. The avalanche fan is fed by two source areas, one significantly larger than the other. Periglacial processes are active the toe of the fan, while debris flows are confined to the sides. The avalanche fan in Adventdalen will also be referred to as only “Adventdalen”.

Chapter 4. Fieldwork and Methods

Note

In order to investigate present avalanche conditions and processes in relation to past and present-day avalanche fan development, both wintertime (avalanche season) and snow-free fieldwork was planned. In September 2019, avalanche deposits were mapped in Todalen. Fieldwork was also planned in Adventdalen and Bjørndalen, but weather conditions made it impossible. Close to one thousand drone pictures from Todalen, Adventdalen, and Bjørndalen were taken during the September 2019 field campaign, to create snow free DEMS using SfM (Structure from Motion). This procedure was originally intended to be repeated during winter, such that snow depth distribution in release areas in multiple aspects could be identified. Unfortunately, the winter season of 2020 proved to be difficult from both avalanche monitoring and public health perspectives. Winter conditions in 2020 were dry and cold with little precipitation, meaning that no avalanches released in Todalen or any surrounding valleys of similar character. Once COVID-19 announced its arrival in Norway in early March, all possibilities for fieldwork and access to the university (UNIS) were eliminated. As such, the intended winter fieldwork for this master's thesis was cancelled, and in effect, the drone pictures were never used. The winter fieldwork would have included scanning fresh avalanche deposits using a terrestrial laser scanner (TLS) and digging snow pits and recording snow characteristics such as temperature, density, and weak layers, each week and before and after storms. The data collected in the field during the winter was planned as input in the dynamical avalanche modelling software RAMMS: Avalanche (Rapid Mass Movement Simulations).

4.1 Workflow

Figure 22 illustrates the conceptual workflow for data collection and processing. Step 1 in figure 22 involves the field work and data processing which laid the foundation for step 2: reconstructing recent and historical avalanche runouts in RAMMS. Extreme precipitation and meteorological analysis were conducted independently for later comparison with modelling results and discussion.

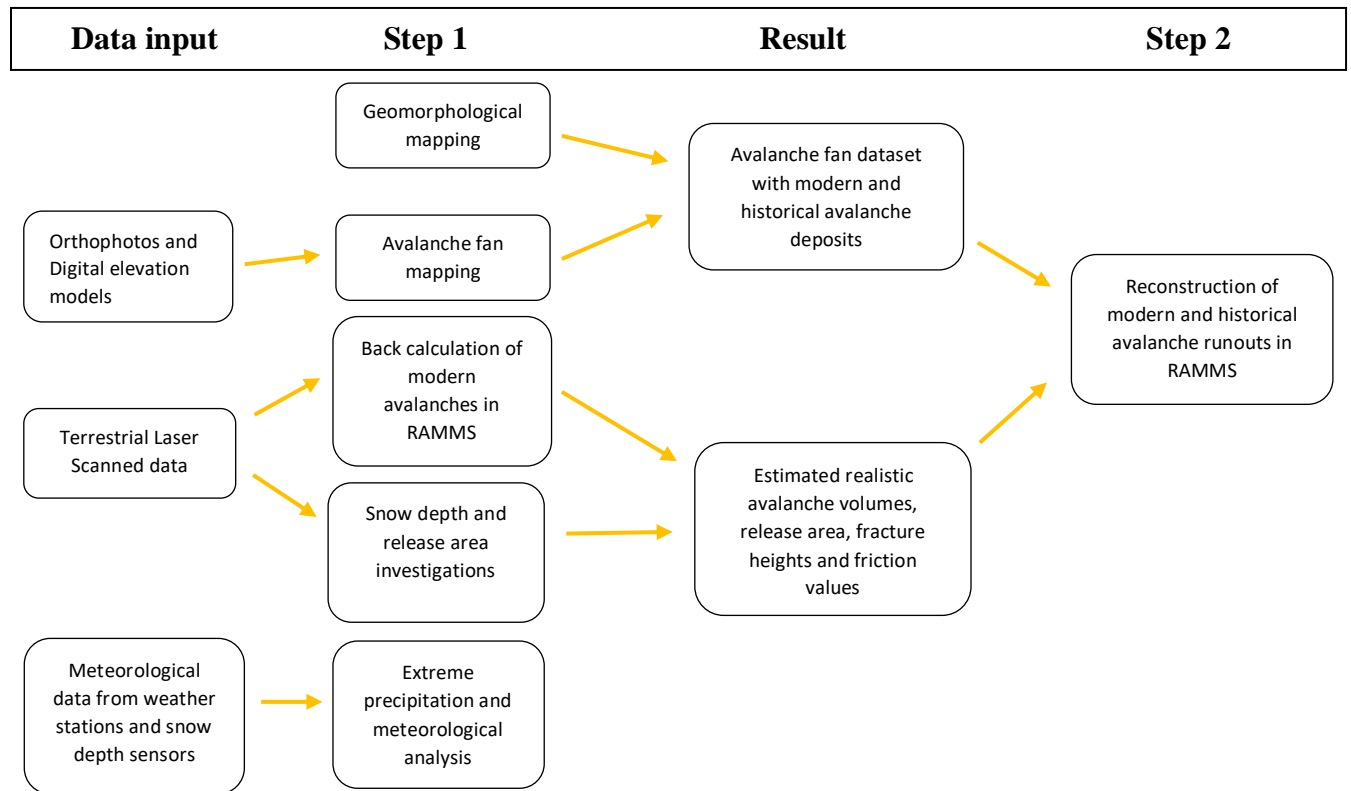


Figure 22. Conceptual workflow for data processing and collection leading up to the reconstruction of modern and historical avalanche runouts in RAMMS.

4.2 Geomorphological mapping

Geomorphological mapping of avalanche fans in the field was conducted between 02.09.2019 and 11.09.2019 with Lena Rubensdotter from the Norwegian Geological Survey (NGU), participating the first two days. Marianne Bredesen participated the remaining days, acting as polar bear guard. Todalen and Adventdalen were chosen as field sites for the geomorphological mapping. Todalen exhibits extensive avalanche fan distribution on both valley sides and is easily accessible from town with a car (Fig. 20c, Fig. 21). Adventdalen (Fig. 20a) was chosen because of a large south-west facing avalanche fan with a visually distinct transition from recent to historical deposits. Due to challenging weather and a polar bear close to town, only the east side of Todalen was mapped. Early snowfall in September partly covered the avalanche fans, consequently making mapping more challenging.

The purpose of the fieldwork was to investigate the avalanche fans, mapping recent and historical avalanche deposits. GPS points on the margins of the historical and recent deposits

were directly plotted into ArcMap installed on a Toughbook. Camera and field notebook were used to take pictures of the deposits and note down observations. Avalanche deposits have previously been described, and the same morphological features were identified in the field to verify avalanche activity and deposition (table 2).

Table 2. Morphological features which are caused by avalanches.

Feature	Description
Perched boulder/cobble	Small rocks lying on top of larger rocks. From melt-out process from an avalanche. Rocks can be balancing on the edge of other rocks or may be stacked on top of each other (Fig. 12h)
Debris tail	Cluster of debris located downslope of an obstacle where erosion is preserved (Fig. 12d).
Debris horn	Cluster of debris located upslope of an obstacle due to plastic freezing of avalanche rich sediments (Fig. 12f)
Re-deposited sediments	Weathered rock with fragment broken off, exposing a fresh surface. Fragment breaks off during re-deposition by a recent avalanche when it collides with other rocks (Fig. 31f)

Each fan was investigated either starting from the toe of the fan and walking up slope, or starting higher up and stopping at the toe. Two GPS points were registered per avalanche fan: One point registered for the recent deposits and one point registered for the historical deposits. Recently deposited sediments were identified according to lichen growth on the surface of the fan debris and imprinting on the underlying rocks. After deposition, lichen starts growing on the surface of the rock. Lichen growth is slow, and it takes several years for growth to begin on the surface (Werner, 1990). If no lichen was observed on the rock debris, it was considered recently deposited. After fan deposition, the underlying surface which the deposited sediment is resting on is shielded from weathering. Over time, the shielding results in a lighter-coloured imprint where little to no lichen growth takes place. If rocks with no lichen had left an imprint on the underlying rock, they were considered historical deposits. Only avalanche deposits with no lichen and no imprint were considered recently deposited and registered with a GPS point.

Historical fan deposits are characterized by lichen growing on the surface of the rock debris. They were mapped at the toe of the fan. Periglacial processes such as frost heave and solifluction can transport deposited sediments downslope post-deposition. Careful investigation of the surface was done to ensure that the historical deposits were not significantly affected by periglacial process. Several fans were affected by debris flows and mapping close to the debris flow tracks was avoided.

4.3 Avalanche fan mapping

Avalanche fan mapping of the valleys surrounding Longyearbyen in ArcGIS PRO was part of an earlier, unrelated project that ultimately lead to the idea for this thesis. The complete dataset is not presented, since it is beyond the scope of this thesis. For this study, all avalanche fans within the selected study areas were mapped in ArcGIS PRO in greater detail, improving the quality of the existing dataset.

Orthophotos and digital elevation models (DEM), using the coordinate system ETRS 1989 UTM Zone 33N from the Norwegian Polar Institute was used as basis for the manual mapping. A significant number of fans on Svalbard are affected by both fluvial flow and debris flow (De Haas et al., 2015). Only fans where avalanches were interpreted to be the dominating factor were included in the digital mapping process. The east-facing slopes in Longyeardalen and Todalen are covered by shade in the orthophotos, making the extent of the fans difficult to map accurately (fig 20b, c). Hillshades were created from the DEMs to assist in identifying fans where shadows in the orthophotos prevented accurate mapping. Each fan was mapped with a polygon representing the entire area of the fan, and a second polygon representing the extension of recently deposited sediments. The extent of the recently deposited sediments was determined by using the orthophotos to identify the boundary between light-coloured sediments and dark-coloured sediments. The GPS points from the field campaign in September 2019 were imported and coupled with the avalanche mapping dataset. Where mapping of recently deposited sediments had been unsuccessful due to shadows, the GPS points were used to help constrain the margins of the recently deposited sediments. This is the case for almost all avalanche fans in Todalen where fieldwork was conducted.

Based on the avalanche mapping and fieldwork, a selection of avalanche fans for the avalanche modelling was made. The inner part of Todalen exhibits large avalanche fans, but the river has cut into some of the fans. Since the entire extent of some of the fans are unknown, they were not included for the modelling. The avalanche fans in the outer part of Todalen are not affected by the river and were therefore chosen for the avalanche modelling.

4.4 Terrestrial Laser Scanning (TLS)

Lidar (light detection and ranging) is an active remote sensing tool which allows for data acquisition of surfaces with high spatial resolution in rough and forested terrain (Lefsky et al., 2002; Deems et al., 2013). Data collection with Lidar is either from airborne (ALS) or ground based instruments (TLS) (Deems et al., 2013). A Terrestrial Laser Scanner (TLS) sends out a laser pulse, which measures the distance from the scanner to the target surface based on time-of-flight principle (Deems et al., 2013). Impenetrable obstacles such as large rocks, can block the scan pulse, and scan shadows emerge with no data behind the feature (Prokop et al., 2015). When the position of the scanner is known, it is possible to detect the absolute position of each individual scan point with x,y,z coordinates (Rees, 2005). Terrestrial Laser Scanners remove the hazard of going into dangerous or inaccessible areas, for example, avalanche prone terrain or rugged alpine terrain because the TLS can be used several hundred meters to a few kilometres away from its target (Prokop, 2008). In recent years, TLS has become a popular tool in snow and avalanche science (Prokop, 2008; Prokop et al., 2008; Prokop, 2009; Deems et al., 2013; Vionnet et al., 2014; Schön et al., 2015; Deems et al., 2015; Hancock et al., 2018; Hancock et al., 2020). An in-depth review of lidar-technology and snow measurements is summarized by Deems et al (2013) and TLS use in snow science by Prokop (2008), and won't be elaborated further here.

4.4.1 TLS data processing

Terrestrial Laser Scanner (TLS) data used in this thesis was originally collected with a Riegl Laser Measurement Systems VZ-6000 ultra-long-range terrestrial laser scanner by PhD student Holt Hancock at the University Center on Svalbard (UNIS). The dataset included 25 scans from Gruvefjellet and 22 scans of Platåberget during the 2016-2017 and 2017-2018 winter season. At both Gruvefjellet and Platåberget, a snow-free surface scan was taken on during September 16th, 2016. The data was prepared in RiSCAN Pro, and ground control points were acquired with

dGPS used to georeference the point cloud data. Ground control points and “Multi-Station Adjustment” were used to align the snow-covered scans to the snow-free scan from 2016. An octree filter with 0.1m increment was applied and exported as an XYZ text file (Hancock et al., 2020). The XYZ files was then imported into ArcGIS PRO, with each file containing a few million points. A geoprocessing model (Fig. 23) was created to iterate through all XYZ .txt files. The output for each .txt file was a natural neighbour interpolation with cell size of 10x10 cm and a hillshade stored in a geodatabase.

Creating a DEM for the purpose of making snow depth measurements has some inherent challenges. Interpolating between points means potentially inducing errors depending on terrain surface complexity and point spacing (Deems et al., 2013). However, the accuracy of the interpolation is determined by the resolution (Prokop, 2008).

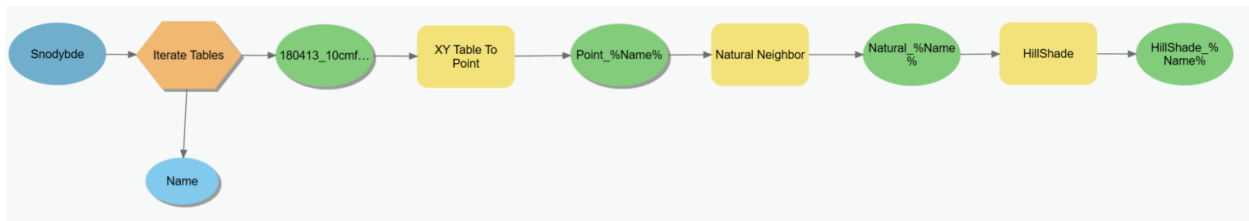


Figure 23. Geoprocessing model in ArcGIS PRO to iterate through TLS data from Gruvefjellet and Platåberget. Output of the model is a XY point file, natural neighbour interpolation and hillshade for each scan.

The output DEMs from the geoprocessing model were used for two purposes: (1) mapping maximum snow depth in the release areas at Gruvefjellet and Platåberget for the two winter seasons; and (2) investigating four avalanche cycles which released multiple avalanches during the same two winter seasons. Volume calculations of the avalanches, release, and runout area would later be used for back-calculations in RAMMS.

4.4.2 DEM calculations

The distribution of snow depth in avalanche release areas are strongly linked with avalanche potential and character (Schweizer et al., 2003). TLS mapping of snow distribution and snow depth in the release area can give important information on differential loading due to precipitation and wind loading events (Deems et al., 2015). Snow depth mapping involved subtracting a snow-free surface from a snow-covered surface. Additionally, snow depth changes can be mapped by subtracting a snow-covered surface with another snow-covered surface, obtained at two different periods within the same snow season. The maximum snow depths are

based on a bare-ground scans from September 2016 and snow-covered scans from 25.04.2017 and 13.04.2018, when snow cover is around its maximum (Eckerstorfer & Christiansen, 2011c). The scans are only based on two snow seasons and are therefore not representative of longer timescales. The Raster minus tool in ArcGIS PRO was used the bare-ground and snow-covered scans to visualize the snow depth changes in the release areas.

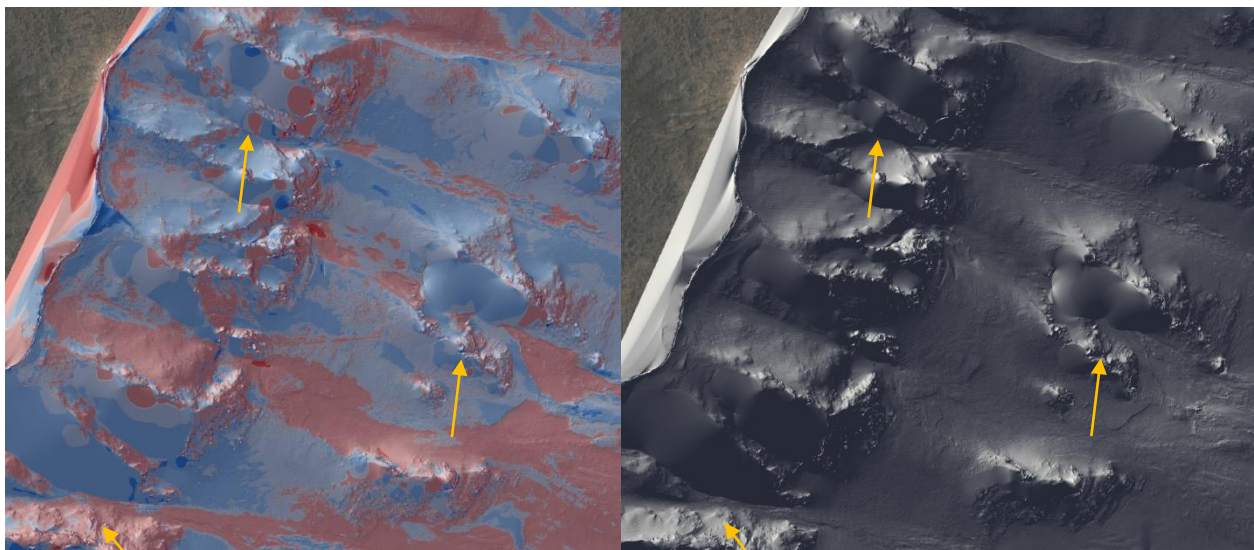


Figure 24: Raster minus calculation and hillshade of the same release area shows scan shadows in the dataset. Yellow arrows indicate three examples of scan shadows in the dataset.

Dynamic avalanche modelling (described below) relies heavily on input parameters such as release area and volumes of snow in the starting zone, which is determined by the fracture height (Sovilla & Bartelt, 2002; Gruber & Bartelt, 2007; Sovilla et al., 2007.) Comparing two different snow surfaces (pre-avalanche scan and post-avalanche scan), allows for identification of avalanche dimensions and retrieving of parameters for dynamic avalanche modelling (Prokop et al., 2015). The Raster minus tool was used to visualize changes in snow depth between the pre-avalanche scan and the post-avalanche scan. Overlain by a hillshade, the avalanche deposits were mapped. The “Cut Fill” tool in ArcGIS PRO was used for volume calculation of the deposited mass. Release areas were drawn based on changes in snow depth. However, scan shadows prevented accurate mapping (Fig. 24). Neither release area nor fracture height could be determined in a way that represented the actual event. Nevertheless, release areas were drawn combining all available data and general avalanche release theory.

4.5 Dynamical Avalanche Modelling

RAMMS: Avalanche (Rapid Mass Movements Simulations) is a two-dimensional numerical simulation program which calculates the motion of snow avalanches on a three-dimensional terrain. RAMMS is developed towards hazard mapping and planning by the WSL Institute for Snow and Avalanche Research SLF. The model is calibrated to observed avalanches at the Vallée de la Sionne test site in Switzerland (Bartelt et al., 2017). The basic input data is a DEM, release area information, forest extent, and maps/orthophoto. RAMMS has been applied to a variety of scientific and practical problems, including back-calculation of observed avalanches. Avalanche modelling has been primarily concerned about with avalanches and the return periods. To the author's knowledge, no scientific articles have considered the differences in past climate and avalanche release over long periods using dynamical avalanche modelling results.

4.5.1 Physical friction model

RAMMS is based on the Voellmy-Salm (VS) model (Salm et al., 1990; Salm, 1993) which is used in Switzerland for avalanche runout calculations (Christen et al., 2010). The VS model is split into two parts. The dry-Coulomb friction (coefficient μ) that scales with the normal stress and the viscous-turbulent friction (coefficient ξ). The frictional resistance S (Pa) is then:

$$S = \mu N + \frac{\rho g u^2}{\xi} \quad \text{with} \quad N = \rho h g \cos(\phi)$$

where ρ is the density, g the gravitational acceleration, ϕ the slope angle, h the flow height and u the vector $u = (u_x, u_y)^T$, consisting of the avalanche velocity in the x- and y-directions. The normal stress on the running surface, $\rho h g \cos(\phi)$, can be summarized in a single parameter N . The friction coefficients determine the behavior of the flow. Coefficient μ dominates when the avalanche is close to stopping, and coefficient ξ dominates when the avalanche is running quickly (Bartelt et al., 2017).

The VS preforms well in modelling flow heights and velocity in the front of the avalanche. However, it falls short in modelling evolution of velocity over the entire length of the avalanche, and works poorly with snow entrainment (Christen et al., 2010). Therefore, the random kinetic energy (RKE) model is implemented to couple the VS model to the random kinetic energy of the

avalanche. The RKE model accounts for the random motion and inelastic interaction between snow granules within an avalanche. This allows for better prediction of the distribution of avalanche deposits, volume increase and velocity (Christen et al., 2010).

The cohesive bonding determines the interaction between grains in the flowing avalanche, and thereby the flow regime (Issler & Gauer, 2008; Bartelt & Mcardell, 2009). Dry snow avalanches are considered non-cohesive and display dispersive granular flow compared to wet snow avalanches, which have a pronounced cohesive, visco-plastic type flow (Bartelt et al., 2015). Cohesion has previously not been included in RAMMS, which was problematic because the avalanche flow often diffused with low velocity and flow height, adding 10s of meters in avalanche width and runout (Bühler et al., 2014). This changed recently when Bartelt et al (2015) included a cohesion parameter into the model. Bartelt et al (2015) showed that the cohesion parameter strongly impacted avalanche flow and runout behaviour, by reducing runout distance with increasing cohesion. In RAMMS cohesion is treated as (1) additional potential energy that must be overcome to pull-apart and break cohesive bonding between snow granules and (2) a normal stress independent shear stress that modifies the Coulomb friction (Bühler et al., 2014). The new equation for the frictional resistance S is then:

$$S = \mu N + \frac{\rho g u^2}{\xi} + (1 - \mu)N_0 - (1 - \mu)N_0 e^{-\frac{N}{N_0}}$$

where N_0 is the yield stress (cohesion) of the flowing material. Unlike a standard Mohr-Coulomb type relation this formula ensures that $S \rightarrow 0$ when both $N \rightarrow 0$ and $U \rightarrow 0$. It increases the shear stress and therefore causes the avalanche to stop earlier, depending on the value of N_0 (Bartelt et al., 2017). Table 3 shows the suggested cohesion parameters in RAMMS for dry and wet snow avalanches.

Avalanche type	Cohesion [Pa]
Dry	0-100
Wet	100-300

Table 3. snow cohesion parameters for dry and wet snow avalanches, as proposed by Bühler et al. (2014)

4.5.2 Topographic data

A clipped DEM (5x5m) of Adventdalen, Todalen and Longyeardalen was converted to ASCII in ArcGIS PRO and imported into RAMMS. The DEM is the most important input requirement, and the resolution has a large impact on modelling results (Bartelt et al., 2017). In complex terrain, a low resolution can lead to inaccurate representation of topographic features such as gullies and ridges. Snow cover small topographic features, and very high resolution (<2m) may not represent the snow-covered terrain (Bühler et al., 2011). High resolution DEMs can be smoothed to account for winter conditions (Maggioni et al., 2013). Smoothing was not done for the selected DEM in this study because the resolution was considered to be representative for a snow-covered terrain. In general, a resolution of 25 meters is sufficient for modelling large scale dry and wet snow avalanches (Bühler et al., 2011).

4.5.3 Release information and orthophotos

All study areas were saved and separated into different project folders containing the additional requirements: orthophoto and release areas. Orthophotos was converted to GEOTIFF-format in ArcGIS PRO. The orthophotos contained the boundaries for recent and historical avalanche deposits. In all study areas, model simulations were run until the output matched the mapped deposits.

In RAMMS, release areas were either imported as shapefile from GIS or manually drawn in the program. Release areas were drawn manually in ArcGIS PRO using a combination of several raster datasets. Aspect was calculated to visualize orientation of the topography. A slope raster was used to illustrate the slope gradient. The slope dataset was reclassified to 30-55 degrees based on slab avalanche release. Hillshades was produced from DEMs to illustrate the topography, especially in shaded areas. The rasters was combined with orthophotos to accurately map the release areas. The resulting polygon shapefiles of the release areas was later imported into RAMMS. The size and shape of release areas have large impact on modelling results (Christen et al., 2010). Inaccurate drawing of the release area can result in different avalanche flow paths than observed (Dreier et al., 2014). Release areas was drawn based on two principles: (1) That most of the potential release area failed, and (2) that a significantly smaller area failed. Failure propagation over the entire release area normally applies for large avalanches with higher return periods under very unstable conditions, while smaller and frequent avalanches tend to be

more restricted under more “normal” conditions (Schmid & Sardemann, 2003; Veitinger & Sovilla, 2016). Multiple release areas were drawn for each fan, representing different release scenarios. Forest information was not included, since Svalbard has no trees. The definitions of release areas and fracture height have a strong impact on the results (Bartelt et al., 2017). RAMMS calculates the volume of the released mass by multiplying the size of the release area with the fracture height. RAMMS takes a simplistic approach, assuming that snow distribution is equal over the entire release area, and no variation in snow depth is considered. Fracture height was adjusted between each simulation until “best-fit” was achieved.

4.5.4 Friction parameters

The coefficient μ and coefficient ξ can be set to either constant or variable when running the RAMMS calculation. Running a calculation with constant friction values, the same values are applied over the entire calculation domain; neither terrain undulations nor forest is considered.

The recommendation is to use the variable friction values. RAMMS automatically classifies the friction values over the domain based on GIS-based DEM analysis, forest information and global parameters (Bartelt et al., 2017). Different friction values are then applied to five different categories: open slope, flat terrain, channelled, gully or forested.

Modelling avalanches at different elevations and potentially with high vertical distance involves flowing through altitudes with different snow properties. Altitude limits are part of the DEM analysis, and assigns different friction values at different elevations. The default limits are set to 1500/1000 m a.s.l. which is based on the Swiss calibrations. These are not necessarily representative for a snow climate such as Svalbard. Figure 25 shows an example of friction parameters used in RAMMS. Friction values has been independently adjusted to fit the snow climate on

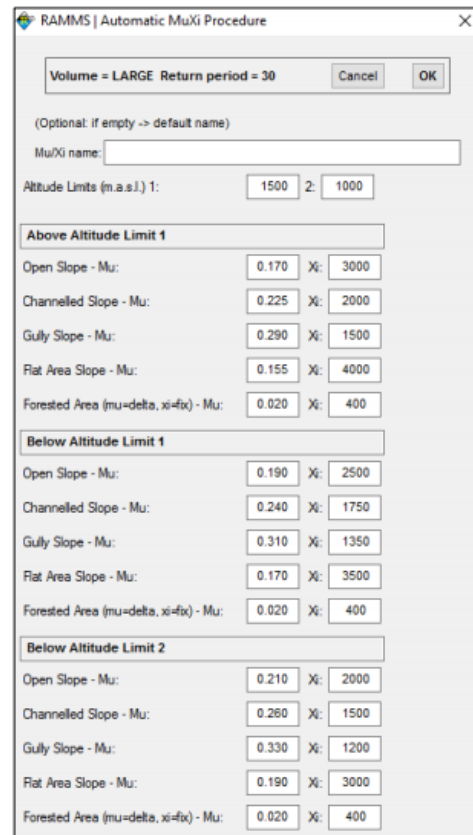


Figure 25: Example of friction values at different altitudes in RAMMS based on Large volume and return period of 30 years (Bartelt et al., 2017)

Svalbard, based on back calculations of observed avalanches (Eiken, 2017). However, Eiken's friction values were not adjusted for all terrain categories. Due to complex terrain and multiple terrain categories in the study areas, it was considered too risky to manually adjust friction values for all categories.

Back calculating the observed avalanches in Longyeardalen served as basis for determining the altitude limits, and thus the friction values. The results would be used as input for the modelling in Todalen and Adventdalen. Three different altitude limits were tested: default (1500/1000 m a.s.l), 150/50 m a.s.l and 50/10 m a.s.l. The latter two are based on RAMMS modelling by NVE and NGI of the 2015 and 2017 avalanche at Sukkertoppen (NVE, 2018). The altitude difference in the study areas are in range of around 450 to 70 m a.s.l in Longyeardalen, 400 to 60 m a.s.l in Todalen and 850 to 130 m a.s.l in Adventdalen. The altitude limits proposed by NGI and NVE implies a lower friction value compared to the default value proposed by RAMMS. Altitude limits was the same for modelling dry and wet slab avalanches.

Global parameters (volume and return period of the avalanche) affects the friction parameters, because avalanches of different sizes and return periods behaves differently (Bartelt et al., 2017). Global parameters had to be assigned before defining the friction values μ and ξ (Fig. 26). Global parameters were set to 10 years return period for all simulations. Default volume category was automatically based on volume of the individual release areas.

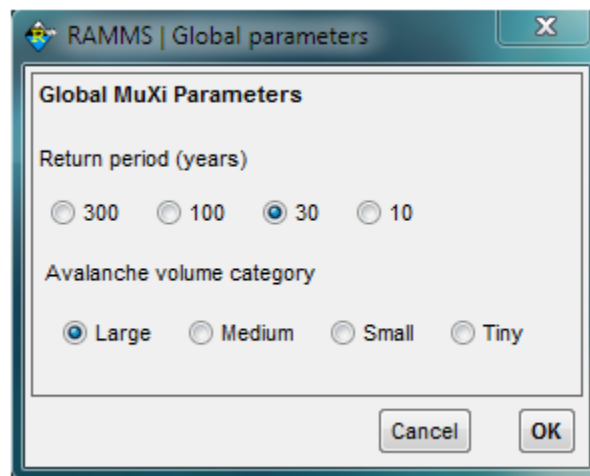


Figure 26: Overview of global parameters. Volume was automatically classified based on volume in the release area. Return period for all avalanches was set to 10 years (Figure from Bartelt et al., 2017)

4.5.5 Snow density and cohesion

Snow density was set to 375 kg/m^3 based on Winther et al. (2003) and Eckerstorfer & Christiansen (2011a) for dry slab avalanches. Density for wet slab avalanches are considered higher, but no real measurements are found in literature from Svalbard. Snow density was therefore set to 450 kg/m^3 . Snow density mainly affects the avalanche pressure, which is not the focus of this thesis.

Cohesion is a powerful parameter which decreases runout distance and flow separation with increasing value. Back calculating the avalanches in Longyeardalen served to find a fitting cohesion parameter for dry and wet slab avalanches. Cohesion was adjusted in the range of 0-100 for dry slab avalanches and 100-300 for wet slab avalanches. The resulting cohesion parameters was used for avalanche modelling in Todalen and Adventdalen.

4.5.6 Simulation output

Avalanche simulation initiated when all parameters and input data were defined. Once the simulation was finished, the modelled runout was inspected. If the results didn't fit the mapped deposits, the fracture height was adjusted to change the release volume. Numerous attempts were made to fine tune the fracture height and volume to match the mapped deposits.

Simulation output shows the flowing avalanche over the three-dimensional terrain. Maximum flow height, pressure and velocity over the entire avalanche domain can be visualized and imported into GIS. Maximum flow height and velocity was imported into GIS, as these two had the furthest runout.

For back calculating avalanches in Longyeardalen, simulation output was three separate scenarios with the applied altitude limits described above. The scenarios were run for both dry slab avalanche and wet slab avalanche. Altitude limit, cohesion, density, volume and fracture height values was registered in a table for comparison. Based on the results of the back-calculation, only one altitude limit and one cohesion value for each avalanche type was applied to dry slab and wet slab modelling in Adventdalen and Todalen. Altitude limit, cohesion, density, volume and fracture height was registered in a table for comparison. The simulation was run twice. The first reaching the recently deposited sediments, and the second reaching the historical deposits.

4.6 Extreme precipitation analysis and Automated snow and weather data

In avalanche hazard mapping, it is common practice to use extreme value analysis of the 1 and 3-day precipitation sum, including snow drift potential to estimate fracture heights for high return periods (Salm et al., 1990). Nevertheless, a common problem are large uncertainties due to short precipitation series, and extrapolation of large return periods such as 1000 and 5000 years (Katz et al., 2002). For this study, the 1 and 3-day precipitation sum was calculated focusing on return periods between 1 and 10 years. Comparison was made between the precipitation values and the modelled fracture height to determine if the modelled results were realistic. A 10% snow increase per 100m (Humlum, 2002) was added to the precipitation value according to the altitude of the release areas. Wind drift was not accounted for since there are no guidelines for accurately determining additional wind drifted snow.

Precipitation data from Svalbard Airport 99840 located ca. 5 km northeast of Longyearbyen, 28 m a.s.l (1975-2020, 45 years) and Longyearbyen 99860 (1911-1977, 66 years) was combined and collected from eklima.met.no. The weather station in Longyearbyen was located at Skjæringa before it was relocated to the new airport in 1975. Precipitation data must be viewed with care, as there are large differences in local precipitation and undercatch of the precipitation gauge (Humlum, 2002). Precipitation was analysed for the winter months, defined as January, February, March, April, May, November and December. During this period the ground is snow covered and precipitation normally comes as snow. Extreme value analysis was based on NVE guidelines, which uses the Bayesian approach and generalized extreme value (GEV) shape parameter (NVE, 2014). The values were computed in R statistical software version 3.6.3, using “Trond Reitan’s R-Script” (NVE, 2014).

To evaluate snow depths and contributing factors to snow accumulation in release areas, data was gathered from a pair of ultrasonic snow depth sensors and meteorological data from Gruvefjellet automated weather station (AWS) and Longyearbyen Airport AWS. Data was analysed both on the hourly and daily average scale. The snow sensors have been active since 17.11.2017, and been monitoring snow depth changes in the release areas at Lia, Gruvefjellet and Platåberget (Prokop et al., 2018). Data is transmitted 4 times a day and is available on the internet (<http://snow.unis.no/data.php>). For this analysis, snow depth data from Gruvefjellet (350

m a.s.l) (Fig. 20b, Fig. 27a) and Platåberget (450 m a.s.l) (Fig 20b, Fig 27b) was used. The data is not publicly available in downloadable form but was provided by PhD student Holt Hancock (01.12.2017-30.06.2018).

Gruvefjellet AWS is located at 464 m a.s.l in the middle of the Gruvefjellet plateau and data has been available online on the UNIS website from 30.11.2006 and onwards. The location of Gruvefjellet AWS is considered representative for the regional airflow, compared to Svalbard Airport which has been shown to be influenced by channelized wind (Christiansen et al., 2013). Gruvefjellet AWS does not record precipitation, and the data was thus collected from Svalbard Airport. The analysis only considers the 2017-2018 winter season, since snow depth data was available only for that period. Acquired measurements relevant for this thesis from Gruvefjellet AWS is temperature (measured 3 m above ground), wind speed and wind direction (measured 10 meters above ground). Measurements are recorded hourly and needed to be computer to daily average. Holt Hancock provided a computed dataset with daily values for the 2017-2018 season, with daily averaged temperature, arithmetically averaged wind speeds, maximum windspeed and vector averaged wind direction.

Additional snow and avalanche observations from Longyearbyen and the surrounding area was collected from the Norwegian Water Resources and Energy Directorate's (NVE) online observation platform regObs (<https://www.regobs.no/>, last access: 10 May 2020). The observations supplement the meteorological observations at Gruvefjellet AWS and Svalbard Airport AWS. Locals and trained avalanche experts publish observations on almost a daily basis.

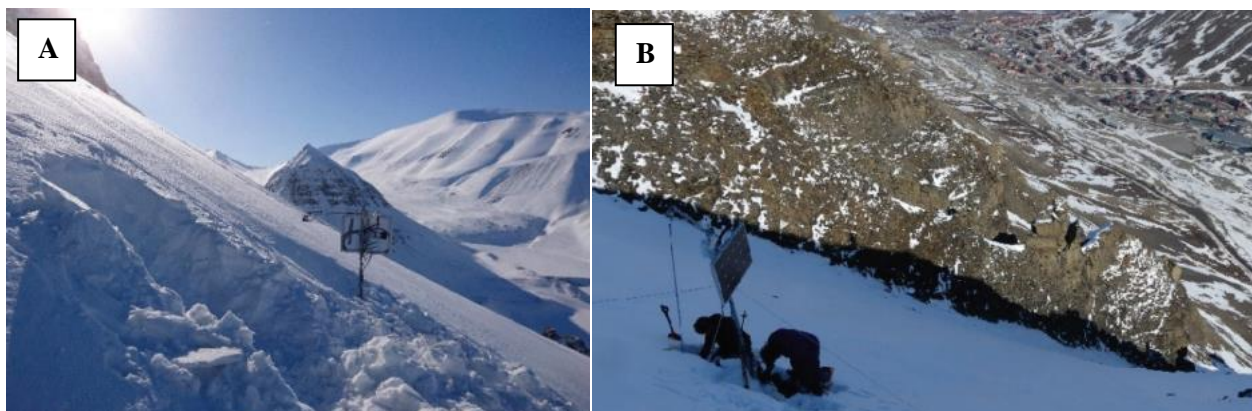


Figure 27. Snow depth sensors at (A) Gruvefjellet and (B) Platåberget (photo: Prokop et al., 2018)

Chapter 5. Results

This section summarizes the results from the avalanche fan mapping, snow depths investigations, RAMMS analysis and extreme precipitation analysis. The results from the geomorphological and avalanche fan mapping are presented first to show the extent of recent and historical deposits.

These maps were then imported and used as basemaps when performing the RAMMS modelling. Back calculation in RAMMS was performed in Longyeardalen to find suitable input parameters is briefly presented, before the results from the RAMMS modelling in Adventdalen and Todalen is presented. Snow depth changes, investigation of released avalanches from the 2016/2017 and 2017/2018 snow season and extreme precipitation analysis are presented for further discussion.

5.1 Geomorphological and Avalanche Fan Mapping

The combined results from the field campaign in September 2019 and avalanche mapping using remote sensing is presented. Todalen was the only location investigated in the field, while Longyeardalen and Adventdalen were mapped in ArcGIS. The mapping results are presented with a short description accompanied by maps and tables summarizing the fan statistics relevant for further discussion.

5.1.1 Todalen

In total, 17 avalanche fans were mapped in the field on the east side of Todalen, and a total of 34 GPS points were registered (Fig. 28). On 15 out of 17 fans, the extent of recent deposits is drawn to the position of the GPS points since shadows in the orthophotos prevented accurate mapping. Only two fans (Fan ID 15 and 16, Fig 28) have their extents drawn based on the orthophotos. A 47-meter gap and a 10-meter gap separate the mapped extent and the GPS points of the recent deposits in Fan 15 and 16, respectively (table 4). One GPS point (Fan ID 2) lies 78 meters outside the mapped extent of historical deposits (Fig. 28).

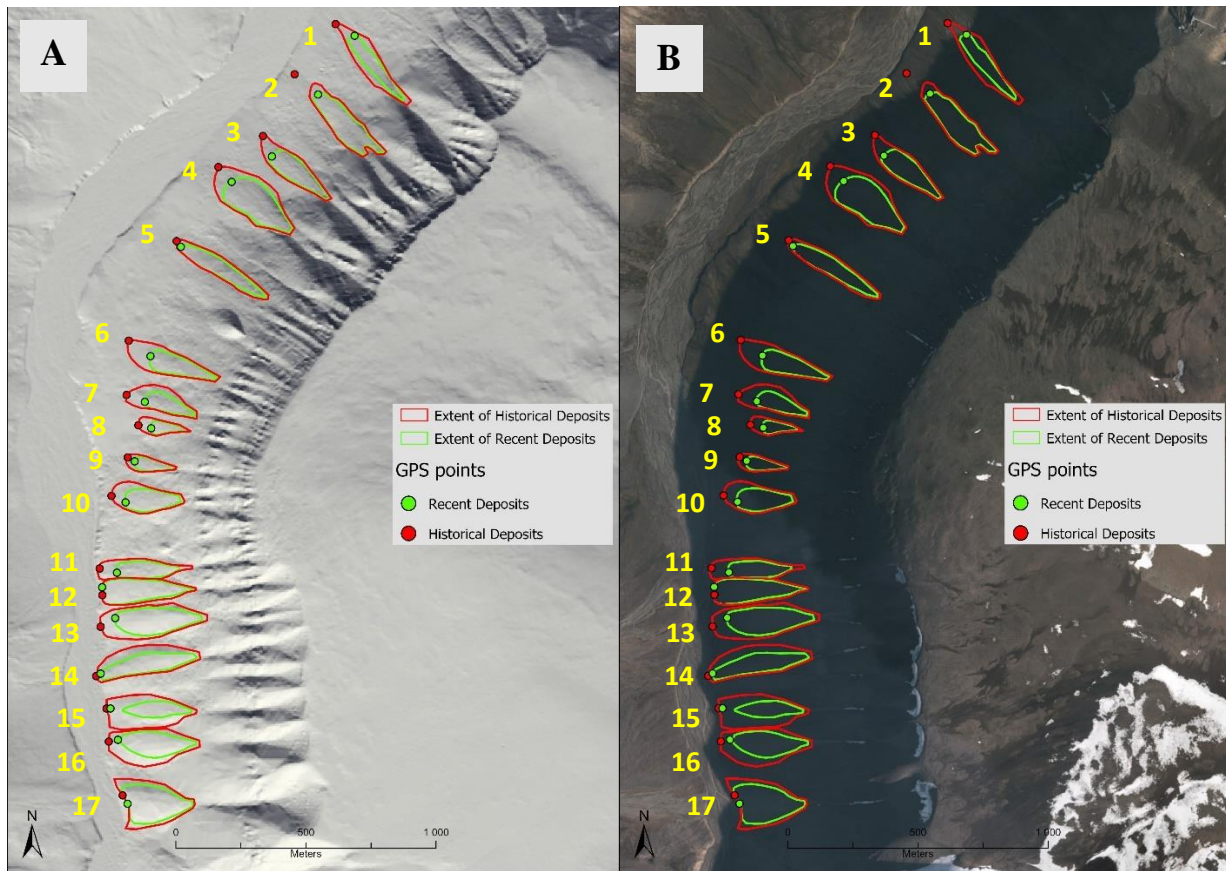


Figure 28: Hillshade (A) and Orthophoto (B) representation of the study area in eastern Todalen. The river Todalselva flows through the valley bottom, eroding into some of the fans in the inner part of the valley. GPS points were collected during the field campaign in September 2019, and the extent was mapped in ArcGIS.

All GPS points represent a registration of perched boulders which are the most common depositional feature. Debris horns and re-deposited sediments were also observed in the field but did not represent a mappable feature due to their location on the fan. Figures 29, 30 and 31 show a selection of the deposits mapped in the field. A clear distinction can be seen between recent (Fig. 29) and historical deposits (Fig. 30). Recent deposits had no lichen nor imprinting, while historical deposits had an abundance of lichen growing on the surface. The historical deposits, had in most cases, a significant imprint on the underlying rock. Size and thickness of the fans increases towards inner Todalen, with the largest located at the innermost part (Fan ID 13-17). However, as the river has eroded into some of the fans in inner Todalen, their true extent is unknown. Surface morphology is dominated by avalanches, but debris flows tracks were identified on almost all fans, and their occurrence increases towards the outer part of Todalen.

Figure 29: A, C and D show typical perched cobbles deposits. B show perched boulder. Perched cobbles and boulders were the most common depositional signature of recent avalanche deposits. Deposits were interpreted as recent if no lichen was growing on the surface and no imprint was left on the underlying rock. GPS receiver for scale.

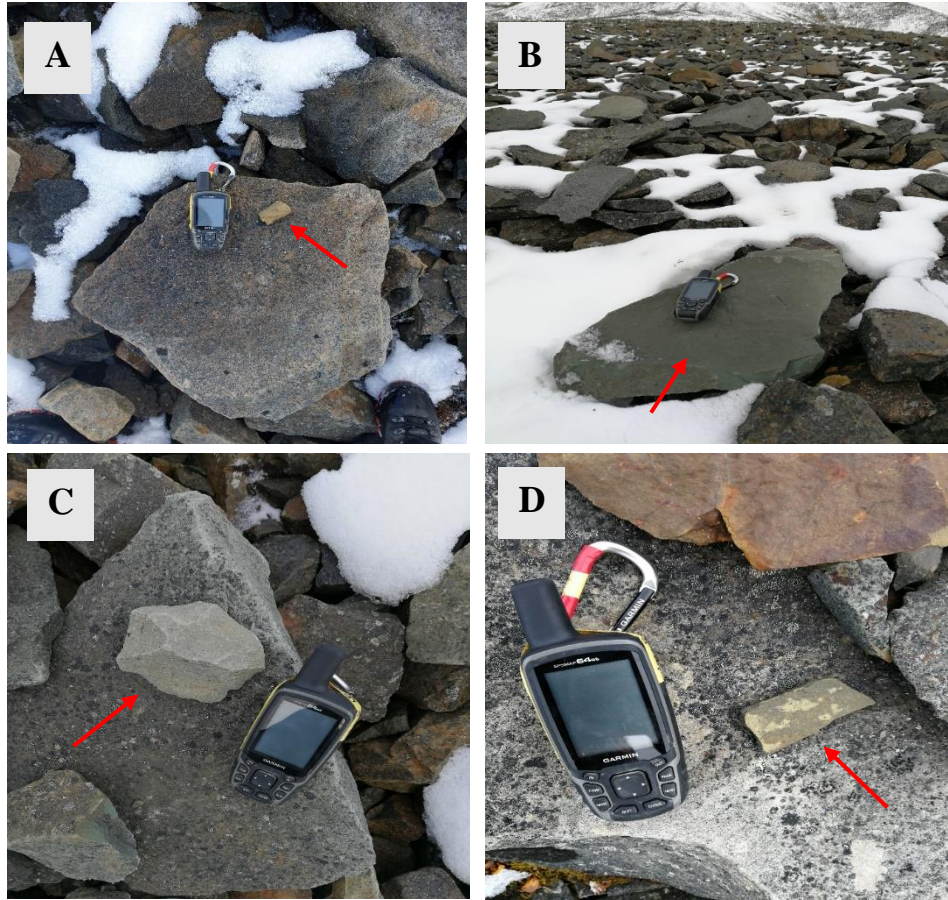


Figure 30: Perched cobbles interpreted as historical deposits because of extensive lichen growth on their surface, and imprint on the underlying rock. GPS for scale. Perched boulders where found far away from the source area, ruling out rockfall as a potential transport agent.

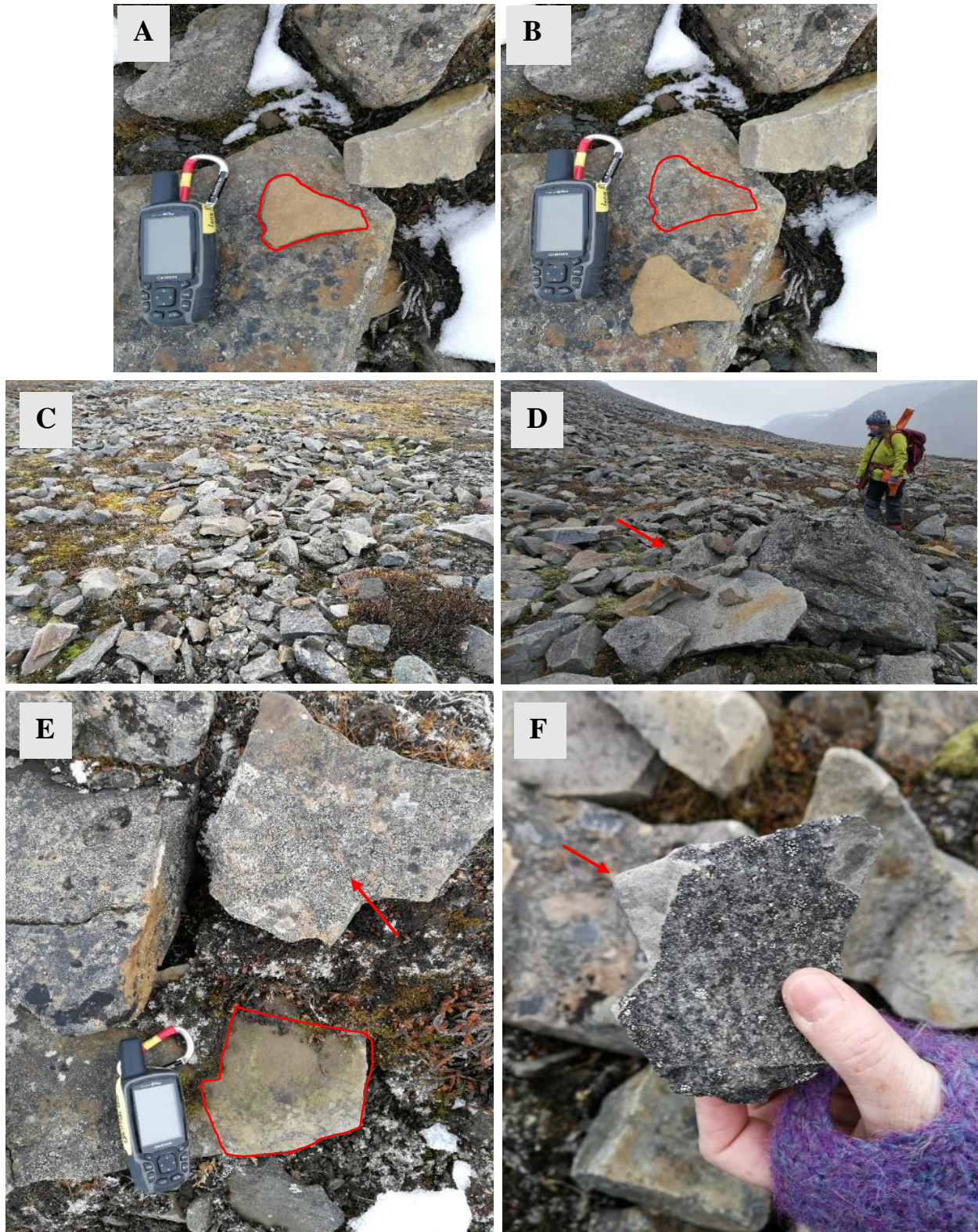


Figure 31: A, B and E show the difference between recent and historical avalanche fan deposits which had left an imprint on the underlying surface. Red outline is the original position. After moving the rock, B shows no imprint while E shows a partly shielded surface. C: shows the scattered avalanche deposits with high frequency of perched boulders. D: debris horn where debris has accumulated on the upward side of a larger obstacle. F: fragment has broken off with a fresh exposed surface, implying re-deposition.

The combined results of the geomorphological and avalanche mapping show a significant difference between recent and old deposits in terms of avalanche runout length (table 4). The length of the older deposits, which represent the total length of the fan, range from 195 to 415 meters, while recent deposits range from 152 to 389 meters (table 4). Differences between older and recent fan lengths range from 0 to 99 meters, and percentage increase from recent to old deposits range from 0% to +36% (table 4). Only two fans (Fan ID 12 and 17, Fig. 28) displayed no difference in length. In the case of Fan 17, it is clear that the result is biased by river erosion of the fan (Fig. 28)

<i>Fan ID</i>	<i>Aspect</i>	<i>Length of historical deposits</i>	<i>Length of recent deposits</i>	<i>Length difference between recent and historical deposits</i>	<i>% increase of length</i>
1	NW	413 m	338 m	75 m	+22 %
2	NW	374 m	332 m	42 m	+13 %
3	NW	351 m	272 m	79 m	+29 %
4	NW	376 m	300 m	76 m	+25 %
5	NW	415 m	389 m	26 m	+7 %
6	NW	372 m	273 m	99 m	+36 %
7	NW	281 m	206 m	75 m	+36%
8	W	202 m	152 m	50 m	+33 %
9	W	195 m	162 m	33 m	+20 %
10	W	282 m	230 m	52 m	+23 %
11	W	366 m	290 m	76 m	+26 %
12	W	372 m	372 m	0 m	0%
13	W	412 m	354 m	58 m	+16 %
14	W	406 m	388 m	18 m	+5 %
15	W	344 m	282 m	62 m	+22 %
16	W	348 m	303 m	45 m	+15 %
17	W	275 m	275 m	0 m	0%
Average		340 m	289 m	51 m	+19 %

Table 4. Summary of fan statistics for the avalanche fans in Todalen

5.1.2 Adventdalen

The SW facing avalanche fan in Adventdalen shows a significant gap between recent and old deposits (Fig. 32). The total length of the old fan is 684 m (table 5), which is significantly longer than the fans in Todalen. Recently deposited sediments reach 400 m down the fan, and the length difference between recent and old deposits is large, with a 284 m gap and a + 71% increase in length (table 5). Minor debris flow tracks are restricted to the sides, and the surface morphology of the fan appears to be fully snow avalanche-dominated (Fig. 32)

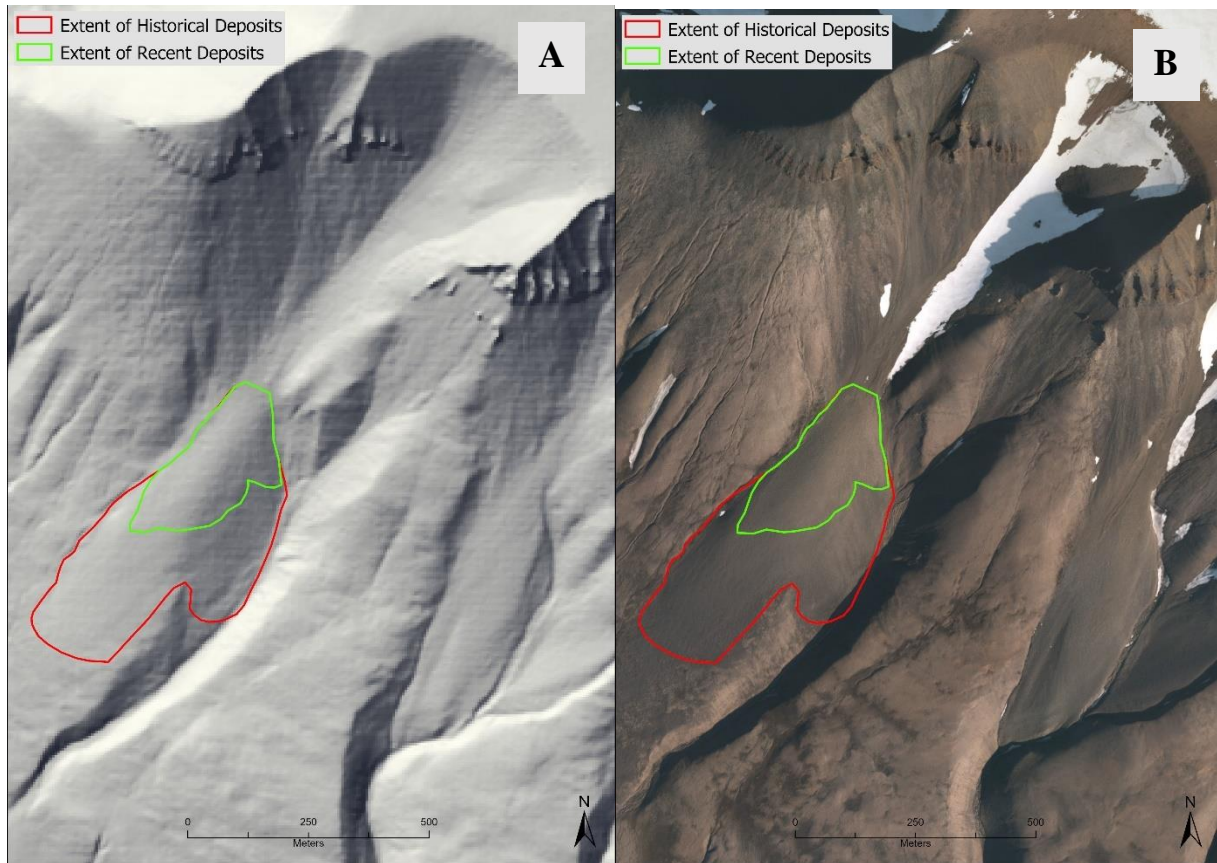


Figure 32. Hillshade (A) and orthophoto (B) of the SW facing avalanche fan in Adventdalen with the mapped extent of recent and old deposits.

FAN ID	ASPECT	LENGTH OF HISTORICAL DEPOSITS	LENGTH OF RECENT DEPOSITS	LENGTH DIFFERENCE BETWEEN RECENT AND HISTORICAL DEPOSITS	% INCREASE OF LENGTH
1	SW	684 m	400 m	284 m	+ 71%

Table 5. Summary of fan statistics for the avalanche fan in Adventdalen.

5.1.3 Longyeardalen

10 avalanche fans were mapped at Platåberget, on the western side of Longyeardalen (Fig. 33). Gruvefjellet on the eastern side was covered in shade in the orthophotos and could not be mapped. The length of the older avalanche fans ranges from 214 m to 352 m, while recent deposits range from 133 to 293 meters (Table 6). Length differences show significant variation, ranging from 0 to 129 meters, and a percentage increase of 0% to +99% (Table 6). Two avalanche fans have recent deposits reaching the toe of the fan (Fan ID 4 and 5, Fig. 33).

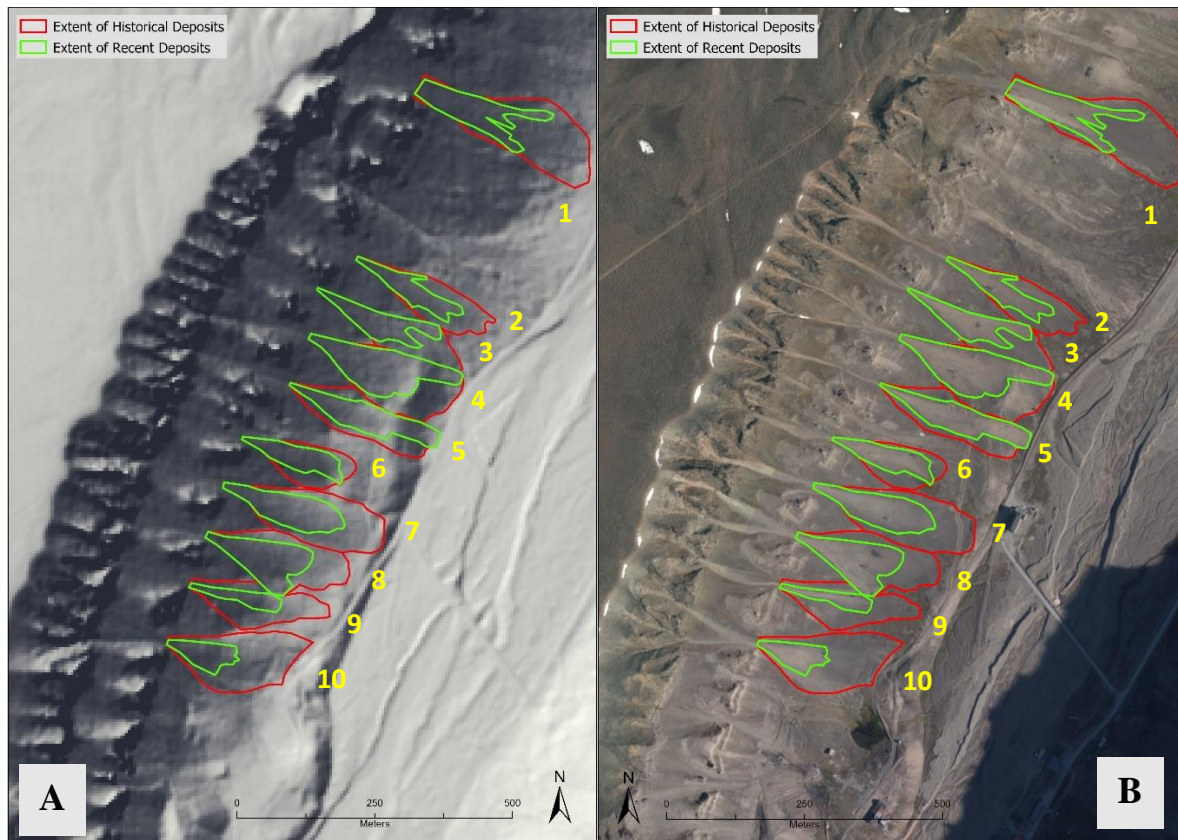


Figure 33. Hillshade (A) and orthophoto (B) of the ESE facing avalanche fans in Longyeardalen with mapped extent of recent and old deposits

<i>Fan ID</i>	<i>Aspect</i>	<i>Length of historical deposits</i>	<i>Length of recent deposits</i>	<i>Length difference between recent and historical deposits</i>	<i>% increase of length</i>
1	ESE	352 m	236 m	116 m	+ 49%
2	ESE	268 m	217 m	51 m	+ 24%
3	ESE	299 m	238 m	61 m	+ 26%
4	ESE	293 m	293 m	0 m	0 %
5	ESE	288 m	288 m	0 m	0 %
6	ESE	214 m	197 m	17 m	+ 9 %
7	ESE	307 m	231 m	76 m	+ 33%
8	ESE	269 m	195 m	74 m	+ 38%
9	ESE	258 m	166 m	92 m	+ 55%
10	ESE	262 m	133 m	129 m	+ 97%
<i>Mean</i>		281 m	219 m	62 m	+ 33%

Table 6. Summary of fan statistics for avalanche fans in Longyeardalen

5.2 Snow depth calculations

Scan results from Platåberget and Gruvefjellet in Longyeardalen document the spatial distribution of snow in the release areas. Two snow depth maps were created for each location, showing the snow depth for 25.04.2017 and 13.04.2018 compared to the ground scan from 16.09.2016. The resolution of the snow depth maps is 10cm, but scan shadows affects both slopes and parts of the release areas lack data, especially at Platåberget. Precipitation measured at Svalbard Airport from 01.12 to the date of the scan show 123.7mm and 86.2 mm, for the 2016-2017 and 2017-2018 winter seasons (yr.no), respectively.

5.2.1 Gruvefjellet

The release areas are made up of several bowls where snow accumulation exceeded 4 m for both winter seasons (Fig. 34). The snow depth maps show significant accumulation in the release areas below the vertical cliff where large cornices are known to develop during the winter. The greatest snow depths are confined to the gullies and debris flow tracks below the release areas, caused by smoothing of the terrain by snowdrift. The variation in snow depth across the entire slope highlights the importance of snowdrift across the terrain. Several meters of snow are separated by patches of only a few tens of centimetres of snow in the release areas (Fig 34). On

the open slope below the gullies, the snow depth rarely exceeds 0.5 m. Cross-loading is evident from southerly winds in the release areas, which correspond to winds following the orientation of the valley (Fig. 34). Scouring occurs on the small ridges separating the release areas. In total, the distribution of snow suggests loading from southerly and westerly winds. The 2017 scan (Fig. 34a) shows a broader snow distribution in the release areas compared to the 2018 scan (Fig 34b). The difference in snow depth between 2017 and 2018 is attributed to the observed difference in precipitation, and partly to already released avalanches which eroded parts of the release area close to when the scan was taken. The 2018 scan was performed at an earlier date, but the precipitation gap from 13.04 to 25.04 only constitutes 5.6mm of precipitation, hence, not enough to explain the difference in snow depth. Nevertheless, enough snow was present during both seasons to release large avalanches if the entire release area failed, especially if triggered by a cornice.

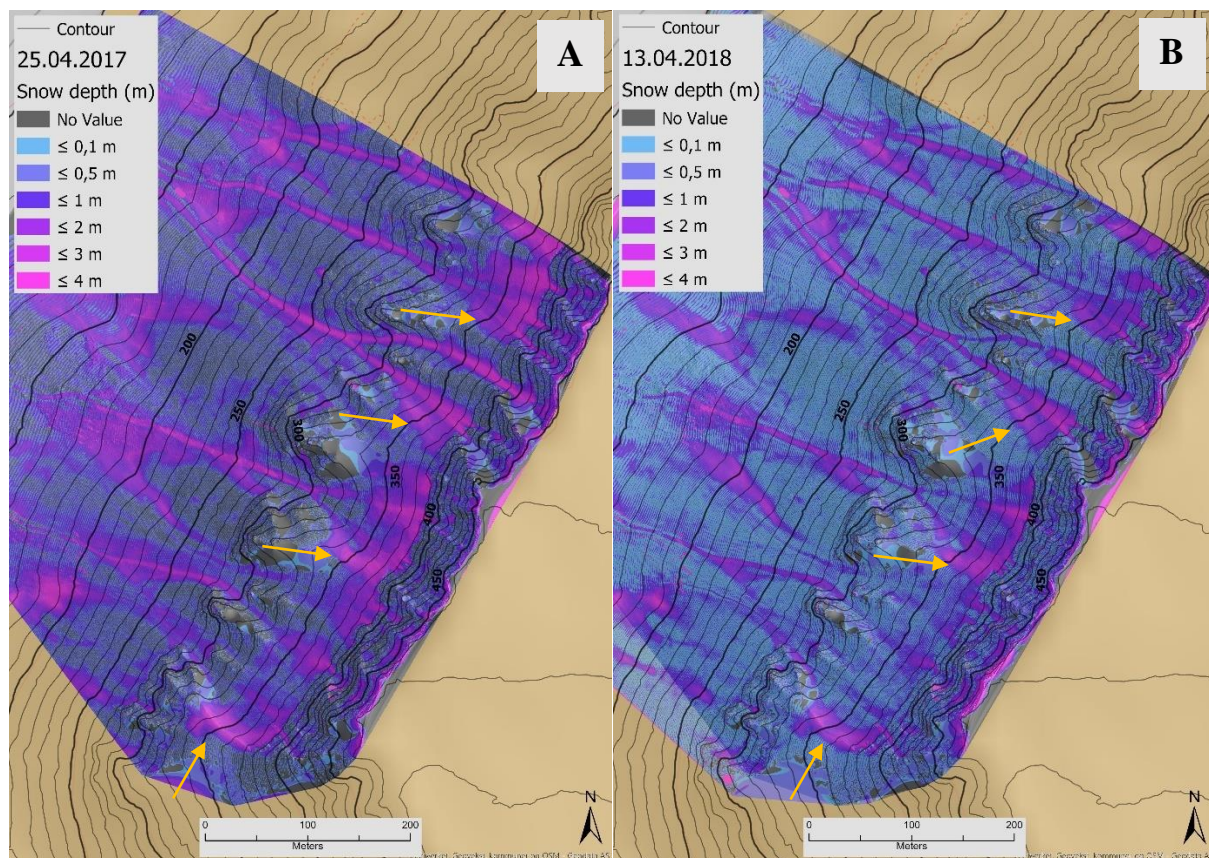


Figure 34. Snow depth maps of the release areas at Gruvefjellet in Longyeardalen. The 2016-2017 snow season (A) has accumulated more snow compared to the 2017-2018 (B) season in the release areas. The figure illustrates the importance of snow accumulation by wind, as over 3 times the snow depth is measured compared to the observed precipitation. The yellow arrows indicate evidence of cross loading.

5.2.2 Platåberget

It is difficult to extract accurate information from the snow depth maps at Platåberget since scan shadows dominate large parts of the release areas and gullies (Fig. 35). Variable snow depths are observed in the release areas, and cross-loading is evident behind ridges separating the individual release area. Platåberget is east facing, against the dominant wind direction which explains why less snow was observed in the release areas compared to the west facing Gruvefjellet (Fig. 34). Snow depths exceed 3 meters in the release areas underneath the upper steep slope and where cross loading is evident. On the open slope, avalanches and terrain smoothing by snowdrift have deposited several meters of snow next to a few 10s of cm of snow. Snow depths on east facing Platåberget is more dominated by cross loading from southerly winds, compared to west facing Gruvefjellet. However, snow depths are large enough to release large avalanches, even though snow distribution is highly irregular. The same seasonal variation as Gruvefjellet is found at Platåberget, where snow depths decreased from 2017 to 2018 (Fig. 35).

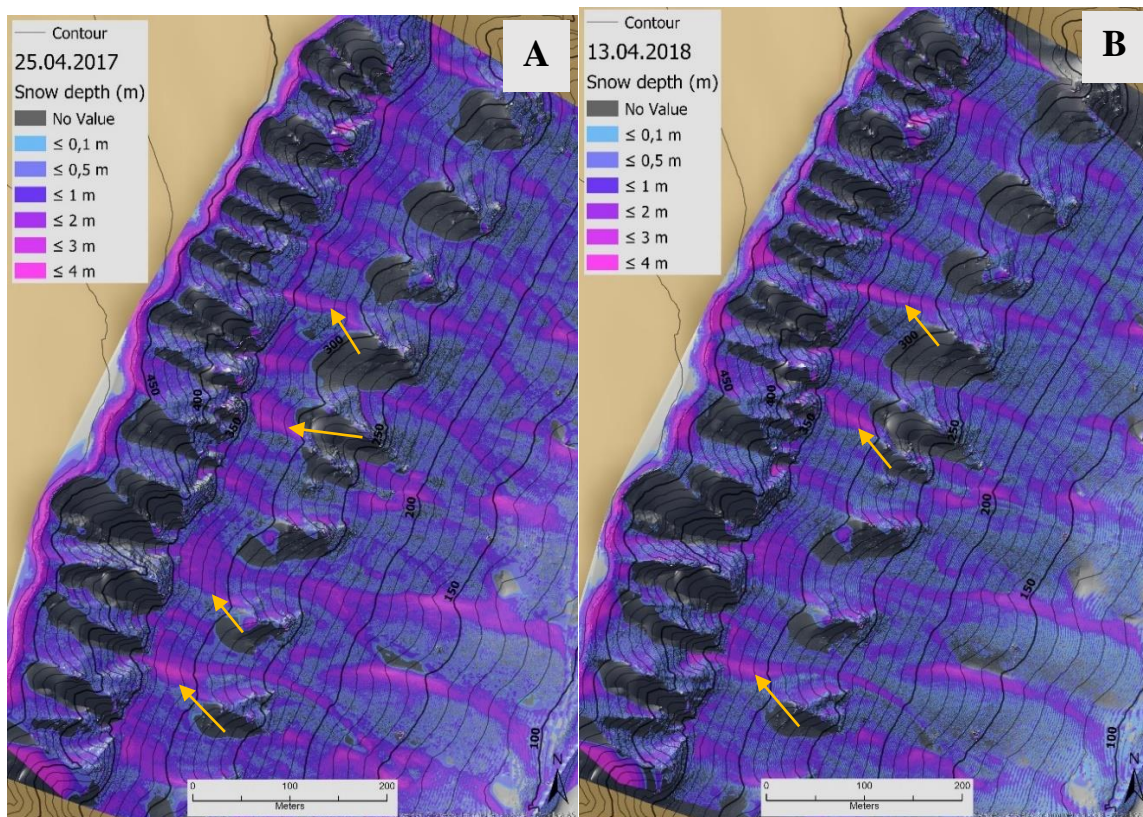


Figure 35. Snow depth maps of the release areas at Platåberget. The 2016-2017 (A) snow season has more accumulated snow than the 2017-2018 (B) season. Cross-loading is pronounced, where over 3 meters have accumulated. The snowpack is highly variable, but data holes are extensive, and the map must be interpreted with care. The yellow arrows some areas with cross loading

5.3 Automated snow and weather data

Snow depths at Gruvefjellet and Platåberget were compared to meteorological data from Gruvefjellet AWS and Longyearbyen Airport AWS to investigate the relationship between snow depth change, precipitation, wind and temperature. Figure 36 shows a summary of the snow depth changes and meteorological factors for the 2017-2018 winter season. A large difference in snow depth is present between east (Platåberget) and west (Gruvefjellet) facing slopes. Maximum snow depth at Gruvefjellet reached 177 cm on 13.04.2018, while maximum snow depth at Platåberget occurred on 03.03.2018 with 73 cm. Snow depths remained relatively stable between precipitation periods, and started to steadily decline from 13.05.2018 at Gruvefjellet and 16.05.2018 at Platåberget when daily temperatures increased. A clear pattern emerges between snow depth changes and the meteorological variables. When snow depth increases significantly, maximum wind speed exceeds 20 m/s, average wind speed generally exceeds 10 m/s and temperature reaches close to 0°C (Fig. 36). This corresponds with the warm and wet low pressure systems from the North Atlantic cyclone track (Hanssen-Bauer et al., 1990). The yellow bar in figure 36 marks the event on the 14.01. Positive air temperatures caused precipitation as rain and combined with little snow available for transport (regobs.no, 2018), no snow depth increase was registered at either snow sensor.

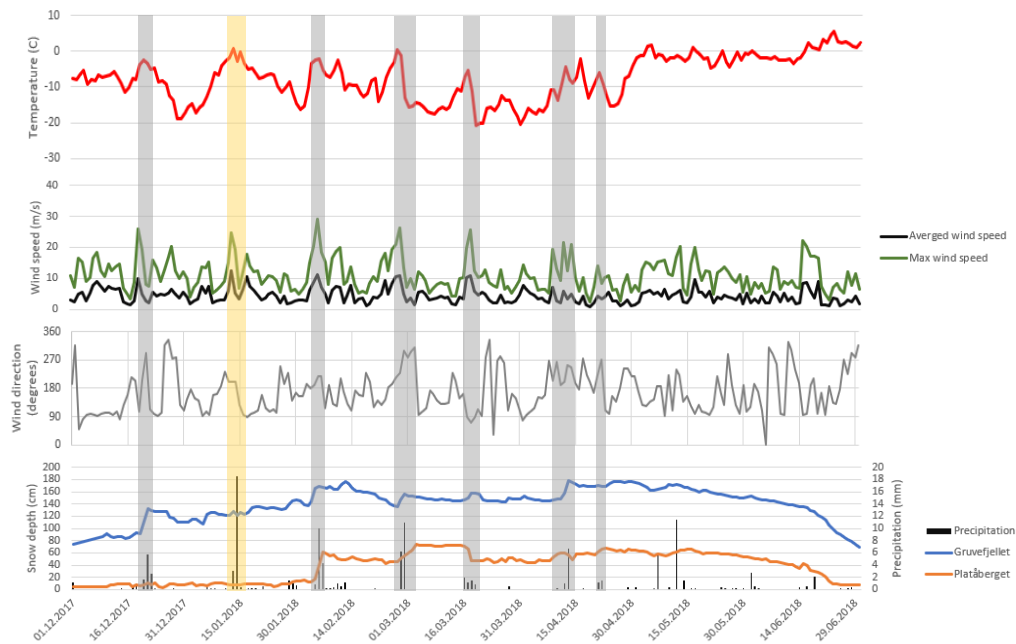


Figure 36. Summary of snow depth and weather data for the 2017-2018 winter season. Precipitation is measured at Longyearbyen Airport (28 m a.s.l.). Snow depth values are from snow sensors at Gruvefjellet (350 m a.s.l) and Platåberget (450 m a.s.l). Wind and temperature data were collected from Gruvefjellet AWS (464 m a.s.l). Temperatures are daily average values, wind speed is arithmetical average, wind direction is vector averaged, and maximum wind speed is the daily measured maximum. The highlighted bars in grey represent precipitation periods where snow depths significantly increased at one or both snow sensors. Yellow bar represents precipitation period when no snow depth increase was registered.

Accumulation period	Snow depth change	Precipitation 1 week prior to event	Total Precipitation	Percentage of accumulation by snowdrift	Maximum windspeed	Average windspeed	Percentage of hours with average wind speed > 7.7 m/s	Wind direction	Temperature range (°C)	Regobs observations
19.12.2017-20.12.2017	+ 50 cm	1.6 mm	7.3 mm	584 %	26 m/s	7.4 m/s	43 %	85 - 270	-6.1 / -1.4	15 cm dry new snow from 0-800 m a.s.l available for transport observed on the 18 th (regobs, 2017x). On the 20 th , 20-50 cm has accumulated on some slopes
05.01.2018-06.01.2018	+ 19 cm	0 mm	0.9 mm	2011 %	13.7 m/s	6.4 m/s	47 %	81 - 218	-15.6/ -11.6	1-3 cm new snow in Longyearbyen between 5 th and 6 th . On the 6 th , reported 20 cm accumulated in gullies
27.01.2018-29.01.2018	+ 17 cm	0.5 mm	3.1 mm	448 %	11.4 m/s	2.7 m/s	5 %	10-330	-12.7 / -7	10 -15 cm new snow in Longyearbyen and Larsbreen reported on the 28 th
04.02.2018	+ 36 cm	3.1 mm	10.9 mm	230 %	20.3 m/s	8.7 m/s	66 %	170 -209	-3.8 / -1.1	5-30 cm loose snow available for transport from Nybyen up to Lars Hiertafjellet on the 3 rd . Wet and wind drifted snow between the 4 th and 5 th
11.02.2018	+ 20 cm	16.9 mm	1.8 mm	1011 %	20.1 m/s	7.1 m/s	50 %	186 -235	-9 / -4.3	10-20 cm precipitation on the 11 th in combination with wind from the S
27.02.2018	+ 19 cm	0.2 mm	17.2 mm	10 %	26.1 m/s	10.9 m/s	87 %	211 - 280	-7.5 / +1	Above 250 m a.s.l, wind drifted snow is substantial. 5 cm new snow on the 26 th . Wet slab avalanches observed on the 27 th
17.03.2018-19.03.2018	+ 15 cm	2 mm	3.6 mm	316 %	25.5 m/s	8.9 m/s	68 %	66 - 172	-22.3 / -3.8	5-10 cm loose snow reported on the 16 th around Longyearbyen. Hard snow on exposed terrain, lee sides has wind accumulated snow due to winds from the east reported on the 20 th
12.04.2018	+ 28 cm	0.1 mm	7.7 mm	263 %	21.5 m/s	5.8 m/s	2.0 %	151 - 344	-8.1 / -0.1	7 cm new snow in Longyearbyen. Much snow available for transport on the 12 th . Wind from S and W have accumulated snow on lee-slopes, reported on the 13 th

Table 7. Summary of major snow depth changes at Gruvefjellet in Longyeardalen during the 2017-2018 snow season. Significant accumulation occurred within a single to a few days due to substantial snowdrift, often in combination with precipitation. Regobs observations have been inspected up to 3 days before and after the event, including the day(s) of the event. Precipitation is measured at Svalbard Airport AWS, snow depth data are from the snow sensor installed at Gruvefjellet, windspeeds and temperature are from Gruvefjellet AWS. The investigated data has been recorded hourly except for precipitation.

Accumulation period	Snow depth change	Precipitation 1 week prior to event	Total Precipitation	Percentage of accumulation by snowdrift	Maximum windspeed	Average windspeed	Percentage of hours with average wind speed > 7.7 m/s	Wind direction	Temperature range (°C)	Regobs observations
04.02.2018-06.02.2018	+ 48 cm	3.1 mm	15.3 mm	213 %	29.1 m/s	9 m/s	66 %	170 -254	-10/ +0	5-30 cm loose snow available for transport from Nybyen up to Lars Hiertafjellet on the 3 rd . Wind averaging 16.5 m/s and snowdrift from the S, reported on the 5 th . Visibility down to 10m at Nybyen.
26.02.2018-28.02.2018	+ 29 cm	0.2 mm	17.2 mm	68 %	26.1 m/s	10.7 m/s	87 %	202 - 280	-7.5 / +1	Above 250 m a.s.l, wind drifted snow is substantial. 5 cm new snow on the 26 th . Wet slab avalanches observed on the 27 th
09.04.2018-10.04.2018	+ 20 cm	0 mm	0.1 mm	19900 %	19.2 m/s	4.9 m/s	29 %	153 - 304	-14.2 / -9	3 cm new snow around Longyearbyen/Larsbreen, which lead to accumulation up to 30 cm in N/NØ/Ø aspects, reported on the 9 th
21.04.2018	+ 11 cm	0.1 mm	2.6 mm	323 %	13.9 m/s	4.4 m/s	0 %	185 - 262	-7.8 / -3.7	10 cm new snow reported on the 21 th in northerly and easterly aspects. Southerly winds

Table 8. Summary of major snow depth changes at Platåberget in Longyeardalen during the 2017-2018 snow season. Significant accumulation occurred within a single to a few days due to substantial snowdrift, often in combination with precipitation. Regobs observations have been inspected up to 3 days before and after the event, including the day(s) of the event. Precipitation is measured at Svalbard Airport AWS, snow depth data are from the snow sensor installed at Platåberget, windspeeds and temperature are from

Table 7 and 8 summarizes the major snow depth changes at Gruvefjellet and Platåberget snow sensor, respectively. In total, Gruvefjellet had 8 events where snow depth increased between 15 cm - 50 cm within a single or a few days. Platåberget had 4 events where snow depth increased between 11 cm – 48 cm. There is a lack of agreement between the Regobs observations and measured precipitation at Svalbard Airport AWS. Generally, several cm to tens of cm more is reported by Regobs, than what is officially recorded at the Airport (table 7 and 8). Large snow depth increase at both locations are attributed to either significant precipitation, much snow available for transport, or both. Regardless, snow drift accounts for most of the accumulated snow, expect for one event on the 27.02.2018 (table 7). Hourly wind direction changes significantly during most events. Accumulation on Gruvefjellet is dominated by easterly, south easterly, southerly and south-westerly winds, which agrees with general lee side or cross-loading accumulation. The placement of the Gruvefjellet snow sensor is placed on the lee side of a small ridge within the release area, and should be affected by cross-loading from southerly, and south-westerly wind being channelled by the valley (Fig. 20b). Accumulation on Platåberget is more dependent on south-easterly and easterly winds which brings precipitation. Wind direction during the 2017-2018 winter season is mostly from the E, SE and S (Fig. 37). High wind speeds enabling snow drift, largely comes from the east, and is a strong indicator why snow depths are higher at Gruvefjellet compared to Platåberget. Based on only one season of snow sensor data, new snow sum regularly exceeds 20 cm (table 7 and 8). A longer observation period is necessary to conclude if new snow depths between 40 cm-50 cm occurs regularly. On two occasions on Platåberget (table 8) and three at Gruvefjellet (table 7), the new snow sum is about 30 cm or more, which is the critical sum for new snow instabilities (Schweizer et al., 2003). However, avalanche release is strongly linked with cornice falls (Hancock et al., 2020), which trigger avalanches independently of the new snow sum reaching 30 cm or not.

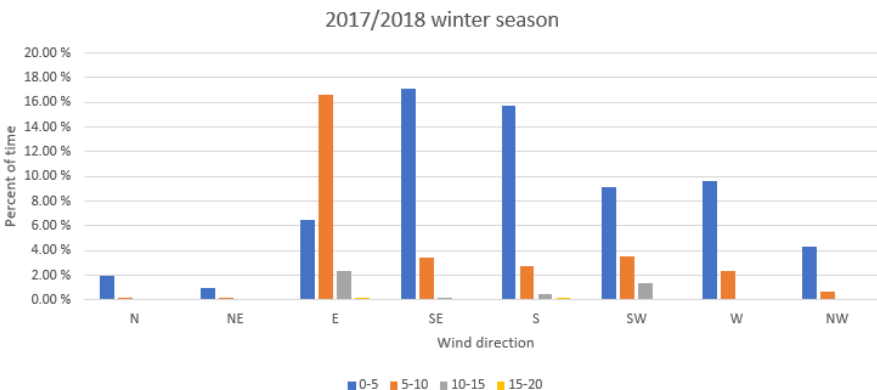


Figure 37. Frequency analysis of windspeed and direction at Gruvefjellet AWS for the 2017/2018 snow season. The snow season is defined as November-May.

5.4 Extreme precipitation analysis

To estimate fracture heights, the 1 and 3-day precipitation sum was calculated using the Bayesian approach for generalized extreme value (GEV) analysis, based on precipitation data from Longyearbyen Airport and Longyearbyen Station. The total data series spans 109 years of observation, but some gaps in the data exist at the old Longyearbyen station. A common issue with extreme precipitation analysis is the extrapolation of values for large return periods (Katz et al., 2002). As this thesis investigates avalanches with small return periods, there is enough data that the uncertainty is small up until a 10 - 20 year return period. The results of the extreme precipitation analysis are presented in figure 38 and 39. The blue line represents the 95 % confidence interval and represents the degree of uncertainty. It is considered that 1 mm of precipitation represents 1 cm of snow. The values from the extreme precipitation analysis should be considered the minimum representation of the actual precipitation. Large uncertainties exist regarding the catch rate of the precipitation gauge at Longyearbyen Airport (Humlum, 2002).

The vertical precipitation gradient is not considered since precipitation is measured at 28 m a.s.l and the release areas are located at 300-500 m a.s.l in Todalen, 300-470 m a.s.l in Longyeardalen and 650-850 m a.s.l in Adventdalen. The calculated values presented in table 9 and 10 represent return values for 2, 5, 10, 20, 50 and 100 years. Three different sums are calculated for each return period (table 9 and 10): (1) extreme precipitation analysis, (2) corrected for vertical gradient of 10% per 100 m based on Humlum (2002) and (3) 100% upwards correction of precipitation values based on Humlum (2002) and the vertical gradient of 10% per 100 m.

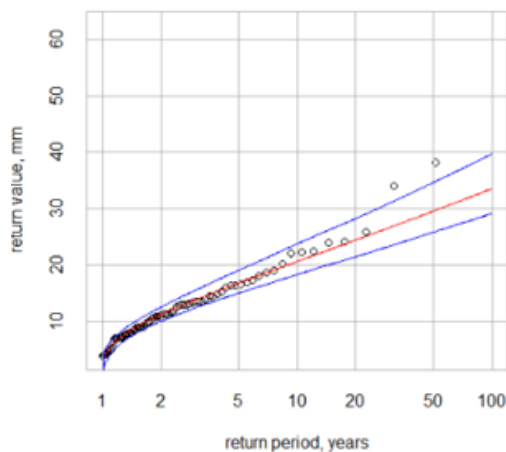


Figure 38. Extreme precipitation analysis of 1-day precipitation. X-axis represents the precipitation values, which translates into snow depth in cm. Y-axis is return periods in years.

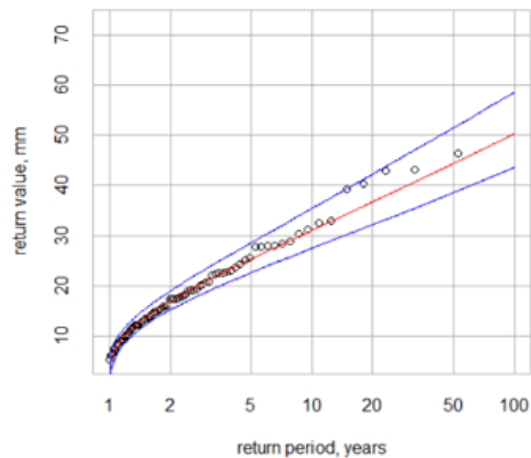


Figure 39. Extreme precipitation analysis of 3-day precipitation. X-axis represents the precipitation values, which translates into snow depth in cm. Y-axis is return periods in years.

TODALEN AND LONGYEARDALEN (300-500 M A.S.L)

RETURN PERIOD (1-DAY SUM)	GEV (Bayesian)	GEV + vertical gradient of 10% per 100 m	GEV + upwards correction of 100% and 10% per 100 meters
2 YEARS	11 cm	14.3 – 16.5 cm	28.6 – 33 cm
5 YEARS	16 cm	20.8 – 24 cm	41.6 – 48 cm
10 YEARS	21 cm	27.3 – 31.5 cm	54.6 – 63 cm
20 YEARS	25 cm	32.5 – 37.5 cm	65 – 75 cm
50 YEARS	30 cm	39 – 45 cm	78 – 90 cm
100 YEARS	33 cm	42.9 – 49.5 cm	85.8 – 99 cm
RETURN PERIOD (3-DAY SUM)			
2 YEARS	17 cm	22.1 – 25.5 cm	44.2 – 51 cm
5 YEARS	25 cm	32.5 – 37.5 cm	65 – 75 cm
10 YEARS	31 cm	40.3 – 46.5 cm	80.6 – 93 cm
20 YEARS	37 cm	48.1 – 55.5 cm	96.2 – 111 cm
50 YEARS	44 cm	57.2 – 66 cm	114.4 – 132 cm
100 YEARS	50 cm	65 – 75 cm	130 – 150 cm

Table 9. Estimated fracture height values based on extreme precipitation analysis for release areas in Todalen and Longyear dalen. Three different fracture heights are presented based on correction for the vertical gradient and upwards correction of measured precipitation in addition to the vertical gradient.

ADVENTDALEN (650-850 M A.S.L)

RETURN PERIOD (1 DAY SUM)	GEV (Bayesian)	GEV + vertical gradient of 10% per 100 m	GEV + upwards correction of 100% and 10% per 100 meters
2 YEARS	11 cm	18.1 – 20.3 cm	36.3 – 40.7 cm
5 YEARS	16 cm	26.4 – 29.6 cm	52.8 – 59.2 cm
10 YEARS	21 cm	34.6 – 38.8 cm	69.3 – 77.7 cm
20 YEARS	25 cm	41.2 – 46.2 cm	82.4 – 92.4 cm
50 YEARS	30 cm	49.5 – 55.5 cm	99 – 111 cm
100 YEARS	33 cm	54.4 – 61 cm	108.8 – 122 cm
RETURN PERIOD (3-DAY SUM)			
2 YEARS	17 cm	28 – 31.4 cm	56.1 – 62.9 cm
5 YEARS	25 cm	41.2 – 46.2 cm	82.5 – 92.5 cm
10 YEARS	31 cm	51.1 – 57.3 cm	102.3 – 114.7 cm
20 YEARS	37 cm	61 – 68.4 cm	122 – 136.8 cm
50 YEARS	44 cm	72.6 – 81.4 cm	145.2 – 162 cm
100 YEARS	50 cm	82.5 – 92.5 cm	165 – 185 cm

Table 10. Estimated fracture height values based on extreme precipitation analysis for release area in Advent dalen. Three different fracture heights are presented based on correction for the vertical gradient and upwards correction of measured precipitation in addition to the vertical gradient.

5.5 Avalanche cycles and the release properties

Four major avalanche cycles were detected from the scan data, in which multiple avalanches released. Two events occurred Platåberget on the 21.01.2017 and 29.04.2017 (Fig. 40), and two at Gruvefjellet on the 09.04.2017 and 13.03.2018 (Fig. 41) (Hancock et al., 2020). Table 11 shows a summary of the avalanche cycles, weather history and the time between pre and post avalanche scan. Hancock et al. (2020) recently described the avalanches as cornice fall avalanches which also triggered secondary slab avalanches.

Pre scan date	Post scan date	Avalanche date	Scan site	Number of mapped avalanches	Weather history prior to avalanche release and between scans (from yr.no)
12.01.2017	22.01.2017	21.01.2017	Platåberget	3	-15.4/+2.2°C. 18.5 mm precipitation. One period over two days with temperatures above 0°C. Strong westerly wind prior to avalanche release. Average wind speed 6.7 m/s.
25.04.2017	01.05.2017	29.04.2017	Platåberget	4	-12.8/+2.9°C. 4.4 mm precipitation. One period over two days with temperatures above 0°C. Prevailing wind from SE Average wind speed 5.7 m/s
21.03.2017	25.04.2017	09.04.2017	Gruvefjellet	2	-21,3/-1,1°C. 5.3 mm precipitation. Wind from SW, W, E, SE, S, NW, N. Average wind speed 5.3 m/s
02.03.2018	23.03.2018	18.03.2018	Gruvefjellet	3	-19.3/+1.4°C, 5.6 mm precipitation. One day with temperatures above 0°C. Prevailing wind from E and SE. Average wind speed 6.2 m/s.

Table 11. Summary of avalanche cycles with weather history between the two scans.

Figure 40 and 41 show the avalanche cycles that occurred during the 2016/2017 and 2017/2018 snow season. Multiple avalanches released, which is visible on the TLS scan. The scan from 01.05.2017 is from spring when snowmelt has started, and received less precipitation compared to the 21,01,2017 event (table 11), and is probably the reason why large parts of the southern slope is red (indicating a reduction in snow depth). The avalanche track is clearly visible on just a few avalanches. Snow accumulation between the time of avalanche failure and the TLS scan, in addition to scan shadows is probably the reason why avalanche tracks are hard to identify. An unknown error in ArcGIS resulted in volume calculation for only some of the avalanches.

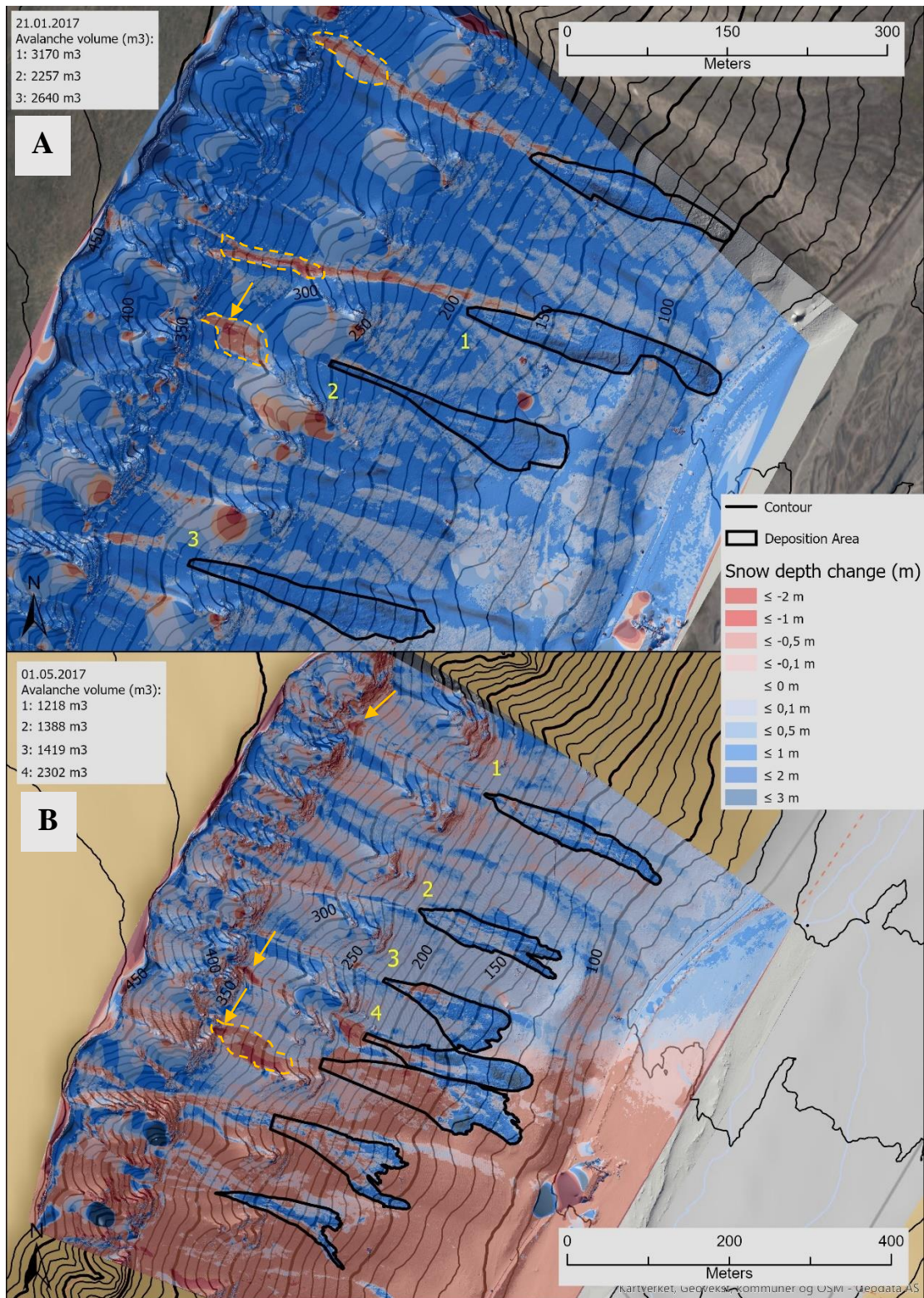


Figure 40. Map showing the avalanche deposits from multiple avalanches released during two avalanche cycles at Platåberget during the 2016/2017 winter season. The yellow arrows indicate impact craters from cornice fall avalanche, and dotted outline shows the extent of the release area which was clearly visible in the scan.

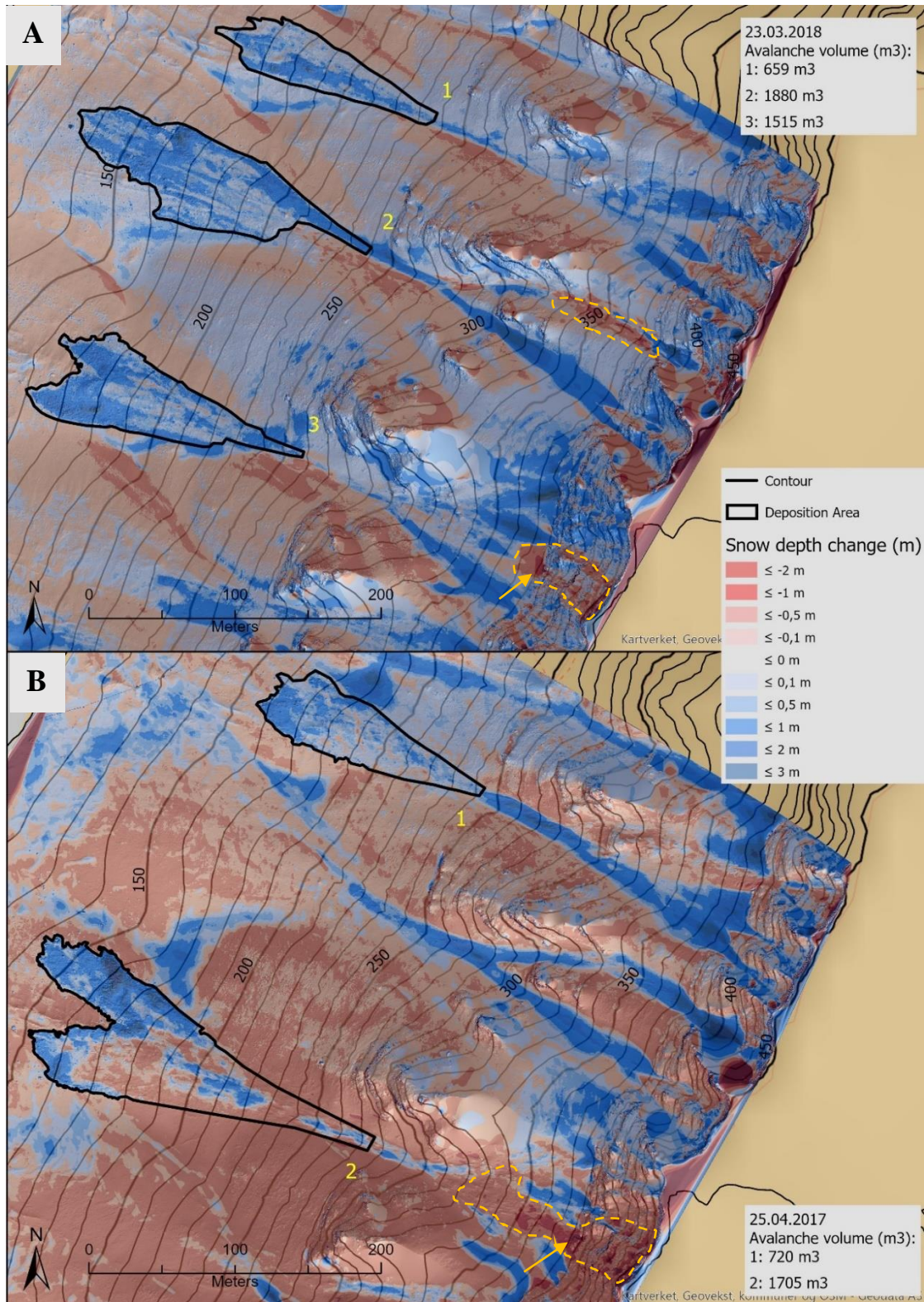


Figure 41. Map showing the avalanche deposits from multiple avalanches released during two avalanche cycles at Gruvefjellet during the 2016/2017 (B) 2017/2018 (A) winter season. The yellow arrows indicate impact craters from cornice fall avalanche, and dotted outline shows the extent of the release area which was clearly visible in the scan.

Release areas has also accumulated snow after the avalanches released and some were affected by scan shadows, making it harder to map accurately (Fig. 40 and 41). Platåberget consist of two potential release areas; the upper bowl-shaped areas just beneath the plateau edge, and a second just above the rock noses (Fig. 40). The bowls range in size and act source areas for the lower release areas and avalanche paths. It was not possible to see whether one or more source areas released, especially for the larger avalanches, due to scan shadows. Gruvefjellet has one main zone above the rock noses which acts as release area for avalanches. Small ridges or rock noses divide the release area into two parts which feeds the avalanche fan below in all but one.

Only one avalanche is registered to have triggered a large part of the release area. A cornice detached and eroded part of the rock wall and triggered a slab avalanche underneath (Fig 41b, ID 2). Instead, almost all avalanches triggered only a small part of the release area, even the largest avalanche which reached the road on 21.01.2017 (Fig. 40a, ID 1). Six avalanches (Fig. 40 and 41) have impact craters visible in the release area, indicating a cornice fall avalanche. Since most of the upper release areas are filled with scan shadows, it remains inconclusive from the scans whether most of the released mass is from the upper, rather than the lower release area at Platåberget. At both Platåberget and Gruvefjellet, fracture heights are highly variable and range from about 0.1 m to 1m. The depth of the impact craters ranges from 0.6 m – 1.7 m, but not weak layers were triggered at the maximum depth of the impact craters. The general observation was that larger release area and fracture height caused longer runout. Volumes of the deposited masses ranged from 659 m³ to 3170 m³. If cornice fall avalanches don't trigger a secondary slab avalanche, the deposited mass is mostly the cornice itself and some entrained snow. Two avalanches are strictly cornice falls as deposited volume was 659 m³ and 720 m³, while the rest are either cornice falls which triggered a secondary slab avalanche, or strictly slab avalanche.

5.6 Back calculation in RAMMS

Prior to the RAMMS modelling of recent and historical avalanches in Todalen, parameters for dry slab and wet slab avalanche release were tested and tuned to the observed avalanches in Longyeardalen (Fig. 40 and 41). The main parameters determining avalanche runout include the size of the release area, fracture height, friction parameters and cohesion. These values where changed until best fit was achieved.

Due to the uncertainty regarding the actual size of the release areas, multiple were tested. Release areas based on the TLS scan gave unrealistically high fracture heights between 1-2 m. RAMMS recommends using a larger release area to accommodate for entrainment, and the most accurate results came from enlarging the release area to almost the entire theoretical release area for all avalanches. Enlarging the release areas gave a fracture height ranging between 0.15m – 0.6m for dry slab release and 0.30-0.72 m for wet slab release. Fracture heights observed on the TLS data ranged between 0.1m – 1m, but these values were not constant within the same release area. Therefore, the fracture height from RAMMS represents the average height, which is expected to be lower. Cohesion had a big influence on the results. Low cohesion caused the avalanche flow to diffuse at low velocities, adding 10s of meters to the deposited mass as described by Bühler et al. (2014). Increasing the cohesion lead directly to shorter runout, which had to be compensated for by increasing the fracture height. For modelling dry slab release, cohesion value of 100 was found to be the best fit. The cohesion value was increased to 200 for modelling wet slab avalanches. Beyond 200 in cohesion, the fracture height had to be increased by an amount which was interpreted as unrealistic in order to reach the targeted runout.

Friction values were automatically classified by global parameters (return period and avalanche size) and altitude limits. Emphasis was placed on the altitude limits 150/50 m a.s.l as they seemed to have a slightly better fit. Although, not much difference was found between the altitude limits used by NVE (150/50 m a.s.l) and NGI (50-10 m a.s.l) (NVE, 2018). On the other hand, the default altitude limits (1500/1000m) was deemed to high based on the modelling results compared to the other two altitude limits. Volumes were hard to accurately back calculate while maintaining realistic input parameters. None of the modelling results managed to accurately recreate deposited volumes. This is partly believed to be caused by the fact that several avalanches are cornice fall avalanches. Cornice fall have different volumes, dynamics and runout compared to regular slab avalanches. For modelling cornice fall avalanches, it had to be assumed that they triggered a secondary slab avalanche. Table 12 shows the combination of parameters which was considered to be the best fit for modelling observed avalanches in Longyeardalen. Parameters are the representation of modern avalanches and do not take into account that historical avalanches could have released under different conditions, which would require different parameters.

	DRY SLAB AVALANCHE	WET SLAB AVALANCHE
ALTITUDE LIMIT (FRICTION VALUES)	150m-50m	150m-50m
COHESION	100	200
DENSITY	375	450
RETRUN PERIOD	10 years	10 years
AVALANCHE SIZE	Small	Small
FRACTURE HEIGHT	0.15m - 0.4 m	0.30m - 0.72m

Table 12. Summary of parameters in RAMMS which gave the best fit in back-calculation observed avalanches which released during 4 avalanche cycles between the 2016-2017 and 2017-2018 winter season.

5.7 Reconstruction of recent and historical avalanche runouts

The results of the back calculation and avalanche fan mapping of recent and historical served as starting point for the reconstruction of recent and historical avalanche runouts in Todalen and Adventdalen. The altitude limit, cohesion, density values and return period from the back-calculation (table 12) was kept constant throughout the modelling. Avalanche size was automatically determined based on the input volume. The only changed parameter was fracture height and size of the release area. As previously observed, release areas were generally drawn a bit larger to compensate for entrainment. In Adventdalen, modelling was done with a small release area and a large release area to compare and discuss the impact. For recent and historical runout lengths, two scenarios are presented: dry slab avalanche which typically release mid-winter and wet slab avalanche which typically release during rain-on-snow events or during spring (Eckerstorfer & Christiansen, 2011c). The modelling results from Adventdalen and Todalen will be presented below, before being discussed in the next chapter.

5.7.1 Adventdalen

RAMMS was able to reconstruct recent and historical runouts on the avalanche fan in Adventdalen with good accuracy (Fig. 42 and 43). Modelling results show that the avalanches almost fit entirely within the outline of historical deposits. The only misrepresentation is that parts of the avalanche flowed into the fluvial gorge farther than expected. Accuracy decreased slightly within the outline of recent deposits, but RAMMS is known to overestimate the width of the deposits (Bühler et al., 2014). No significant difference in the shape of the avalanche is found between dry and wet slab avalanche modelling, or between modelling with large or small release area. The largest difference is found comparing the flow height between dry and wet slab avalanches. Wet slab avalanches had higher release volume due to higher fracture height, resulting in slightly higher flow heights. This is observed in the runout zone where flow heights are distributed more in the wet slab avalanche results, compared to the dry slab avalanches, where flow heights of <0.5 m dominates a larger part of the runout zone (Fig. 42 and 43). Three statistical comparisons are made: (1) Impact of release area size on volume and fracture height for the same runout, (2) comparison of recent and historical runout between the same avalanche types, and (3) comparison between the different avalanche types, for the same runout.

Modelling results: small release area

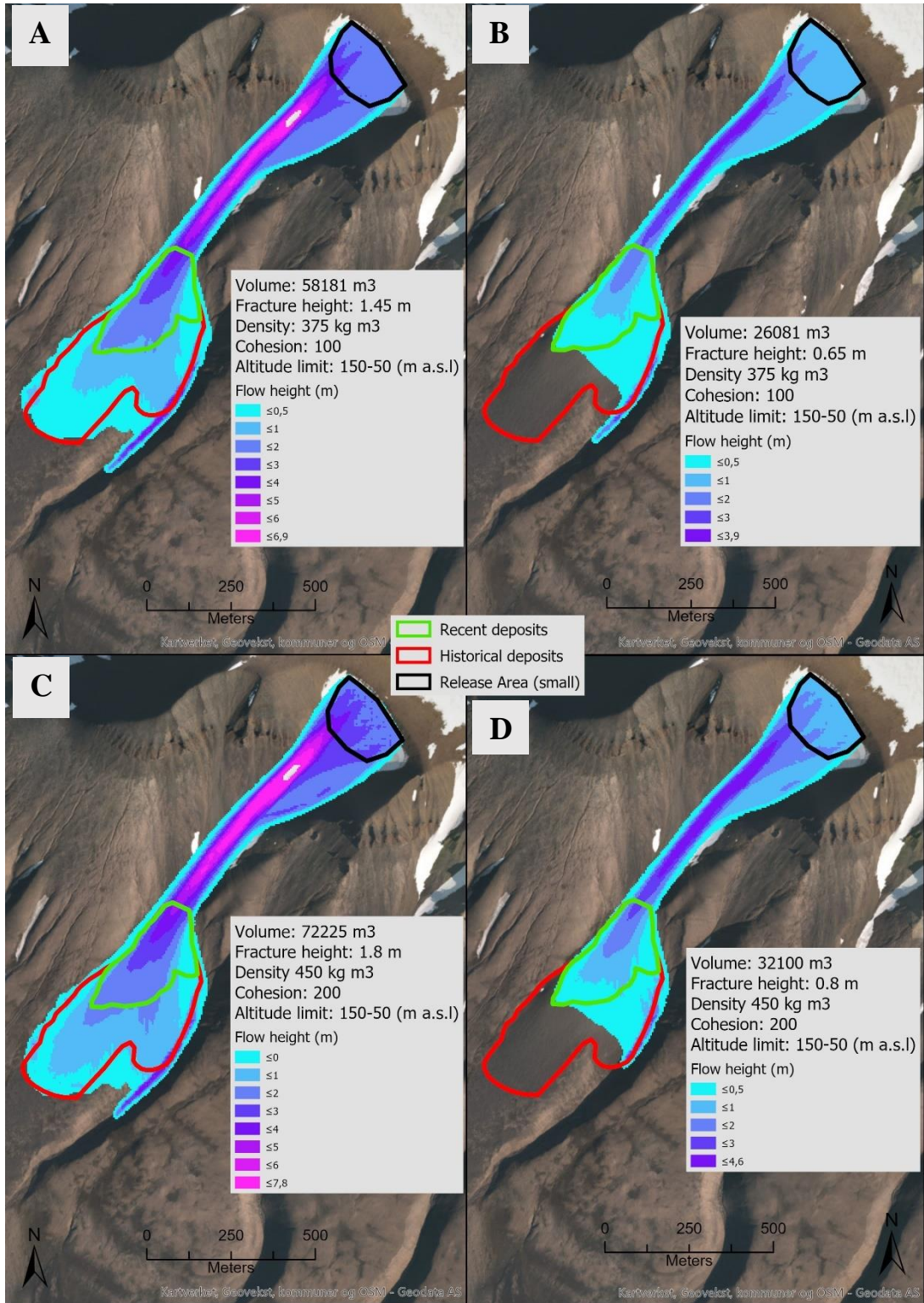


Figure 42. Visualization of RAMMS modelling results from Adventdalen with small release area. A and C show the historical runout result. B and D show the recent runout. A and B represents modeling of dry slab avalanches with a cohesion of 100, compared to C and D which represents wet slab avalanches with a cohesion of 200.

Modelling results: large release

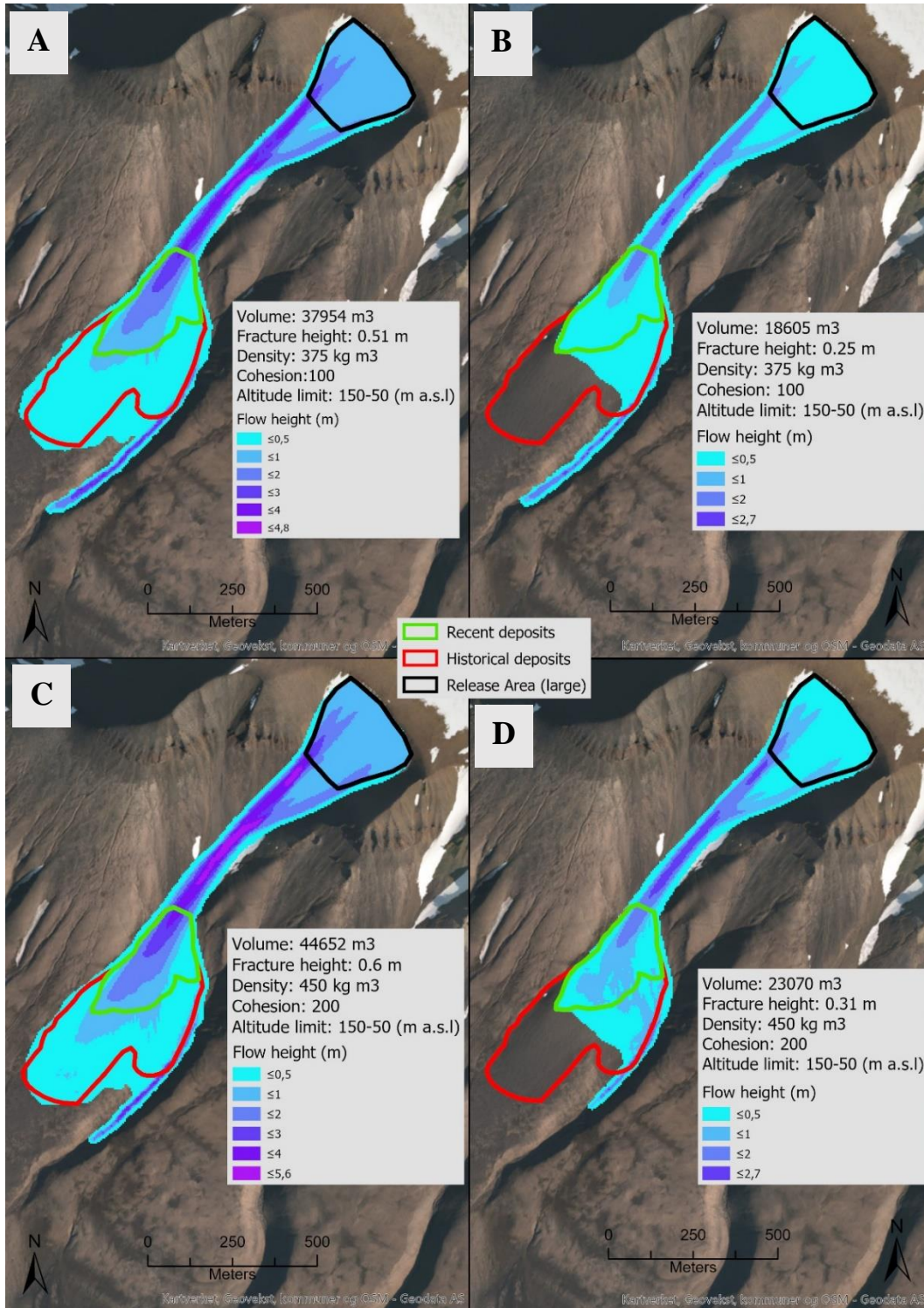


Figure 43. Visualization of RAMMS modelling results from Adventdalen with large release area. A and C show the historical runout result. B and D show the recent runout. A and B represents modeling of dry slab avalanches with a cohesion of 100, compared to C and D which represents wet slab avalanches with a cohesion of 200. Larger release area resulted in lower volume and fracture height compared to smaller release area.

The entire release area connected to the fan in Adventdalen is very large. Therefore, two scenarios were run with one large (Fig. 43) and one small release area (Fig 42). The large release area represents failure of the entire release area, while the smaller release area represents a scenario where a smaller part of the release area fails. Comparison was made to investigate whether it is necessary for the entire release area to fail to produce the necessary runout for fan development, or if partial failure also is probable of producing the same results. The difference in release area size had large impact on the fracture height and volume necessary to reconstruct the recent and historical avalanches. Table 13 shows the comparison between modelling the same runout with small and large release area. Modelling results with small release areas gave a fracture height of 0.65 m to reach the recent deposits and 1.45 m to reach the historical runout for dry slab avalanches. Modelling with the larger release area on the other hand needed 0.25 m and 0.51 m to reach the respective runouts. The same trend is found when modelling wet slab avalanches. Small release area had a fracture height of 0.8m and 1.8m, while large release area needed 0.31 m and 0.6 m in fracture height. Increased fracture height resulted in higher release volumes and in some cases different avalanche volume classification (table 13). An increase from small to medium, and medium to large avalanche volume classification will have impacted the behavior of the avalanche, due to automatic adjustments of the friction parameters set by the global parameters in RAMMS. The large difference is reflected in the percentage increase where smaller release area resulted in 39-62% increase in volume and 158-200% increase in fracture height to reach to same runout (table 13).

AVALANCHE TYPE	COHESION	RUNOUT	RELEASE AREA SIZE	VOLUME (M ³)	VOLUME CLASSIFICATION	FRACTURE HEIGHT (M)	& INCREASE VOLUME	% INCREASE FRACTURE HEIGHT
Dry slab	100	Recent	Large	18605 m ³	Small	0.25 m	40 %	160 %
			Small	26081 m ³	Medium	0.65 m		
Dry slab	100	Historical	Large	37951 m ³	Medium	0.51 m	53 %	184 %
			Small	58181 m ³	Medium	1.45 m		
Wet slab	200	Recent	Large	23070 m ³	Small	0.31 m	39 %	158 %
			Small	32100 m ³	Medium	0.8 m		
Wet slab	200	Historical	Large	44652 m ³	Medium	0.6 m	62 %	200 %
			Small	72225 m ³	Large	1.8 m		

Table 13. Summary of modelling statistics and statistical comparison highlighting the percentage difference between modelling with small and large release area for the same runout.

As presented earlier, the increase in length from recent to historical deposits was 284 m or 71% (table 5). For dry slab avalanches to increase its length by 71%, an increase in fracture height and corresponding volume of 104% for the large release area was needed, and 123% increase for the small release (table 14). For wet slab avalanches, an 125 % increase for the small release area, and 94% for the large release area was needed (table 14). The modelling results indicates that both avalanche types must approximately double their size or more to reach the historical deposits, regardless of the size of the release area.

AVALANCHE TYPE	COHESION	RUNOUT	RELEASE AREA SIZE	VOLUME (M ³)	VOLUME CLASSIFICATION	FRACTURE HEIGHT (M)	% INCREASE VOLUME	% INCREASE FRACTURE HEIGHT
Dry slab	100	Recent		26081 m³	Medium	0.65 m		
		Historical	Small	58181 m³	Medium	1.45 m	+ 123 %	+ 123 %
Dry slab	100	Recent		18605 m³	Small	0.25 m		
		Historical	Large	37954 m³	Medium	0.51 m	+ 104%	+ 104%
Wet slab	200	Recent		32100 m³	Medium	0.8 m		
		Historical	Small	72225 m³	Large	1.8 m	+ 125 %	+ 125%
Wet slab	200	Recent		23070 m³	Small	0.31 m		
		Historical	Large	44652 m³	Medium	0.6 m	+ 94%	+ 94%

Table 14. Summary of modelling statistics highlighting the volume and fracture height increase necessary to reach the historical deposits for the same avalanche type.

Table 15 shows the difference between modelling the same runout with different cohesion values. An increase in cohesion, representing wet slab avalanches, leads to an increase in fracture height and volume compared to dry avalanche release. Regardless of release area size and runout distance, the percentage increase is rather similar. Comparing both runouts with the small release area gave an increase of 23% and 24%, while modelling with the large release area gave an increase of 24% and 18% (table 15). However, a 24% increase lead to a 35 cm increase in fracture height, which is significant (table 15).

AVALANCHE TYPE	COHESION	RUNOUT	RELEASE AREA SIZE	VOLUME (M ³)	VOLUME CLASSIFICATION	FRACTURE HEIGHT (M)	% INCREASE VOLUME	% INCREASE FRACTURE HEIGHT
Dry slab	100			26081 m³	Medium	0.65 m		
Wet slab	200	Recent	Small	32100 m³	Medium	0.8 m	+ 23%	+ 23%
Dry slab	100			58181 m³	Medium	1.45 m		
Wet slab	200	Historical	Small	72225 m³	Large	1.8 m	+ 24%	+ 24%
Dry slab	100			18605 m³	Small	0.25 m		
Wet slab	200	Recent	Large	23070 m³	Small	0.31 m	+ 24%	+ 24%
Dry slab	100			37954 m³	Medium	0.51 m		
Wet slab	200	Historical	Large	44652 m³	Medium	0.6 m	+ 18%	+ 18%

Table 15. Summary of modelling statistics highlighting the volume and fracture height difference between the two avalanche types, when the same runout was compared.

5.7.2 Todalen

In Todalen, RAMMS modelling was conducted on 6 northeast facing avalanche fans. The modelled avalanches were able to reach the desired runout, but in most cases extended too much to the sides. Modelling results for dry slab avalanche release is presented in figure 44 and wet slab avalanche release is presented in figure 45. No significant difference in shape is found between the dry and wet slab avalanches. Due to a general increase in volume for wet slab avalanches, these were found to have the highest flow heights up to 4.5 m and 8.5 m (Fig. 45). Dry slab avalanches reached a maximum flow height of 4.3 m and 7.6 m (Fig. 44). Compared to the avalanche fan in Adventdalen, modelling results only show one release area. The release areas varied in size and shape and had a large impact on the results. Fan nr. 5 and 6, in the southern end of the study area had relatively small release areas drawn. An unrealistically high fracture height had to be applied to reach the recent and historical runout (Fig. 44 and 45). Fan nr. 5 had only a 26 m or 7% increase in length from recent to historical runout (table 4), yet fracture height had to be increased by 57% and 61%, reaching up to 2m (table 15). Fan nr. 6 needed an astronomical 242% and 297% increase in fracture height, reaching up to 2.7 m, to match the historical runout (table 15). The results from fan nr. 5 and 6 are still presented in the tables below and marked with red, as they are not included in any calculations based on the entire dataset. Three statistical comparisons are made: (1) Calculating average fracture height, (2) calculating percentage increase of volume and fracture height from recent to historical runout and (3) Comparison between the different avalanche types, for the same runout.

Dry slab avalanche modelling

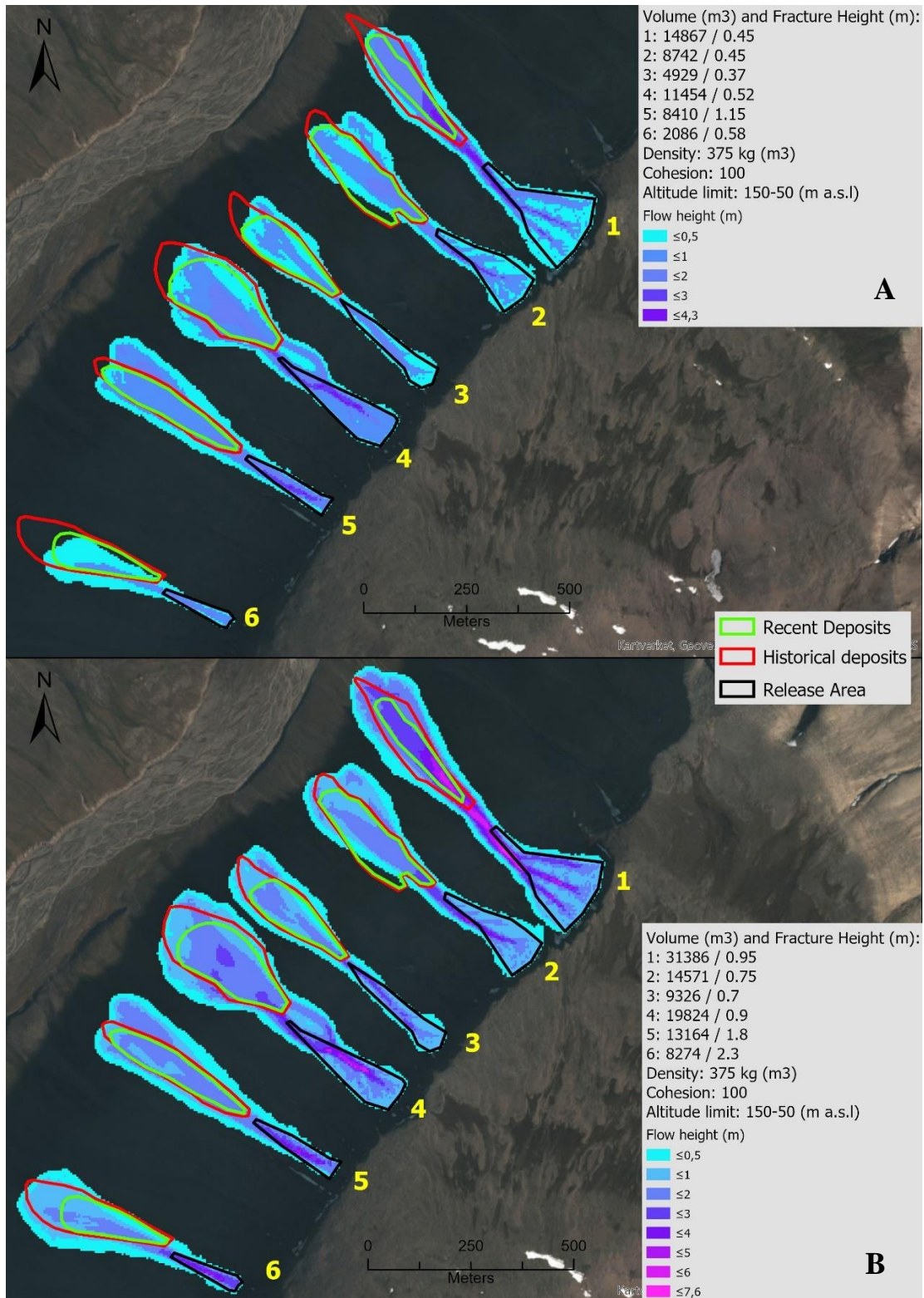


Figure 44. Visualization of the results from modelling dry slab avalanches in Todalen. (A) show the modelled avalanches reaching the recent deposits, and (B) show the modelled avalanches reaching the historical deposits.

Wet slab avalanche modelling

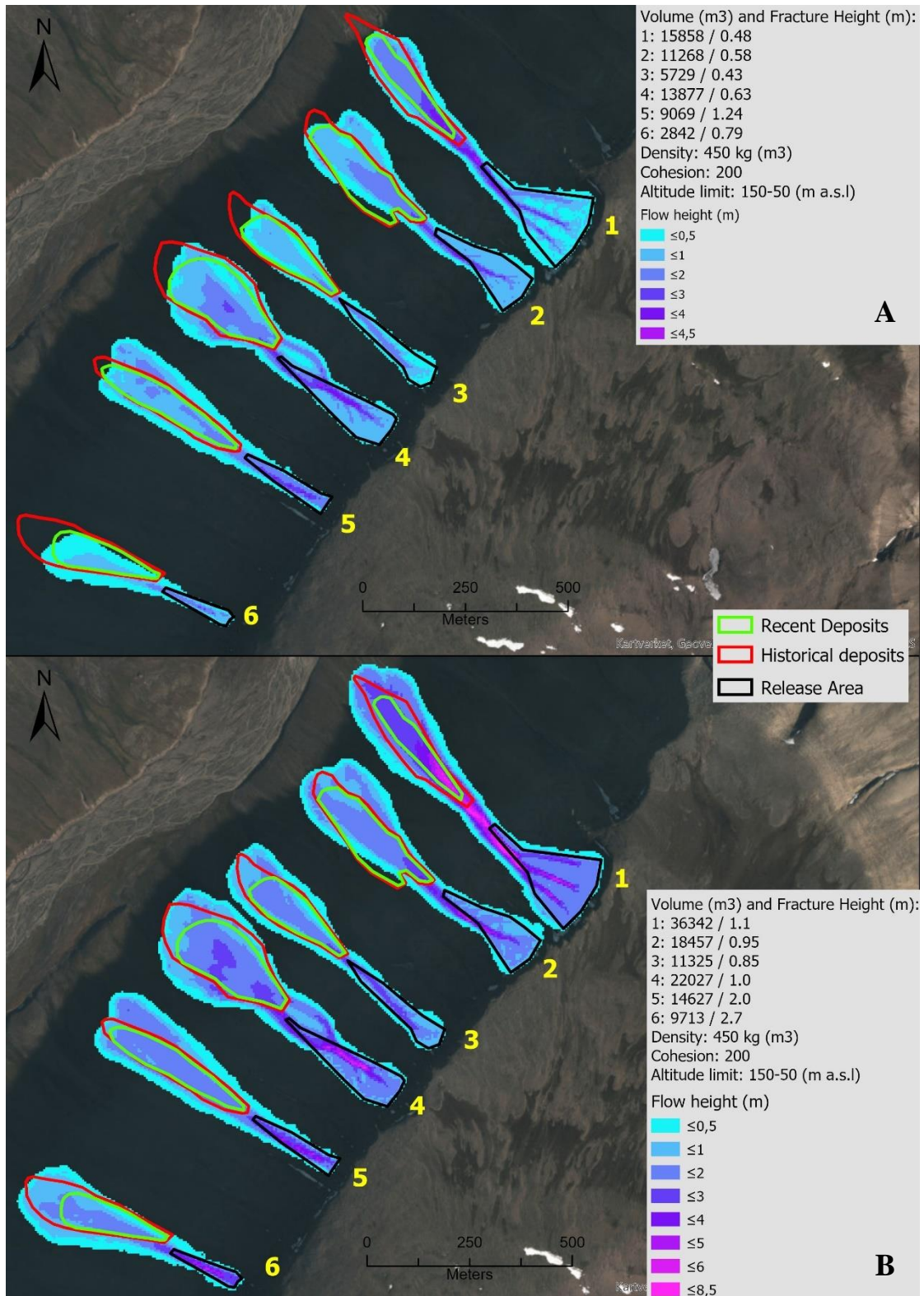


Figure 45. Visualization of the results from modelling wet slab avalanches in Todalen. (A) show the modelled avalanches reaching the recent deposits, and (B) show the modelled avalanches reaching the historical deposits.

Apart from fans 5 and 6, fracture heights were somewhat similar within each scenario (table 16). Fracture heights required for modelling dry slab avalanches reaching the recent deposits ranged from 0.37 m to 0.52 m, with an average fracture height of 0.44 m. To reach the historical runouts, the fracture heights ranged from 0.7 m to 0.95 m, averaging 0.82 m. Fracture heights for wet slab avalanches increased slightly ranging from 0.42 m to 0.62 m, averaging 0.52 m for the recent runout. For the historical runout, they ranged between 0.85 m to 1.1 m, averaging 0.97 m (table 16).

AVALANCHE TYPE	COHESION	RUNOUT	FAN ID	VOLUME (M ³)	VOLUME CLASSIFICATION	FRACTURE HEIGHT (M)	AVERAGE FRACTURE HEIGHT
Dry slab	100	Recent	1	14867	Small	0.45 m	0.44 m
			2	8742	Small	0.45 m	
			3	4929	Tiny	0.37 m	
			4	11454	Small	0.52 m	
			5	8410	Small	1.15 m	
			6	2086	Tiny	0.58 m	
Dry slab	100	Historical	1	31386	Medium	0.95 m	0.82 m
			2	14571	Small	0.75 m	
			3	9326	Small	0.7 m	
			4	19824	Small	0.9 m	
			5	13164	Small	1.8 m	
			6	8274	Small	2.3 m	
Wet slab	200	Recent	1	15858	Small	0.48 m	0.52 m
			2	14571	Small	0.58 m	
			3	9326	Small	0.42 m	
			4	19824	Small	0.63 m	
			5	13164	Small	1.24 m	
			6	8274	Small	0.79 m	
Wet slab	200	Historical	1	36342	Medium	1.1 m	0.97 m
			2	18457	Small	0.95 m	
			3	11325	Small	0.85 m	
			4	22027	Small	1 m	
			5	14627	Small	2 m	
			6	9713	Small	2.7 m	

Table 16. Summary of fan statistics from the avalanche modelling in Todalen, highlighting the average fracture height among all avalanches for each runout and avalanche type. The two fans (ID 5 and 6) marked in red is not included in the average fracture height calculation.

Both the dry slab scenario and the wet slab scenario show a significant increase in fracture height and volume in order to reach the historical runout (table 17). The average increase is almost identical, + 85 % for dry slab release and + 87%. However, large variation between the individual release areas exists, ranging from + 59% to + 129 % for wet slab avalanches and + 67 % to + 111 % for dry slab avalanches.

AVALANCHE TYPE	COHESION	RUNOUT	FAN ID	VOLUME (M ³)	VOLUME CLASSIFICATION	FRACTURE HEIGHT (M)	% INCREASE VOLUME	% INCREASE FRACTURE HEIGHT
Dry slab	100	Recent	1	14867	Small	0.45 m	+ 111%	+ 111%
		Historical	1	31386	Medium	0.95 m		
Wet slab	200	Recent	1	15858	Small	0.48 m	+ 129%	+ 129%
		Historical	1	36342	Medium	1.1 m		
Dry slab	100	Recent	2	8742	Small	0.45 m	+ 67%	+ 67%
		Historical	2	14571	Small	0.75 m		
Wet slab	200	Recent	2	11268	Small	0.58 m	+ 64 %	+ 64 %
		Historical	2	18457	Small	0.95 m		
Dry slab	100	Recent	3	4929	Tiny	0.37 m	+ 89%	+89%
		Historical	3	9326	Small	0.7 m		
Wet slab	200	Recent	3	5729	Small	0.42 m	+ 98 %	+102 %
		Historical	3	11325	Small	0.85 m		
Dry slab	100	Recent	4	11454	Small	0.52 m	+ 73 %	+ 73 %
		Historical	4	19824	Small	0.9 m		
Wet slab	200	Recent	4	13877	Small	0.63 m	+ 59 %	+59%
		Historical	4	22027	Small	1 m		
Dry slab	100	Recent	5	8410	Small	1.15 m	+ 57%	+57%
		Historical	5	13164	Small	1.8 m		
Wet slab	200	Recent	5	9069	Small	1.24 m	+ 61%	+ 61%
		Historical	5	14627	Small	2 m		
Dry slab	100	Recent	6	2086	Tiny	0.58 m	+ 297%	+ 297%
		Historical	6	8274	Small	2.3 m		
Wet slab	200	Recent	6	2842	Tiny	0.79 m	+ 242%	+ 242%
		Historical	6	9713	Small	2.7 m		
AVERAGE:	ALL						+ 86 %	+ 86 %
	DRY SLAB						+ 85 %	+ 85 %
	WET SLAB						+ 87 %	+ 88 %

Table 17. Summary of fan statistics from the avalanche modelling in Todalen, highlighting the increase in fracture height and volume necessary to reach the historical runouts. The two fans (ID 5 and 6) marked in red is not included in the average fracture height and volume calculation.

A general increase in volume and fracture height is also observed when comparing dry slab release and wet slab release with the same runout. The increase in cohesion lead to fracture heights increasing by +7% to + 29 %, averaging + 18% (table 18). The results indicate that wet slab avalanches need to be larger and trigger a weak layer deeper in the snowpack in order to run the same distance as a dry slab avalanche (explained further in discussion). However, the differences in cm are not very significant, especially at fan nr. 1, where + 7 % only represented a +3 cm increase in fracture height, and + 16% increase at fan nr. 3 constituted + 5 cm (table 18). When fracture heights were larger in general, the difference in cm increase became bigger.

AVALANCHE TYPE	COHESION	RUNOUT	FAN ID	VOLUME (M ³)	VOLUME CLASSIFICATION	FRACTURE HEIGHT (M)	% INCREASE VOLUME	% INCREASE FRACTURE HEIGHT
Dry slab	100	Recent	1	14867 m ³	Small	0.45 m		
Wet slab	200	Recent	1	15858 m ³	Small	0.48 m	+ 7%	+ 7%
Dry slab	100	Historical	1	31386 m ³	Medium	0.95 m		
Wet slab	200	Historical	1	36342 m ³	Medium	1.1 m	+ 16%	+ 16%
Dry slab	100	Recent	2	8742 m ³	Small	0.45 m		
Wet slab	200	Recent	2	11268 m ³	Small	0.58 m	+ 29%	+ 29%
Dry slab	100	Historical	2	14571 m ³	Small	0.75 m		
Wet slab	200	Historical	2	18457 m ³	Small	0.95 m	+ 27%	+ 27%
Dry slab	100	Recent	3	4929 m ³	Tiny	0.37 m		
Wet slab	200	Recent	3	5729 m ³	Small	0.42 m	+ 16%	+ 14%
Dry slab	100	Historical	3	9326 m ³	Small	0.7 m		
Wet slab	200	Historical	3	11325 m ³	Small	0.85 m	+ 21%	+ 21%
Dry slab	100	Recent	4	11454 m ³	Small	0.52 m		
Wet slab	200	Recent	4	13877 m ³	Small	0.63 m	+ 21%	+ 21%
Dry slab	100	Historical	4	19824 m ³	Small	0.9 m		
Wet slab	200	Historical	4	22027 m ³	Small	1 m	+ 11%	+ 11%
Dry slab	100	Recent	5	8410 m ³	Small	1.15 m		
Wet slab	200	Recent	5	9069 m ³	Small	1.24 m	+ 8%	+ 8%
Dry slab	100	Historical	5	13164 m ³	Small	1.8 m		
Wet slab	200	Historical	5	14627 m ³	Small	2 m	+ 11 %	+ 11%
Dry slab	100	Recent	6	2086 m ³	Tiny	0.58 m		
Wet slab	200	Recent	6	2842 m ³	Tiny	0.79 m	+ 36%	+ 36%
Dry slab	100	Historical	6	8274 m ³	Small	2.3 m		
Wet slab	200	Historical	6	9713 m ³	Small	2.7 m	+ 17 %	+ 17%
AVERAGE							+ 18 %	+ 18 %

Table 18. Summary of fan statistics from the avalanche modelling in Todalen, highlighting the volume and fracture height difference between the two avalanche types, when the same runout was compared.

Chapter 6. Discussion

This chapter considers the reconstruction of recent and historic avalanches in the Longyearbyen area, with the overall aim of determining what caused longer runouts observed in the past. The first section will discuss the results of the geomorphological and avalanche fan mapping, before moving on to the modelling results and a comparison of them to the meteorological and extreme precipitation analysis. An examination of what climatological changes could have been responsible for the larger avalanches of the past, observed in the geomorphological and avalanche fan mapping, follows.

6.1 Geomorphological mapping of avalanche fans

The primary goal of the geomorphological and avalanche fan mapping was to investigate the relationship between recent and historical avalanche runout lengths. Both De Haas et al. (2015) and Eckerstorfer (2013) noted the occurrence of recent, light-coloured sediments, draped over older, more extensive avalanche deposits in the Longyearbyen area, and interpreted as being from recent avalanche deposits.

All avalanches in this study displayed a snow avalanche-dominated surface morphology, even though debris flows were also present on several fans. All mapped avalanche deposits consist of perched boulders/cobbles, and GPS registration of the deposits was done with care to minimize the potential to incorrectly mapping debris flow deposits. The basic assumption underlining this thesis is that fan development is caused by avalanches during the entire, or large parts of the Holocene. The avalanche dominated surface morphology can mask other fan developing processes such as fluvial flow and debris flow, which could have been the major contributor to fan development in the past (De Haas et al., 2015). It is possible that the avalanche fan deposits that are visible today may only reflect a few major events which are draped over older debris flow deposits. Investigating the internal structure of the fan deposits would give answers to these questions (Blikra & Selvik, 1998). Nevertheless, the topography above the avalanche fans in Todalen, Longyeardalen and Adventdalen are not typical of fluvial flow, and the shape of the fans do not resemble that of fluvial flow or debris flow. In periglacial or paraglacial environments, avalanche landforms are considered short lived if conditions become less favorable for development (André, 2003, Ballantyne & Benn, 1994). Therefore, for large

avalanche fans to develop, enough debris needs to be available for transport, avalanche frequency must be high enough to transport the debris downhill, and the climate must be favourable for erosional avalanches (Luckman, 1977). Debris flows are active on the fans at present in Longyeardalen and Todalen, and in a significantly warmer climate, could potentially be a larger contributor to fan accretion if snow avalanches were absent. However, avalanches are considered the most important agent for fan development, due to the plateau margins favouring cornice growth and the characteristic tongue-shape of several large fans in the study area (Eckerstorfer et al., 2013a, 2013b; De Haas et al., 2015).

Twenty-four out of 28 avalanche fans investigated in Todalen, Adventdalen and Longyeardalen showed an increase in length between recent and historical deposits. Previous avalanche mapping demonstrated that these are not isolated phenomena in the area surrounding Longyearbyen (Fig. 1). All slope aspects show an increase in length from recent to historical deposits (Fig. 28, 33 and 34). The single WSW facing avalanche fan in Adventdalen showed the largest increase of 71% (table 5). The ESE facing fans in Longyeardalen showed the second highest increase by 33% on average (table 6), and the W and NW facing fans in Todalen had an average of 19% increase (table 4). Thus, the findings suggest that the length gap between recent and historical avalanche deposits is a result of larger avalanches that occurred in the past. The basic assumption underlying this statement is that only repeated avalanching occurring in the same location can develop distinct avalanche fans (Luckman, 1977). Large, but infrequent avalanches that run beyond the terminus of the fans do occur rarely, are not representative of the average, more frequent events necessary for fan formation. To summarize, at some point in the past, avalanches were consistently larger than they are today and occurred for a long enough period of time to produce distinct avalanche fans on the slopes around Longyearbyen. Eventually these avalanches decreased in size, and appear as lighter, smaller fan deposits resting on older, more extensive, and darker fan deposits.

Although the results show a clear trend of increasing length of historical deposits compared to recent deposits, there are still error margins in the methods to be discussed. A limitation of the study is the fact that the observations from Todalen are only based on GPS points rather than in combination with remote sensing. Orthophotos from Longyeardalen and Adventdalen clearly show the transition from the shorter, more recent, light colored sediments overlying darker, older

and more extensive fan deposits. In Todalen however, this cannot be seen on aerial imagery due to shadows on the orthophotos. As such, it was not possible to definitely verify if the GPS points accurately outline the boundary between recent and older deposits. Another drawback of the lack of remote sensing data at this site is that, without remote sensing to verify the deposits in the field (often one or two recently deposited rocks) could represent a single infrequent large avalanche event which does not represent the long-term average depositional pattern. On most fans, geomorphological mapping progressed from the historical deposits, upslope towards the younger deposits.

Consequently, there is a possibility that GPS points marking recent deposits were mapped according to the first visible deposits fan deposits, which may be related to larger events, not reflecting the long-term average events. An example of this is that only on two occasions the depositional boundary was identified on the orthophotos in Todalen. On those two occasions it was determined that there were 47 m and 10 m gaps between the GPS points and the outlines of recent deposits drawn on the aerial imagery (Fig. 28). Comparing the fan outline mapped through remote sensing and the GPS points, one GPS point representing historical deposits was also mapped 78 m outside the avalanche fan. Therefore, a combination of remote sensing and field mapping is preferable for obtaining the most accurate results. A second limitation, which remains largely unquantifiable, is to what degree snow cover limited the identification of recent deposits in the field. Ideally, the geomorphological mapping should have been conducted on a snow-free surface. Aerial photos taken by a drone would have been more effective without snow cover as well. Based on the outliers and the fact that geomorphological mapping occurred on the lower part of the fan, there is some probability that length differences between recent and historical deposits have been underestimated, could actually be even greater than that which was mapped in Todalen.

6.2 RAMMS modelling

Runout distances representing recent and historical avalanches were modelled on one avalanche fan in Adventdalen and 6 avalanche fans in Todalen. The purpose of the modelling was to identify to what degree the model parameters needed to be adjusted to reconstruct the longer historical runouts. The avalanche modelling in RAMMS show that a significant percentage increase in fracture height and volume is necessary to reproduce the larger historical avalanches.

In Todalen, the average increase in fracture height between recent and historical deposits was + 86 % (table 15), and in Adventdalen up to + 125 % (table 12). This implies a significant increase in snow depth or triggering of a persistent weak layer much deeper within the snowpack, both of which results in higher fracture height. A slight increase in fracture height and volume of 18 % on average in Todalen (table 16) and between 18-24 % in Adventdalen (table 13) was necessary for the wet slab avalanches to reach the recent and historical deposits compared to the dry slab avalanches. The increase is caused by the cohesion parameter, which helps the avalanche to stop earlier and limit diffusion of the flow (Bartelt et al., 2015). Cohesion was only recently implemented into RAMMS (Bühler et al., 2014), and previous modelling on Svalbard does not appear to have used the cohesion parameter when modelling the catastrophic avalanches in 2015 and 2017 (Issler et al., 2016; NVE, 2018). The cohesion parameter was based on the guidelines by Bühler et al. (2014), and the exact value was subjectively decided based on the back-calculation in Longyeardalen. The back-calculation turned out to be very important because low cohesion values increased the width and length of the avalanche by 10s of meters to the deposited mass (Bühler et al., 2014). However, the results indicate that wet slab avalanches need to be larger and trigger a weak layer deeper in the snowpack in order to run the same distance as the dry slab avalanches.

The size of the release areas had a big impact on the fracture heights and volumes. Modelling in Todalen was based on failure of the entire release area, but on two occasions (fan 5 and 6, Fig. 44 and 45), the release area used was so small that it resulted in fracture heights up to 2.7 m (table 14), which is unrealistic in the current avalanche climate on Svalbard. Compared to the other fans (1-4), the release areas of 5 and 6 does not exhibit the same pronounced bowl-shaped release areas as the first four (Fig. 28). A more open slope beneath the plateau margin with several small chutes represent the release areas of fan 5 and 6 (Fig. 28). Avalanches must therefore have released on the open slope and been channelized by one or several chutes. Modelling with two different release area sizes on the Adventdalen fan resulted in an 158-200% increase in fracture height and 39-62 % increase in volume between the smaller and larger release area size for the same runout (table 11). This resulted in modelled fracture heights for wet and dry slab avalanches of 0.25 - 0.31 m for recent avalanches and 0.51 - 0.6 m for historical avalanches modelling with the large release area. Modelling with small release gave 0.65 – 0.8 m for recent avalanches and 1.45 - 1.8 m for historical avalanches. Based on the present avalanche

climate and TLS observations, fracture heights below 1 meter is common. However, fracture heights close to 1 meter or above is believed to cause large, destructive and infrequent avalanches (Landrø et al., 2016; Hancock et al., 2018; NVE, 2018). In Todalen, the fracture height ranged between 0.37 – 0.63 m for recent wet-and dry slab avalanches, and 0.7 -1.1 m for the historical avalanches. The fracture height of recent avalanches in Todalen and Adventdalen are within the range of what is interpreted as adequate for frequent avalanche release. Historical fracture depths on the other hand are considered with the range of infrequent, large avalanches. The variation in fracture depth is a combination between different sizes in release area, and different lengths of the avalanche fans. All fans have a slight variation in length, resulting in different avalanche volumes and fracture heights. In addition, each release area has different shapes and sizes, with impacts the size of the drawn release area in RAMMS. The difference in modelled release area size will impact the fracture height, as previous examples show by the difference between smaller and larger release area in Adventdalen, and the extreme values from Todalen (fan 5 and 6). For example, fracture heights up to 1.8 m in Adventdalen can be considered excessive. However, the length from the release area to the toe of fan is 1.5 km, which is around twice the distance as in Todalen and Longyeardalen. Thus, the 0.25-0.6 m modelled fracture height with large release area in Adventdalen appears to be an underestimation. This shows how sensitive the fracture heights and volumes are to the size of the release area, and thus, it would be wrong to claim with certainty that the modelled fracture heights are the precise representation of reality. Since deglaciation, rockwall retreat by cornice plucking and erosion by avalanches and rockfall has enlarged the release areas to the present size. Meaning that historical avalanches released in potentially smaller release areas, which would accumulate less snow than the larger release areas of today. If avalanches were bigger in the past, and they had smaller release area, it indicates that in order to reach the historical runout, more snow (thicker snowpack) had to be present to release the same volume.

It is difficult to determine changes in past meteorological conditions based on the modelling results alone. Avalanche frequency and size are determined by several factors (Luckman, 1977), in which the fracture height and volume only tell the size of the avalanche, but not what changes in meteorological or climatic conditions are responsible for the observed increase from recent to historical deposits. An increase weak layer depth, winter precipitation or storm intensity is perceived as a most common cause for an increase in avalanche size (Fitzharris & Bakkehøi,

1986; Eckert et al., 2010; Marienthal et al., 2012). However, a change in wind direction or higher average windspeeds would increase the snow accumulation in certain aspects without changing the amount of precipitation. Snow stratigraphy plays a large role in triggering depth of the weak layer and fracture propagation potential (Schweizer et al., 2003), while a change in temperature can lead to a change in snow metamorphism, which in turn influences the properties of the snowpack (Colbeck, 1991). Nevertheless, based on both the RAMMS modelling and the geomorphological mapping, a clear change in avalanche environment occurred at some point during the Holocene, which has caused larger fracture heights and volumes of frequent avalanche, compared to today. The results must be tied to climatic and meteorological conditions in order to give them some context, and the historical avalanche deposits should be dated and connected the Holocene climate records in order evaluate the timing and palaeoclimatic relevance.

The resolution of the digital elevation model (DEM) and fine-tuning the input values for parameters such as friction values, size of the release area, cohesion, and fracture height showed that model outputs are sensitive to small changes in input values. The DEM is considered the most important input requirement, and the resolution has a large impact on modelling results (Bartelt et al., 2017). Based on previous research (Bühler et al., 2011), the DEM resolution of 5x5m used in this thesis can be considered adequate for the modelling. However, avalanche fans develop over time, meaning that modelling on a DEM based on present-day topography does not perfectly represent the surface of the historical fan, especially during early development, when no deposits existed yet. The difference in fan shape would have impacted the avalanche flow and potentially runout length to an unknown extent. Similarly, along the plateau margins where cornice fall avalanches occur frequently, multiple avalanches can release in the same location within a single season (Eckerstorfer et al., 2013a), which was observed during the 2016/2017 winter season (Fig. 40). Additional snow deposited by a previous avalanche would have influenced the flow of the second avalanche releasing in the same location. Additional snow deposited by a previous avalanche can technically be added to the DEM in RAMMS (Bartelt et al., 2017), but this was not done in this thesis.

Back-calculations of avalanches in the same study area, or from observed avalanches in precisely the same location, are common methods used to validate the selected parameters (Christen et al.,

2010; Maggioni et al., 2012; Dreier et al., 2014). In this study, back calculations were performed in Longyeardalen, where several avalanches have been mapped with TLS. Longyeardalen has a similar valley profile to Todalen and was therefore considered representative. Along the plateau margins, cornice fall avalanches are the most frequent avalanche type (Eckerstorfer & Christiansen, 2011c), and cornice fall avalanches were responsible for several avalanches that released during four avalanche cycles in 2016/2017 and 2017/2018 (Hancock et al., 2020). The runout distance and volume of cornice fall avalanches are different to those of slab avalanches, and only 16 % of the cornice falls trigger a secondary slab avalanche (Eckerstorfer et al., 2011c). RAMMS was developed to model slab avalanches (Bartelt et al., 2017), and for the modelling to be valid, we must assume that the falling cornice triggered a secondary slab avalanche, or that the runout of cornice fall avalanches is equal to slab avalanches.

Friction values in RAMMS used in this study are based on case studies from Switzerland (Bartelt et al., 2017). Applying them to the high Arctic maritime snow climate on Svalbard will introduce uncertainties, as the avalanches in Switzerland behave differently than avalanches on Svalbard. However, friction values were based on the altitude limits used by NVE for back-calculating the 2015 and 2017 avalanches in Longyearbyen (NVE, 2018), and are considered adequate based on today's practice. Historical avalanches with friction values based on the present-day avalanche climate, might be a sub-optimal representation, because the avalanche climate was probably different in the past. An attempt to model with different friction parameters could have been made for the historical avalanches, but since there is no knowledge on previous avalanche climates on Svalbard, and friction values are already subject to uncertainties, adjusting the friction parameters even more would probably not yield any valuable results.

Apart from snow density, which was set to 375 kg m^3 (Winther et al., 2003) for dry slab avalanche release and 450 kg m^3 for wet slab avalanche release, fracture height and cohesion was the only parameter which was adjusted. Small changes in density values were found to have little impact on the runout results. Thus, friction values and size of the release area for each individual fan were unchanged to make comparison between the results easier. Based on the uncertainty regarding the size of the release area, and the applied fracture height and volume, to model recent and historical avalanches, emphasis should be placed on the percentage increase of the fracture heights and volumes, rather than their numerical value. During the RAMMS modelling when

adjustments to the fracture height was made in order to model the correct runout, the percentage increase of fracture height and volume remained rather similar, even if fracture height and volume changed between the different attempts, when the same fan-respective modelling parameters were kept.

6.3 Comparing modelled fracture heights with snow depth and extreme precipitation analysis

To verify whether the fracture heights used in the modelling are representative for the environment and give an indication on possible return period, they were compared to the extreme precipitation analysis and the snow depth changes. The analysis is suitable for direct-action avalanches, releasing in new snow, rather than climax-released avalanches. The values are only accurate if: (1) all the precipitation is measured at Svalbard Airport and (2), that precipitation at Svalbard Airport is representative of precipitation in Adventdalen and Todalen. As precipitation tends to come with high windspeeds and temperatures (Christiansen et al., 2013), the accumulation is strongly dependent on the wind direction and elevation. What falls as rain at Longyearbyen Airport, probably falls as snow in the release areas at higher elevations, especially the release area in Adventdalen, situated 650-850 m a.s.l. The fracture heights based on the 3-day sum cannot be applied across all aspects, as storm events and snow accumulation are controlled by the dominant wind direction. For example, northerly winds never bring precipitation in central Svalbard, in today's climate (Christiansen et al., 2013). Thus, applying the 3-day sum to the SSE facing avalanche fan in Adventdalen to estimate the return period is speculative.

High return periods of around 100 years or more are calculated for the historical deposits. Considering that the modelled release areas in Todalen have a westerly aspect, they would under current conditions, accumulate snow during winter storms. This implies that a significantly wetter climate had to be present in the past for frequent direct-action avalanches to release at such fracture heights. Since precipitation during the Holocene is unknown (Farnsworth, 2018), it is impossible to verify whether this statement is true or not. The fracture height for the historical runout is considered very high, especially since fracture heights greater than 1 m is large in the current avalanche climate (Hancock et al., 2018). Achieving a fracture height above 1 m would probably require meteorological events similar those that triggered the 2015 and 2017 avalanches in Longyearbyen (Issler et al., 2016; Landrø et al., 2017; Hancock et al., 2018). For avalanches

to release frequently on such fracture heights, a climate like the Norwegian Coastal climate (Bakkehoi, 1987) would be required. The high return periods can also imply that direct-action avalanches didn't contribute much to fan development due to their high fracture heights. Rather it strengthens the possibility that full-depth wet slab avalanches are the main contributor to fan development.

AVALANCHE TYPE	FAN ID	RUNOUT	LOCATION	FRACTURE HEIGHT	RETURN PERIOD: GEV + V. GRADIENT (3 DAY SUM)	RETURN PERIOD: GEV + UPWARDS CORRECTION + V. GRADIENT (3 DAY SUM)
Dry slab	1	Recent	Todalen	0.45 m	10 years	2 years
Dry slab	2	Recent	Todalen	0.45 m	10 years	2 years
Dry slab	3	Recent	Todalen	0.37 m	5 years	< 2 years
Dry slab	4	Recent	Todalen	0.52 m	20 years	2 years
Dry slab	1	Recent	Adventdalen (large)	0.25 m	< 2 years	< 2 years
Dry slab	1	Recent	Adventdalen (small)	0.65 m	20 years	2 years
Dry slab	1	Historical	Todalen	0.95 m	>100 years	20 years
Dry slab	2	Historical	Todalen	0.75 m	100 years	5 years
Dry slab	3	Historical	Todalen	0.7 m	100 years	5 years
Dry slab	4	Historical	Todalen	0.9 m	>100 years	10 years
Dry slab	1	Historical	Adventdalen (large)	0.51 m	10 years	< 2 years
Dry slab	1	Historical	Adventdalen (small)	1.45 m	>100 years	50 years

Table 19. The combined results showing the fracture height and the corresponding return periods, using the 3-day sum. Emphasis is placed on the GEV + V. gradient rather than the GEV analysis with upwards correction.

The estimated return periods of the avalanches heavily depend on which interpretation of the results are used (table 19). Return periods are much higher when only considering the Generalized Extreme Value (GEV) analysis without any correction. The 3-day sum with return period of 20 years gave a precipitation value of 36 cm, but snow depth changes from Gruvefjellet and Platåberget show that this occurred on multiple occasions during the same season. A clear uncertainty is that snow depth changes in this study are only based on one season of observations. However, as snow depth increased with over 28 cm five times within a single season, in the lack of better data, approximately 30 cm is considered to represent a 1-year return period. Therefore, it is interpreted that the GEV analysis without any correction is an underestimation of the true values.

Emphasis must be placed on either the GEV analysis corrected for the vertical gradient, or the GEV analysis with upwards correction based on Humlum (2002) and the vertical gradient. The calculations do not include correction for snowdrift, which would significantly increase the values based on estimations in table 9 and 10. The maximum snow depth change during the 2017-2018 winter season was 48 cm and 50 cm at Platåberget and Gruvefjellet, respectively (table 7 and 8). Those snow depths correlate with roughly a 5-year return period with the GEV analysis with upwards and vertical correction at both Todalen and Adventdalen (table 9 and 10). Nevertheless, at return periods of 10 years or more, precipitation values become very high. A comprehensive evaluation of the 2015 and 2017 avalanche that destroyed several houses in Longyearbyen was conducted by several organizations (NVE, 2018), including the Norwegian Geotechnical Institute (NGI) and the Norwegian Water Resources and Energy Directorate (NVE). NVE calculated with additional snowdrift, a 115 cm snow depth with 100-year return period, 160 cm and 195 cm for 1000 year and 5000-year return period, respectively. Comparing the results with the GEV analysis with upwards and vertical correction, indicates an overestimation of the true value, compared to 2015 and 2017 avalanche report (NVE, 2018).

The return periods based on the GEV analysis corrected for only the vertical gradient is interpreted as the most representative, since the other two analysis either underestimates, or overestimates the precipitation values. The return period for recent avalanches, based on 20th and 21th century precipitation measurements, range from less than 2 years to 20 years (table 19). The return periods should be viewed with relative care, as the return periods are calculated from the 2, 5, 10, 20, 50- and 100-year interval. Based on the snow depth analysis (table 7 and 8), a 20-year return period might be too conservative.

6.4 Comparison between factors determining avalanche release and fan sedimentation in Todalen, Longyeardalen and Adventdalen

6.4.1 The effect of snow depths, snow distribution and meteorological variables

The definition of potential snow depths in the release areas is crucial information for the potential runout distance, as the location of the weak layer within the snowpack and fracture propagation properties will determine the initial volume of the avalanche (Schweizer et al., 2003). Generally, a small initial volume leads to smaller run out distances, and large initial volume leads to larger avalanches with longer runout distances (Maggioni et al., 2002).

Snow accumulation on Svalbard is determined by the prevailing winter wind direction, and the wind direction of storms (Eckerstorfer et al., 2011c). The results from the meteorological and snow depth analyses show that even with little to no precipitation, several tens of cm of snow can accumulate on lee sides of ridges and plateau margins depending on the wind direction and windspeed (Table 7 and 8). Humlum (2002) discussed the uncertainties of precipitation measurements when modelling late 20th century precipitation in central Svalbard. The lack of agreement between precipitation measurements at Svalbard Airport AWS and observations made by locals (table 7 and 8), supports the notion that precipitation values are underestimated. However, an important factor determining snow accumulation is the availability of snow for transport prior to storm events. The combination of loose snow available for transport prior to the event, combined with significant amounts of precipitation showed the largest snow depth increases at both Gruvefjellet and Platåberget (table 7 and 8).

The differences in snow depths in the release area is reflected in snow sensor data from Platåberget and Gruvefjellet (Fig. 36). During the 2017/2018 snow season, wind speeds exceeding the threshold for snowdrift mainly came from the east, while the highest windspeeds were recorded from the south and east (Fig. 37). As a result, the NW facing Gruvefjellet not only had more than twice the snow depth compared to the SE facing Platåberget, but also experienced more episodes with significant snow depth increase (Fig. 36). The observed trend is also visible on the snow depth scans from Gruvefjellet and Platåberget. The snow depth is generally higher on the Gruvefjellet slope, but both locations have several meters of snow due to cross-loading from winds being redirected through the valley. Considering the influence of topography on local

wind direction (Christiansen et al., 2013), it can be assumed that even though Gruvefjellet AWS show regional trends, winds are redirected through the valleys, resulting in more cross loading than expected.

With the lack of snow depth measurements at Todalen and Adventdalen, assumptions must be made based on the data from Longyeardalen. The topography in Longyeardalen and Todalen have similar characteristics. Todalen exhibits the same plateau landscape and roughly the same valley orientation. Therefore, similar snow depositional patterns are expected. Additionally, the release areas in Todalen are located at approximately the same altitudes (300-500 m a.s.l) as the release areas in Longyeardalen (300-470 m a.s.l). Snow depths are therefore considered similar. The release area in Adventdalen is oriented towards the SSW, while the valley itself is oriented NE-SW. This makes estimation of snow distribution in the release area difficult, and a precise quantification of the snow depth cannot be made based on the data from Longyeardalen. Wind measurements from Svalbard Airport AWS show that winter wind direction is influenced by the valley orientation, and wind direction from the SE is pronounced due to the channelling effect (Christiansen et al., 2013). The eastern edge of the release area in Adventdalen is bound by a large ridge (Fig. 32), which can enhance cross loading accumulation into the release area with south-easterly winds. Considering the amount of cross loading in Longyeardalen, and the altitude of the release area (650-850 m a.s.l), it is interpreted that significant amounts of snow can accumulate in the SSW facing release area. This assumption is further strengthened by the fact that snow patches are visible on the aerial imagery of the release area during summer (Fig. 32), even though solar insolation is strong on southerly slopes.

The results suggest that with present day precipitation and wind direction during periods with snowdrift, enough snow can accumulate on both westerly and easterly slopes to produce large avalanches. An example of this is shown in figure 33, where two avalanche fans at Platåberget in Longyeardalen show no difference between recent and historical deposits (table 6). Additionally, one avalanche occurring on 21.01.2017 reached the road at the bottom of the valley at easterly facing Platåberget (Fig. 40). Prior to the 21.01.2017 avalanche, 18.5 mm precipitation came with westerly winds (table 9), causing significant accumulation in the release areas at Platåberget (Fig. 40). The combination of above average precipitation and cornice failure caused the release of a large enough avalanche to reach the toe of the fan. Therefore, a possible

explanation for the observed differences between recent and historical deposition can be a decrease in critical new snow accumulation, possibly in combination with the absence of cornice failure triggering a secondary avalanche in the new snow. However, this explanation only works for direct-action avalanches, which have restricted erosional capacity (Luckman, 1977).

Eckerstorfer & Christiansen (2011a) describes slab-avalanche release on Svalbard as being triggered in the upper snowpack due to presence of ice layers. The ice layers on Svalbard are caused by the mid-winter rain-on-snow events (Eckerstorfer & Christiansen, 2012), and Vikhamar-Schuler et al. (2016) found that these extreme winter warming events have increased in frequency during the 20th century. Buried ice masses favour facet growth, and can serve as bed surface, which is one of the prerequisites for slab avalanching. Eckerstorfer & Christiansen (2011a) noted that these ice layers usually survive most of the winter, and also that slab avalanches often trigger a weak layer in the old snowpack due to overburden from additional snow loading. Ice layers in the upper snowpack would therefore restrict the triggering depth of climax avalanches (Eckerstorfer & Christiansen, 2011a). The ice layers can protect the ground from avalanche erosion, limiting the number of erosional avalanches during a season.

Eckerstorfer & Christiansen (2012) analysed two mid-winter rain-on-snow events, where several slush and wet slab avalanches released and ran down to either flat or very gently sloped terrain. They concluded that the avalanche release was meteorologically controlled, as the avalanche cycles were characterized by high air temperatures above 0°C, precipitation as rain, and high wind speeds. The recurrence interval was, on the other hand high, falling in line with previous research in high latitude mountains (André, 1995; Rapp, 1985). However, no debris was found in either the slush or wet slab avalanche deposits during two mid-winter rain-on-snow events.

Sliding was suggested to have occurred on an ice layer within the snowpack, which prohibited full depth avalanches (Eckerstorfer & Christiansen, 2012). Thus, another potential explanation for the observed differences between recent and historical deposits on the avalanche fans is the potential triggering of deeper weak layers in historic events, due to the absence of, or decrease in ice layers in the upper snowpack, caused by extreme mid-winter rain-on-snow events.

6.4.2 The enigmatic Adventdalen fan; proposed mechanism to explain observed results

During the modelling and investigation of the avalanche fans, it became apparent that the avalanche fan in Adventdalen is controlled by other mechanisms outside of the current understanding that cornice fall avalanches are the controlling factor for fan development in central Svalbard (Siewert et al., 2012; Vogel et al., 2012; Eckerstorfer et al., 2013a, 2013b). As such, an alternative theory is developed for the avalanche fan in Adventdalen.

Avalanche activity in central Svalbard follows a temporal pattern, where activity increases significantly following the initiation of solar insolation from early March, and peaks in May (Vogel, 2010; Eckerstorfer & Christiansen, 2011c). Low-pressure systems are the primary cause for avalanche release, and over 50 % of the avalanches triggered are direct-action avalanches, releasing in new snow (Eckerstorfer & Christiansen, 2011c). Assuming that dirty spring avalanches and cornice fall avalanche are the primary contributor to avalanche fan sedimentation, the critical new snow depth should be of little importance to fan development. Only during spring when cornice fall trigger full-depth avalanches, can erosion occur along the avalanche track (Eckerstorfer et al., 2013a). The timing of avalanche release, especially cornice fall avalanches is therefore an important factor for the fan development. Since cornices form and detach annually in the same location, 45 % of all reported avalanches around Longyearbyen are cornice fall avalanches (Eckerstorfer & Christiansen, 2011c), which reflects why cornice fall avalanches are cited as the controlling factor on avalanche fan development and rockwall retreat rates (Siewert et al., 2012; Humlum et al., 2007; Eckerstorfer et al. 2013a, 2013b; De Haas et al., 2015).

In Longyeardalen, which has been investigated by several researchers (Vogel et al., 2012; Siewert et al., 2012; Eckerstorfer et al., 2013a, 2013b), the evidence is clear that cornice fall avalanches are the dominant factor on fan development today. Cornice formation above steep rockwalls allow rockfall and cornice plucking to feed the slope with fresh material (Vogel et al., 2012), so that direct-action avalanches can add sediments to the fan even at mid-winter (Eckerstorfer et al., 2013a). This is not the case for the release area and track feeding the SSW facing avalanche fan in Adventdalen (Fig. 46). Rockfall occurs from the steep left slope, but the topography and prevailing wind direction today limit the potential for cornice development.

Compared to the release areas in Longyeardalen and Todalen, which have a rock face above 50°, the release area in Adventdalen has a mean slope angle of only around 35°. If cornices and rockfall are of little importance due to the absence of a pronounced steep rockwall and the lack of a favourable wind direction for cornice development, only full-depth avalanches and slush avalanches can contribute to fan sedimentation in Adventdalen. Comparing the size of the release area in Adventdalen with the release areas in Todalen and Longyeardalen (fig 46), the release area in Adventdalen is much bigger. Indicating that even without cornice fall avalanches, rockwall retreat is more pronounced than in Todalen and Longyeardalen, where cornice fall avalanches are present. The SSW avalanche fan in Adventdalen (Fig. 46) does not exhibit the surface morphology, nor the release area characteristics of slush avalanches. Therefore, it seems highly unlikely that the fan is dominated by slush avalanches. This leaves us with the conclusion that the avalanche fan in Adventdalen is most likely dominated by full-depth wet slab avalanches rather than cornice fall avalanches. However, as pointed out by Eckerstorfer & Christiansen (2012), meteorologically controlled wet slab avalanches do not necessarily erode due to significant ice layers within the snowpack. This implies that, assuming ice layers were present in the past, the SSW avalanche fan in Adventdalen most likely developed during late spring when the lower slope would be more or less snow free, allowing for erosion along the track at lower elevations. As discussed earlier, ice layers may have been non-existent or less significant in the past. Even if rain-on-snow events were of little importance, wet slab failure would occur during spring, as they would not be meteorologically controlled by the extreme mid-winter events. Rather rain-on-snow events could have occurred primarily during spring when temperatures naturally started rising.

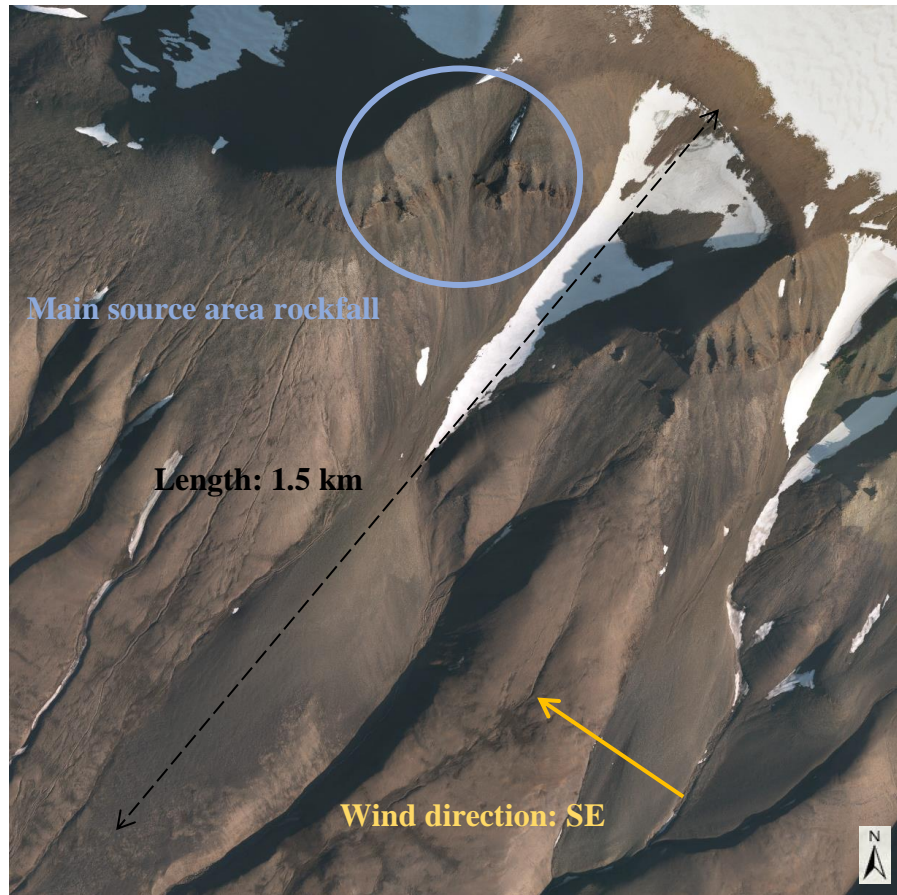


Figure 46. Overview of the avalanche fan in Adventdalen. Main source area for rock fall feeding the avalanche fan is marked with blue circle. The prevailing wind direction from the southeast is marked with yellow arrow. The total length is approx. 1.5 km and a vertical drop of 650 m from 850 m a.s.l to 200 m a.s.l

The avalanche fan in Adventdalen is 1.5 km long (Fig. 46) which is over twice the length compared to fans in Longyeardalen and Todalen. In addition, the Adventdalen fan exhibits the largest gap between recent and historical deposits of + 77%. Modelling results showed that fracture heights potentially reaches up to 1.8 m and avalanches volumes up to 72225 m³ is needed for the wet slab avalanches to reach the historical runout (table 14). Considering the length at which the sediments are deposited and the RAMMS results, very large avalanches, uncommon in today's avalanche climate, are needed to frequently release. Such fracture heights and volumes are interpreted to only be achievable by full-depth avalanches, because they can trigger a persistent weak layer deep within the snowpack. The interpretation is further strengthened by the fact that the fan is south-facing, and would receive a significant amount of solar insolation during spring. The solar insolation causes increased snowmelt and probability of

wet slab avalanche release (Baggi & Schweizer, 2009). Eckerstorfer & Christiansen (2012) noted that meteorologically controlled avalanches had unusual long runout, and based on the avalanche monitoring over several years by Eckerstorfer (2013), modern dry slab avalanches is not likely to reach the same runout as the modern wet slab avalanches. To the author's knowledge, no avalanches have been observed to release onto the fan in Adventdalen in recent years. If large meteorologically controlled wet slab avalanches are infrequent today, and the avalanche fan in Adventdalen is interpreted as dominated by wet slab avalanches. Development must have occurred under a slightly different climatic setting that favoured wet slab avalanches more than today.

My interpretation that the avalanche fan in Adventdalen is the result of full-depth wet slab avalanches, is of potential importance since it indicates that cornice fall avalanches are only an important factor in fan development where topography favours them. Hence, cornice fall avalanches are not a requirement for significant bedrock weathering, erosion rates and fan sedimentation in central Svalbard, as full-depth wet slab avalanches, under favourable climatic and topographical settings, can be an equally effective geomorphological agent. Within the study areas, differences in the sizes of the source areas are observed at the slope scale, even when topography and orientation were similar (Fig. 28 and 33).

6.5 The palaeoclimatic significance of avalanche fans

The results from this thesis has shown that avalanche-dominated fans indicate important palaeoclimatic signals. Linking the observations and earlier discussion about determining factors on avalanche release and fan sedimentation to known Holocene climate fluctuations is difficult without dating the deposits, but the observations themselves can be used as a indication of earlier Holocene climatic and/or meteorological conditions.

The effect of morphological slope conditions is reflected in the previously discussed difference between the wet slab avalanche dominated fan in Adventdalen, and the cornice-fall dominated fans in Longyeardalen and Todalen. Source areas facing west have large potential of accumulating snow with the present wind conditions, but since all aspects have shown an increase in length for historical events, a general increase in precipitation is interpreted as the most logic explanation for the observed increase. Modern observations from Svalbard indicate

that avalanches release in cycles due to incoming low-pressure systems (Eckerstorfer & Christiansen, 2011b). This indicates that storm intensity was higher, bringing more precipitation in the past. An increase in precipitation could lead to larger direct-action avalanches, but also an increase in long term snow depth, which would cause larger wet slab avalanches during spring. The increase in modelled fracture depth and volume of + 86 % average in Todalen + 94 – 125 % in Adventdalen needed to reconstruct the historical deposits cannot be directly transferred into an equal amount of increase in precipitation. Important factors such as wind direction and windspeed will also influence snow accumulation rates, and has a bigger effect on the slope snow accumulation than the precipitation itself (Jaedicke & Sandvik, 2002). An example of the impact of wind direction on snow accumulation and avalanche size is the 2015 and 2017 avalanches, which destroyed several houses in Longyearbyen (Hancock et al., 2018). An abnormal wind direction caused extreme accumulation and avalanche release on a slope which previously had not been associated with such snowdrift events (Hancock et al., 2018). This highlights the fact that a slight shift in wind direction can have large implication on the spatial distribution of avalanche release and size. Even a small increase in precipitation does not necessarily explain the observed difference in snow depths in all aspects. Assuming that today's pattern with dominating wind direction from the SE was also valid for the past, an increase in precipitation would probably lead to mostly localized increase in snow depth on westerly slopes. Therefore, in the heavily wind-affected landscape on Svalbard, an increase in historical runouts on the easterly slopes is a strong indicator of a shift in palaeo-wind direction. Humlum et al (2007) argued that avalanche-derived rock glacier are indicators of palaeo-wind direction. What seems to be avalanche derived rock glaciers are frequently found on easterly aspects in the valleys around Longyearbyen (Tolgensbakk et al., 2001; Rubensdotter et al., 2015b; Geldard, 2019), many of which are found under plateau margins, suggesting cornice fall avalanches as the dominant factor in rock glacier formation (Humlum et al., 2007). The occurrence of avalanche derived rock glaciers on easterly slopes supports the suggestion that a shift wind direction has occurred until today, and that cornice fall activity was higher on the corresponding slopes in the past. More easterly winds, possibly in combination with higher precipitation would explain the +33 % increase between recent and historical deposits in Longyeardalen (Fig. 33 and table 6). Applying the High Arctic nivation process-form-sediment model by Christiansen (1998) could also help reconstruct palaeo-wind direction, and around Longyearbyen, evidence of potential

relict nivation hollows are found. Figure 47 shows what is interpreted as a nivation hollow just beneath Platåberget, facing NE towards Longyearbyen. The interpretation is further strengthened by the V-shaped fluvial gorge below, since a significant water source must have fed the stream in order to cause the gorge. At present no water source are found above, indicating that a permanent snowpatch must have been present. Due to the orientation towards the NE, prevailing snow-bearing winds must have come from W or SW, since today's SE wind direction is not able to sustain a permanent snowpatch.

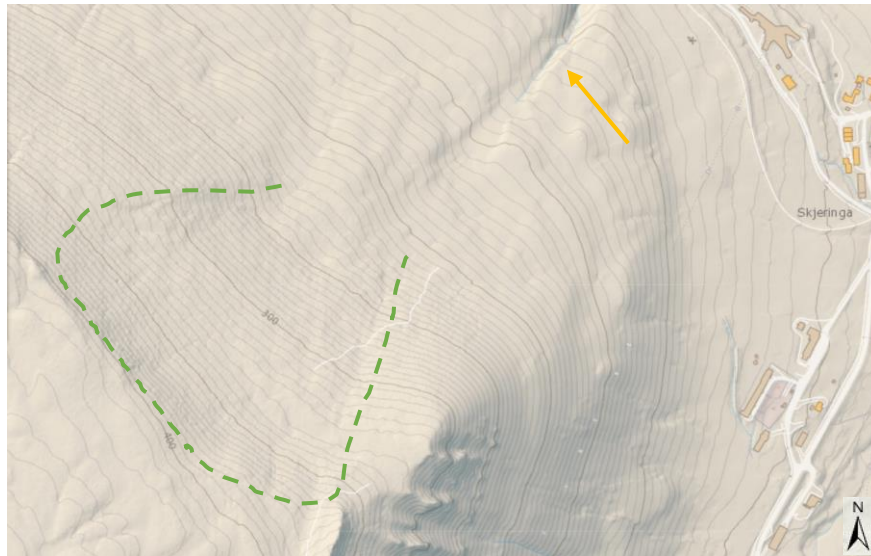


Figure 47. The dotted green line indicates the location of the relict nivation hollow, which during melting season fed the stream (yellow arrow) which created the V-shaped gorge underneath.

Past climatic changes during the Holocene on Svalbard, and air-ocean-land interactions may also help establishing an understanding of periods of increased and decreased avalanche activity and size. Retreating and re-advancing glaciers on Svalbard during the Holocene indicate changes in climate (Bond et al., 2001; Wanner et al., 2011; Farnsworth, 2018). Previous studies have shown correlation between glacier fluctuations and avalanche activity (Blikra & Selvik, 1998; Seierstad et al., 2002; Nesje et al., 2007; Vasskog et al., 2011). Glacial advance is closely linked with air temperature and precipitation, and glaciers can grow in response to an increase in snowfall and/or decrease in temperature (Nesje et al., 2008). Thus, the glacial advances on Svalbard during the Holocene might be connected to an increase in precipitation and correspondingly an increase in avalanche frequency and size. On Svalbard, climatically driven glacial re-advances

have been identified during both Early Holocene and Late Holocene (LIA) (Farnsworth, 2018). However, Longyearbyen and the surrounding area is believed to have deglaciated 10 ka BP (Svendsen & Mangerud, 1997), thus, many of the re-advances during Early Holocene before 10 ka BP would not have affected fan development here, as it would still be ice-covered. Interestingly, historical deposits in Bjørndalen show possible signs of having terminated in water, as one avalanche fan seems to have wave erosion at the toe at 27 m a.s.l (Fig. 48) (Rubensdotter et al., 2015a). A study of leaf wax hydrogen isotopes from north-western Svalbard indicate warmer and wetter climate during early the Holocene (12.8-7.5 ka BP), and Farnsworth (2018) argues that precipitation probably had a large, but unquantifiable, influence on the regional hydroclimate and glacier mass balance. If the interpretation is true, large snow avalanches must have occurred shortly after deglaciation in Bjørndalen when sea levels was still high (Salvigsen, 1984), indicating a wetter winter climate and high avalanche frequency during Early Holocene. Debris availability would in this period also be high due to paraglacial adjustment (Ballantyne, 2002), and dirty avalanches could therefore in effect carry more debris than avalanches to today.

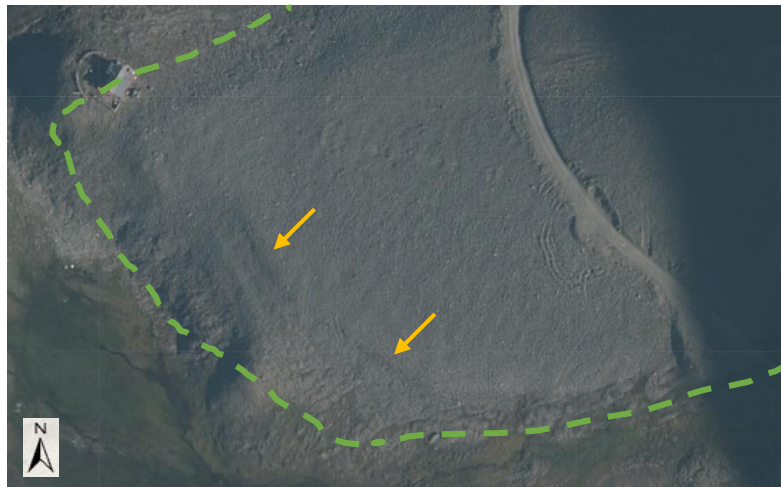


Figure 48. (A) Yellow arrows indicate where wave action possibly has eroded into the fan deposits. Dotted line shows the outline of the avalanche fan.

Considering that glacier re-advanced during the Late Holocene, this could be a strong indicator for increased precipitation, because one of the potential factors determining glacial advances is an increase in precipitation (Nesje et al., 2008). Assuming that an increase in precipitation caused the glacial re-advances, this means that precipitation came as snow at least down to the altitude of the release areas (minimum 300 m a.s.l). Glacial expansion during late Holocene is also linked with a general cooling in the North Atlantic region (Dansgaard, 1980; Nesje &

Kvamme 1991; Svendsen & Mangerud, 1997) which would have expanded the winter season and more precipitation would fall as snow. However, D'Andrea et al. (2013) argued that increased wintertime precipitation led to glacier advance rather than colder climate during the Little Ice Age (LIA). Evidence from western Scandinavia also suggest that changes in The North Atlantic oscillation (NAO) during the 18th century caused increased winter precipitation rather than low summer temperature (Nesje et al., 2008), which was positively correlated with winter precipitation in both Scandinavia and Svalbard (Dickson et al., 2000). If the LIA was controlled by winter precipitation, historical avalanche deposits might have a relatively young age. André (1995) also concluded that mass movements such as slush flows and debris flows were triggered by heavy rainfall during Late Holocene. This could imply that the fan in Adventdalen could have partly been developed by large, meteorologically triggered, wet slab avalanches.

A major influence on the regional climate is the West Spitsbergen current sea surface temperature, which strongly affects the regional sea ice extent (Walczowski & Piechura, 2011; Hanssen-Bauer, 2019). Modern field observations suggest a connection between increased temperature, decreasing sea ice extent and increase in precipitation on Svalbard (Nowak & Hudson, 2013; Isaksen et al., 2016; Kopec et al., 2016), and increased precipitation has been associated with warmer autumns and decrease in sea ice extent (Nowak & Hudson, 2013; Christiansen et al., 2013). Increasing ocean temperatures and a decrease in sea ice extent will for typically also increase the air temperature, and in effect increase moisture content the atmosphere (Christiansen et al., 2013). Thus, the complex relation between ocean temperatures, sea ice extent, air temperature and atmospheric circulation patterns has influenced the precipitation patterns during the Holocene, and could therefore in effect have governed avalanche regime. The unknown factor regarding precipitation increase is the seasonal timing, and how much the increase influences winter precipitation rather than summer precipitation. In addition, if the increase in precipitation comes as mild mid-winter rain-on-snow events and ice layers in the snowpack, the precipitation increase would most likely have no effect on the avalanche runoff. This conclusion comes from, as previously discussed, multiple ice layers are believed to restrict the avalanche release to the upper part of the snowpack, reducing avalanche size and runoff length and limit erosional capacity. The ideal scenario for longer avalanche runoff is interpreted from the modelling results as the combination between increased winter precipitation and the absence of internal ice layers.

Chapter 7. Conclusion

Svalbard is an ideal location to study snow avalanche deposits as the island is not influenced by high vegetation covering the deposits. This study is the first of its kind on Svalbard, trying to move beyond the previous research on Svalbard, in its attempt to obtain palaeoclimatic information, such as changes in precipitation and wind direction from observed changes in runout lengths of avalanches. The geomorphological impact of avalanches on past and present fan sedimentation is a complex relationship involving avalanche climatology, avalanche dynamics and terrain, all of which vary across short distances and time periods. Svalbard is one of the most climate sensitive places on earth, where small changes in ocean currents and temperatures, air temperature, sea ice extent, large-scale atmospheric circulation and glacial extent causes significant changes to the region's overall climate.

The results of this study indicate that avalanche fans on Svalbard contain important information about past climate conditions. The geomorphological and remote sensing evidence mapping show that in the modern avalanche climate, avalanche debris does not travel the full extent of the fan, which implies that larger avalanches released for an extended period of time in the past. Using dynamical avalanche modelling, the larger avalanche sizes and runout lengths of the past were shown to be dependent on much larger fracture heights and snow volumes. An increase in fracture heights and snow volumes were likely related to increased precipitation in the past. Furthermore, the long-term rockwall retreat and concomitant enlarging of release areas above the fans indicates that historical avalanches must have had smaller release areas, which indicates that a thicker snowpack had to be present to release the same volume. Mid-winter rain-on-snow events have reportedly increased during the 20th century (Vikhamar-Schuler et al., 2016), and a second explanation for the increase in avalanche size is the absence of ice layers caused by the mild warming events, which restrict avalanche release to the upper part of the snowpack.

Snow distribution on Svalbard is governed by the prevailing wind direction, and the largest snow depths are found in westerly slopes. Large avalanche fans are found in aspects not oriented according to the dominant wind direction, and the presence of relict snow patches and avalanche-derived rock glaciers in northeasterly and easterly aspects indicate a shift in wind direction from the west, which caused snow accumulation and larger avalanches on easterly slopes. Thus, this

study suggests that the larger avalanches of the past were related to increased precipitation, fewer rain-on-snow events, and possibly a different prevailing wind direction compared to today.

This investigation of avalanche fans suggests that the current hypothesis that cornice fall avalanches are the main factor controlling bedrock weathering, erosion rates, and fan sedimentation in central Svalbard (Eckerstorfer et al., 2013a), does not adequately explain the development of at least one avalanche fan in Adventdalen. Although avalanche fans in Todalen and Longyearbyen appear to be a result of cornice fall avalanches triggering secondary avalanches, the fan in Adventdalen (Fig. 46) has primarily been controlled by large and frequent full-depth wet slab avalanches during spring. This discovery indicates that further research into the cornice fall avalanches as a requirement for avalanche fan build-up is needed, and that climate conditions of the past favored large wet slab avalanches more than today in some settings.

Even though the avalanche deposits in central Svalbard must be dated to establish a solid link to the Holocene climatic record, periods of glacial re-advances and changes in air-ocean-land interactions can give clues to the timing of periods with increased avalanche size. Glacial re-advances during both Early Holocene and Late Holocene are sometimes connected to an increase in precipitation, and based on previous research, the longer avalanche runouts may have occurred. What appears to be wave erosion on the base of an avalanche fan in Bjørndalen indicates an Early Holocene age, when sea level was much higher, while other palaeo-precipitation studies indicate an increase in winter precipitation during the Little Ice Age (LIA), which would suggest a relatively young age for the historical deposits.

7.1 Future Studies

This thesis has tried to shed light on the interesting and complex subject of the spatial and temporal variability of avalanche release in central Svalbard. Due to the limited dataset, few field observations from the study sites due to cancellation of fieldwork, and the limited resources and scope of a master's thesis, more research is needed to answer the research question: on historical runout lengths of snow avalanches and what conditions had to be present for the larger avalanches to release. Further studies would increase our understanding of climate changes in the Holocene, especially palaeo-precipitation and wind, which remains largely unknown (Farnsworth, 2018). A better understanding of the climate and meteorological conditions required to produce larger avalanches would improve predictions of whether avalanches will become a greater hazard for the Longyearbyen community in the future. Below is a list of possible future research areas to explore:

1. Determine the age of the avalanche fan deposits by dating the material, and establish a link to the Holocene climate record.
2. Investigate the sedimentary facies/internal structure of the avalanche fans to get a better understanding of the palaeoclimatic signals, similar to the study by Blikra & Selvik (1998).
3. Reconstruct palaeo-wind direction by applying Christiansen's (1998) High Arctic nivation process-form-sediment model in order to understand whether avalanche size increased due to a shift in wind direction
4. Deepen our understanding of avalanche sedimentation in both cornice fall avalanches and slab avalanches, in order to establish the importance of each avalanche type, and the rate at which avalanche fans develop.
5. Investigate the influence of mid-winter rain-on-snow events, and how ice layers might restrict avalanche size and erosion.
6. Gain a better understanding of patterns of snow distribution and its importance for avalanche release and size, including triggering mechanism for wet slab avalanches and how they might have increased in frequency in response to climate change of the past.

References:

- Åkerman, H. J. (1984). Notes on talus morphology and processes in Spitsbergen. *Geografiska Annaler: Series A, Physical Geography*, 66(4), 267-284.
- Akitaya, E. (1974). Studies on depth hoar. *Contributions from the Institute of Low Temperature Science*, 26, 1-67.
- Albert, M. R., & Perron Jr, F. E. (2000). Ice layer and surface crust permeability in a seasonal snow pack. *Hydrological Processes*, 14(18), 3207-3214.
- André, M. F. (1990). Geomorphic impact of spring avalanches in Northwest Spitsbergen (79 N). *Permafrost and Periglacial Processes*, 1(2), 97-110.
- André, M. F. (1994). Rock glaciers in Svalbard: tentative dating and inferred long-term velocities. *Geografiska Annaler: Series A, Physical Geography*, 76(4), 235-245.
- André, M. F. (1995). Holocene climate fluctuations and geomorphic impact of extreme events in Svalbard. *Geografiska Annaler: Series A, Physical Geography*, 77(4), 241-250.
- André, M. F. (1996). Geological control of slope processes in northwest Spitsbergen. *Norsk Geografisk Tidsskrift-Norwegian Journal of Geography*, 50(1), 37-40.
- André, M. F. (1997). Holocene rockwall retreat in Svalbard: a triple-rate evolution. *Earth Surface Processes and Landforms: The Journal of the British Geomorphological Group*, 22(5), 423-440.
- André, M. F. (2003). Do periglacial landscapes evolve under periglacial conditions?. *Geomorphology*, 52(1-2), 149-164.
- Armstrong, R. L. (1980). An analysis of compressive strain in adjacent temperature-gradient and equi-temperature layers in a natural snow cover. *Journal of Glaciology*, 26(94), 283-289.
- Armstrong, R. L. (1985). *Metamorphism in a subfreezing, seasonal snow cover: The role of thermal and vapor pressure conditions* (Doctoral dissertation, University of Colorado).
- Armstrong, R. L., & Armstrong, B. R. (1987). Snow and avalanche climates of the western United States: a comparison of maritime, intermountain and continental conditions. *IAHS Publ*, 162, 281-294.
- Armstrong, R.L. & Brun, E., 2008. Snow and climate. *Physical Processes, Surface Energy Exchange and Modeling*. Cambridge University Press, Cambridge, UK.
- Arons, E. M., Colbeck, S. C., & Gray, J. M. N. T. (1998). Depth-hoar growth rates near a rocky outcrop. *Journal of Glaciology*, 44(148), 477-484.
- Baggi, S., & Schweizer, J. (2009). Characteristics of wet-snow avalanche activity: 20 years of observations from a high alpine valley (Dischma, Switzerland). *Natural Hazards*, 50(1), 97-108.
- Bakkehoi, S. (1987). Snow avalanche prediction using a probabilistic method. *IAHS Publ*, 162.
- Balascio, N. L., D'Andrea, W. J., Gjerde, M., & Bakke, J. (2018). Hydroclimate variability of High Arctic Svalbard during the Holocene inferred from hydrogen isotopes of leaf waxes. *Quaternary Science Reviews*, 183, 177-187.
- Ballantyne, C. K., & Benn, D. I. (1994). Paraglacial Slope Adjustment and Resedimentation following Recent Glacier Retreat, Fåbergstølsdalen, Norway. *Arctic and Alpine Research*, 26(3), 255-269.
- Ballantyne, CK, 2002. Paraglacial geomorphology. *Quaternary Science Reviews*, 21(18-19), 1935-2017. doi: 10.1016/S0277-3791(02)00005-7.
- Balstad, L, 1956. Kvinna på Svalbard. Forum, Stockholm.
- Bartelt, P., & McARDell, B. W. (2009). Granulometric investigations of snow avalanches. *Journal of Glaciology*, 55(193), 829-833.

- Bartelt, P., Bühler, Y., Christen, M., Deubelbeiss, Y., Salz, M., Schneider, M., Schumacher, L. (2017). RAMMS::AVALANCHE User manual v1.7.0. Available at: https://ramms.slf.ch/ramms/downloads/RAMMS_AVAL_Manual.pdf
- Bartelt, P., Valero, C. V., Feistl, T., Christen, M., Bühler, Y., & Buser, O. (2015). Modelling cohesion in snow avalanche flow. *Journal of Glaciology*, 61(229), 837-850.
- Bell, I., Gardner, J., & Scally, F. D. (1990). An estimate of snow avalanche debris transport, Kaghan Valley, Himalaya, Pakistan. *Arctic and Alpine Research*, 22(3), 317-321.
- Birkeland, K. W. (1998). Terminology and predominant processes associated with the formation of weak layers of near-surface faceted crystals in the mountain snowpack. *Arctic and Alpine Research*, 30(2), 193-199.
- Birkeland, K. W., Johnson, R. F., & Schmidt, D. S. (1998). Near-surface faceted crystals formed by diurnal recrystallization: A case study of weak layer formation in the mountain snowpack and its contribution to snow avalanches. *Arctic and Alpine Research*, 30(2), 200-204.
- Blair, T. C., & McPherson, J. G. (1994). Alluvial fans and their natural distinction from rivers based on morphology, hydraulic processes, sedimentary processes, and facies assemblages. *Journal of sedimentary research*, 64(3a), 450-489.
- Blair, T. C., & McPherson, J. G. (2009). Processes and forms of alluvial fans. In *Geomorphology of desert environments* (pp. 413-467). Springer, Dordrecht.
- Blake Jr, W. (2006). Occurrence of the *Mytilus edulis* complex on Nordaustlandet, Svalbard: radiocarbon ages and climatic implications. *Polar Research*, 25(2), 123-137.
- Blikra, L. H., & Nemeč, W. (1998). Postglacial colluvium in western Norway: depositional processes, facies and palaeoclimatic record. *Sedimentology*, 45(5), 909-960.
- Blikra, L. H., & Selvik, S. F. (1998). Climatic signals recorded in snow avalanche-dominated colluvium in western Norway: depositional facies successions and pollen records. *The Holocene*, 8(6), 631-658.
- Bond, G., Kromer, B., Beer, J., Muscheler, R., Evans, M. N., Showers, W., ... & Bonani, G. (2001). Persistent solar influence on North Atlantic climate during the Holocene. *science*, 294(5549), 2130-2136.
- Breyfogle, S. R. (1986). *Growth characteristics of hoarfrost with respect to avalanche occurrence* (No. FINAL TECH). Washington State Department of Transportation, Research Department.
- Brierley, G. J., Liu, K., & Crook, K. A. (1993). Sedimentology of coarse-grained alluvial fans in the Markham Valley, Papua New Guinea. *Sedimentary Geology*, 86(3-4), 297-324.
- Bühler, Y., Christen, M., Dreier, L., Feistl, T., & Bartelt, P. (2014). Merging of recent developments in avalanche simulation technology into practice. In *International Snow Science Workshop ISSW*.
- Bühler, Y., Christen, M., Kowalski, J., & Bartelt, P. (2011). Sensitivity of snow avalanche simulations to digital elevation model quality and resolution. *Annals of Glaciology*, 52(58), 72-80.
- Burrows, R., & McClung, D. M. (2006). Snow Cornice Development and Failure Monitoring. In *International Snow Science Workshop, Telluride Colorado* (Vol. 101, p. 21920).
- Cabanes, A., Legagneux, L., & Dominé, F. (2003). Rate of evolution of the specific surface area of surface snow layers. *Environmental science & technology*, 37(4), 661-666.
- Christen, M., Bartelt, P., & Kowalski, J. (2010). Back calculation of the In den Arelen avalanche with RAMMS: interpretation of model results. *Annals of Glaciology*, 51(54), 161-168.
- Christen, M., Kowalski, J., & Bartelt, P. (2010). RAMMS: Numerical simulation of dense snow avalanches in three-dimensional terrain. *Cold Regions Science and Technology*, 63(1-2), 1-14.
- Christiansen, H. H. (1998). Nivation forms and processes in unconsolidated sediments, NE Greenland. *Earth Surface Processes and Landforms: The Journal of the British Geomorphological Group*, 23(8), 751-760.

- Christiansen, H. H., Humlum, O., & Eckerstorfer, M. (2013). Central Svalbard 2000–2011 meteorological dynamics and periglacial landscape response. *Arctic, antarctic, and alpine research*, 45(1), 6-18.
- Colbeck, S. C. (1980). Thermodynamics of snow metamorphism due to variations in curvature. *Journal of Glaciology*, 26(94), 291-301.
- Colbeck, S. C. (1986). Classification of seasonal snow cover crystals. *Water Resources Research*, 22(9S), 59S-70S.
- Colbeck, S. C. (1987). A review of the metamorphism and classification of seasonal snow cover crystals. *IAHS Publication*, 162, 3-24.
- Colbeck, S. C. (1991). The layered character of snow covers. *Reviews of Geophysics*, 29(1), 81-96.
- Colbeck, S. C., & Jamieson, J. B. (2001). The formation of faceted layers above crusts. *Cold Regions Science and Technology*, 33(2-3), 247-252.
- Colbeck, S.C., 1982. An overview of seasonal snow metamorphism. *Reviews of Geophysics*, 20(1), pp.45–61.
- Colbeck, S.C., 1983. Theory of Metamorphism of Dry Snow. *J. Geophys. Res.*, 88(C9), pp.5475–5482. Available at: <http://dx.doi.org/10.1029/JC088iC09p05475>.
- Conway, H., & Raymond, C. F. (1993). Snow stability during rain. *Journal of Glaciology*, 39(133), 635-642.
- D’Andrea, W. J., Vaillencourt, D. A., Balascio, N. L., Werner, A., Roof, S. R., Retelle, M., & Bradley, R. S. (2012). Mild Little Ice Age and unprecedented recent warmth in an 1800 year lake sediment record from Svalbard. *Geology*, 40(11), 1007-1010.
- Dallmann, W.K., 2015. Geoscience atlas of Svalbard, Tromsø: Norsk Polarinstitut
- Dansgaard, W., Johnsen, S. J., Clausen, H. B., Dahl-Jensen, D., Gundestrup, N. S., Hammer, C. U., ... & Bond, G. (1993). Evidence for general instability of past climate from a 250-kyr ice-core record. *Nature*, 364(6434), 218-220.
- De Haas, T., Kleinhans, M. G., Carboneau, P. E., Rubensdotter, L., & Hauber, E. (2015). Surface morphology of fans in the high-Arctic periglacial environment of Svalbard: Controls and processes. *Earth-Science Reviews*, 146, 163-182.
- Decaulne, A., & Saemundsson, T. (2006). Geomorphic evidence for present-day snow-avalanche and debris-flow impact in the Icelandic Westfjords. *Geomorphology*, 80(1-2), 80-93.
- Deems, J. S., Gadowski, P. J., Vellone, D., Evanczyk, R., LeWinter, A., Birkeland, K., & Finnegan, D. C. (2015). Mapping starting zone snow depth with a ground-based Lidar to improve avalanche control and forecasting. In *Proceedings of the International Snow Science Workshop* (pp. 101-108).
- Deems, J. S., Painter, T. H., & Finnegan, D. C. (2013). Lidar measurement of snow depth: a review. *Journal of Glaciology*, 59(215), 467-479.
- Delmas, L., 2013. Spontaneous avalanche releases in Svalbard: influence of climate parameters on snow mechanical properties. Trondheim: Norwegian University of Science and Technology, Faculty of Engineering Science and Technology, Department of Civil and Transport Engineering.
- Dickson, R. R., Osborn, T. J., Hurrell, J. W., Meincke, J., Blindheim, J., Adlandsvik, B., ... & Maslowski, W. (2000). The Arctic ocean response to the North Atlantic oscillation. *Journal of Climate*, 13(15), 2671-2696.
- Divine, D., Isaksson, E., Martma, T., Meijer, H. A., Moore, J., Pohjola, V., ... & Godtlielsen, F. (2011). Thousand years of winter surface air temperature variations in Svalbard and northern Norway reconstructed from ice-core data. *Polar Research*, 30(1), 7379.
- Dorn, R. I. (1994). The role of climatic change in alluvial fan development. In *Geomorphology of Desert Environments* (pp. 593-615). Springer, Dordrecht.
- Dreier, L., Bühler, Y., Steinkogler, W., Feistl, T., & Bartelt, P. (2014). Modelling small and frequent avalanches. In *Proceedings of the International Snow Science Workshop ISSW, Banff* (Vol. 29, pp. 135-138).

- Dubé, S., Fillion, L., & Héту, B. (2004). Tree-ring reconstruction of high-magnitude snow avalanches in the northern Gaspé Peninsula, Québec, Canada. *Arctic, Antarctic, and Alpine Research*, 36(4), 555-564.
- Eckerstorfer, M. (2013). Snow avalanches in central Svalbard: a field study of meteorological and topographical triggering factors and geomorphological significance, Doctoral thesis, 56 pp, University of Oslo.
- Eckerstorfer, M., & Christiansen, H. H. (2011a). The “high Arctic maritime snow climate” in central Svalbard. *Arctic, Antarctic, and Alpine Research*, 43(1), 11-21.
- Eckerstorfer, M., & Christiansen, H. H. (2011b). Relating meteorological variables to the natural slab avalanche regime in High Arctic Svalbard. *Cold Regions Science and Technology*, 69(2-3), 184-193.
- Eckerstorfer, M., & Christiansen, H. H. (2011c). Topographical and meteorological control on snow avalanching in the Longyearbyen area, central Svalbard 2006–2009. *Geomorphology*, 134(3-4), 186-196.
- Eckerstorfer, M., & Christiansen, H. H. (2012). Meteorology, topography and snowpack conditions causing two extreme mid-winter slush and wet slab avalanche periods in High Arctic Maritime Svalbard. *Permafrost and Periglacial Processes*, 23(1), 15-25.
- Eckerstorfer, M., 2013. Snow avalanches in central Svalbard: A field study of meteorological and topographical triggering factors and geomorphological significance. Ph.D. Thesis. Available at: <https://www.duo.uio.no/handle/10852/34832>.
- Eckerstorfer, M., Christiansen, H. H., Rubensdotter, L., & Vogel, S. (2013a). The geomorphological effect of cornice fall avalanches in the Longyeardalen valley, Svalbard. *The Cryosphere*, 7(5), 1361.
- Eckerstorfer, M., Christiansen, H. H., Vogel, S., & Rubensdotter, L. (2013b). Snow cornice dynamics as a control on plateau edge erosion in central Svalbard. *Earth Surface Processes and Landforms*, 38(5), 466-476.
- Eckert, N., Baya, H., & Deschatres, M. (2010). Assessing the response of snow avalanche runout altitudes to climate fluctuations using hierarchical modeling: application to 61 winters of data in France. *Journal of Climate*, 23(12), 3157-3180.
- Eiken, M. (2017). *Dynamic avalanche modeling in Svalbard's arctic environment Terrestrial laser scanning as a tool for model verification* (Master's thesis). Available at: <https://www.duo.uio.no/handle/10852/55786>
- Ellehauge, J. 2003. Influence of meteorological and topographic conditions on snow avalanches in central Spitsbergen, Svalbard. MSc, University Centre in Svalbard, Longyearbyen.
- Farnsworth, W. R. (2013). The Topographical and Meteorological Influence on Snow Distribution in Central Svalbard: How the spatial variability of snow influences slopescale stability, permafrost landform dynamics and regional distribution trends, Master Thesis, 150 pp, University of Oslo
- Farnsworth, W. R., Ingólfsson, Ó., Noormets, R., Allaart, L., Alexanderson, H., Henriksen, M., & Schomacker, A. (2017). Dynamic Holocene glacial history of St. Jonsfjorden, Svalbard. *Boreas*, 46(3), 585-603.
- Farnsworth, W. R., Ingólfsson, Ó., Retelle, M., Allaart, L., Håkansson, L. M., & Schomacker, A. (2018). Svalbard glaciers re-advanced during the Pleistocene–Holocene transition. *Boreas*, 47(4), 1022-1032.
- Farnsworth, W.R., 2018. Holocene Glacier History of Svalbard: Retracing the Style of (De-)glaciation. Doctoral thesis. UiT The Arctic University of Norway, Tromsø, ISBN 978-82-8236-325-9, p. 226. Available at: <https://munin.uit.no/handle/10037/14378>
- Farnsworth, W.R., Ingólfsson, Ó., Alexanderson, H., Allaart, L., Forwick, M., Noormets, R., Retelle, M., Schomacker, A. (in review.): Holocene glacial and climate history of Svalbard - status, perspectives and challenges. *Earth-Science Reviews* (Oct. 2019 submission).
- Fierz, C., Armstrong, R.L., Durand, Y., Etchevers, P., Greene, E., McClung, D.M., Nishimura, K., Satyawali, P.K. and Sokratov, S.A. 2009. The International Classification for Seasonal Snow on the Ground. IHP-VII Technical Documents in Hydrology N°83, IACS Contribution N°1, UNESCO-IHP, Paris

- Fitzharris, B. B., & Bakkehøi, S. (1986). A synoptic climatology of major avalanche winters in Norway. *Journal of climatology*, 6(4), 431-446.
- Föhn, P. M. (2001). Simulation of surface-hoar layers for snow-cover models. *Annals of Glaciology*, 32, 19-26.
- Førland, E. J., & Hanssen-Bauer, I. (2000). Increased precipitation in the Norwegian Arctic: true or false?. *Climatic change*, 46(4), 485-509.
- Førland, E. J., Benestad, R., Hanssen-Bauer, I., Haugen, J. E., & Skaugen, T. E. (2011). Temperature and precipitation development at Svalbard 1900–2100. *Advances in Meteorology*, 2011.
- Førland, E. J., Hanssen-Bauer, I., & Nordli, P. Ø. (1997). Climate statistics and longterm series of temperature and precipitation at Svalbard and Jan Mayen. *Det Norske Meteorologiske Institutt Klima Report*, 21, 97.
- Fukuzawa, T., & Akitaya, E. (1993). Depth-hoar crystal growth in the surface layer under high temperature gradient. *Annals of Glaciology*, 18, 39-45.
- Gardner, J. (1970). Geomorphic significance of avalanches in the Lake Louise area, Alberta, Canada. *Arctic and Alpine Research*, 2(2), 135-144.
- Geldard, J. (2019). *The production of a Quaternary Geological map of Endalen, Svalbard, and assessment of Holocene geomorphic processes*. (Master thesis), The University of Sheffield.
- Germain, D., Filion, L., & Héту, B. (2009). Snow avalanche regime and climatic conditions in the Chic-Choc Range, eastern Canada. *Climatic Change*, 92(1-2), 141-167.
- Gjelten, H. M., Nordli, Ø., Isaksen, K., Førland, E. J., Sviashchennikov, P. N., Wyszynski, P., ... & Urazgildeeva, A. V. (2016). Air temperature variations and gradients along the coast and fjords of western Spitsbergen. *Polar Research*, 35(1), 29878.
- Glude, B. (2008). Faceted Melt Forms A Deadly And Unpredictable Weak Layer. In *Proceedings of the International Snow Science Workshop* (pp. 784-790).
- Gruber, U., & Bartelt, P. (2007). Snow avalanche hazard modelling of large areas using shallow water numerical methods and GIS. *Environmental Modelling & Software*, 22(10), 1472-1481.
- Hachikubo, A., & Akitaya, E. (1997). Effect of wind on surface hoar growth on snow. *Journal of Geophysical Research: Atmospheres*, 102(D4), 4367-4373.
- Hägeli, P., & McClung, D. M. (2003). Avalanche characteristics of a transitional snow climate—Columbia Mountains, British Columbia, Canada. *Cold Regions Science and Technology*, 37(3), 255-276.
- Hagen, J. O., Liestøl, O., Roland, E. R. I. K., & Jørgensen, T. (1993). *Glacier atlas of svalbard and jan mayen* (Vol. 129). Oslo: Norsk polarinstitutt.
- Hagen, J. O., Melvold, K., Pinglot, F., & Dowdeswell, J. A. (2003). On the net mass balance of the glaciers and ice caps in Svalbard, Norwegian Arctic. *Arctic, Antarctic, and Alpine Research*, 35(2), 264-270.
- Hancock, H. J. (2016). *Snow drift and avalanche activity in a high arctic maritime snow climate* (Doctoral dissertation, Montana State University-Bozeman, College of Letters & Science).
- Hancock, H., Eckerstorfer, M., Prokop, A., & Hendriks, J. (2020). Quantifying seasonal cornice dynamics using a terrestrial laser scanner in Svalbard, Norway. *Natural Hazards and Earth System Sciences*, 20(2), 603-623.
- Hancock, H., Prokop, A., Eckerstorfer, M., & Hendriks, J. (2018). Combining high spatial resolution snow mapping and meteorological analyses to improve forecasting of destructive avalanches in Longyearbyen, Svalbard. *Cold Regions Science and Technology*, 154, 120-132.
- Hanssen-Bauer, I., Førland, E. J., Hisdal, H., Mayer, S., Sandø, A. B., & Sorteberg, A. (2019). Climate in Svalbard 2100—a knowledge base for climate adaptation. *Norsk klimaservicesenter (NKSS)/Norwegian Centre for Climate Services (NCCS)*.

- Hanssen-Bauer, I., Kristensen Solås, M., & Steffensen, E. L. (1990). The climate of Spitsbergen. 39/90. *The Norwegian Meteorological Institute, Oslo*.
- Harris, C., Kern-Luetschg, M., Christiansen, H. H., and Smith, F., 2011. The role of interannual climate variability in controlling solifluction processes, Endalen, Svalbard. *Permafrost and Periglacial Processes*, 22: 239–253, <http://dx.doi.org/10.1002/ppp.727>.
- Harvey, A. M., Mather, A. E., & Stokes, M. (2005). Alluvial fans: geomorphology, sedimentology, dynamics—introduction. A review of alluvial-fan research. *Geological Society, London, Special Publications*, 251(1), 1-7.
- Heierli, J., Gumbsch, P., & Zaiser, M. (2008). Anticrack nucleation as triggering mechanism for snow slab avalanches. *Science*, 321(5886), 240-243.
- Hestnes, E. (1985). A contribution to the prediction of slush avalanches. *Annals of glaciology*, 6, 1-4.
- Hestnes, E. (1998). Slushflow hazard—where, why and when? 25 years of experience with slushflow consulting and research, *Annals of Glaciology*, 26, 370-376.
- Hestnes, E. (2000). Impact of rapid mass movement and drifting snow on the infrastructure and development of Longyearbyen, Svalbard. In *Proceedings of the International Workshop on Permafrost Engineering* (pp. 259-282).
- Heywood, L. (1988). Rain on snow avalanche events—Some observations. In *Proceedings of the 1988 international snow science workshop* (pp. 135-136).
- Humlum, O. (1998). The climatic significance of rock glaciers. *Permafrost and periglacial processes*, 9(4), 375-395.
- Humlum, O. (2002). Modelling late 20th-century precipitation in Nordenskiöld Land, Svalbard, by geomorphic means. *Norsk Geografisk Tidsskrift-Norwegian Journal of Geography*, 56(2), 96-103.
- Humlum, O. (2005). Holocene permafrost aggradation in Svalbard. *Geological Society, London, Special Publications*, 242(1), 119-129.
- Humlum, O., Christiansen, H. H., & Juliussen, H. (2007). Avalanche derived rock glaciers in Svalbard. *Permafrost and Periglacial Processes*, 18(1), 75-88.
- Humlum, O., Instanes, A., & Sollid, J. L. (2003). Permafrost in Svalbard: a review of research history, climatic background and engineering challenges. *Polar research*, 22(2), 191-215.
- Humlum, O., Solheim, J. E., & Stordahl, K. (2011). Identifying natural contributions to late Holocene climate change. *Global and Planetary Change*, 79(1-2), 145-156.
- Ingólfsson, Ó., & Landvik, J. Y. (2013). The Svalbard–Barents Sea ice-sheet—Historical, current and future perspectives. *Quaternary Science Reviews*, 64, 33-60.
- Isaksen, K., Nordli, Ø., Førland, E. J., Łupikasza, E., Eastwood, S., & Niedźwiedz, T. (2016). Recent warming on Spitsbergen—Influence of atmospheric circulation and sea ice cover. *Journal of Geophysical Research: Atmospheres*, 121(20), 11-913.
- Issler, D., & Gauer, P. (2008). Exploring the significance of the fluidized flow regime for avalanche hazard mapping. *Annals of Glaciology*, 49, 193-198.
- Issler, D., Jónsson, Á., Gauer, P., & Domaas, U. (2016). Vulnerability of houses and persons under avalanche impact—The avalanche at Longyearbyen on 2015-12-19. In *ISSW 2016-International Snow Science Workshop, Proceedings* (Vol. 371, p. 8).
- Iturrizaga, L. (2012). Talus cones as key landforms for reconstructing the extent of former glaciations. *Quaternary International*, (279-280), 217.
- Jaedicke, C. (2001). *Drifting snow and snow accumulation in complex Arctic terrain: field experiments and numerical modelling*. Geophysical Institute, University of Bergen.
- Jaedicke, C., and A. D. Sandvik (2002), High resolution snow distribution data from complex Arctic terrain: a tool for model validation, *Natural Hazards and Earth System Science*, 2(3/4), 147-155.

- Jaedicke, C., Thiis, T., Sandvik, A. D., & Gjessing, Y. (2000). Drifting snow in complex terrain-comparison of measured snow distribution and simulated wind field. In *Snow Engineering: Recent Advances and Developments. Proceedings of the Fourth International Conference on Snow Engineering. Norwegian University of Science and Technology*.
- Jahn, A, 1976. Contemporaneous geomorphological processes in Longyeardalen, Vestspitsbergen (Svalbard). *Biuletyn Peryglacjalny*, 26, pp. 25.
- Jahn, A. (1967). Some features of mass movement on Spitsbergen slopes. *Geografiska Annaler: Series A, Physical Geography*, 49(2-4), 213-225.
- Jamieson, B., & Stethem, C. (2002). Snow avalanche hazards and management in Canada: challenges and progress. *Natural Hazards*, 26(1), 35-53.
- Jamieson, B., Geldsetzer, T., & Stethem, C. (2000, October). Case study of a deep slab instability and associated dry avalanches. In *Presented at the International Snow Science Workshop in Big Sky*.
- Jamieson, B., Geldsetzer, T., & Stethem, C. (2001). Forecasting for deep slab avalanches. *Cold Regions Science and Technology*, 33(2-3), 275-290.
- Jamieson, J. B., & van Herwijnen, A. (2002, September). Preliminary results from controlled experiments on the growth of faceted crystals above a wet snow layer. In *Proceedings International Snow Science Workshop, Penticton BC, Canada*(Vol. 29, pp. 337-342).
- Jomelli, V., & Bertran, P. (2001). Wet snow avalanche deposits in the French Alps: structure and sedimentology. *Geografiska Annaler: series A, physical geography*, 83(1-2), 15-28.
- Jomelli, V., & Francou, B. (2000). Comparing the characteristics of rockfall talus and snow avalanche landforms in an Alpine environment using a new methodological approach: Massif des Ecrins, French Alps. *Geomorphology*, 35(3-4), 181-192.
- Jomelli, V., & Pech, P. (2004). Effects of the little ice age on avalanche boulder tongues in the French Alps (Massif des Ecrins). *Earth Surface Processes and Landforms: The Journal of the British Geomorphological Research Group*, 29(5), 553-564.
- Jomelli, V., Delval, C., Grancher, D., Escande, S., Brunstein, D., Hetu, B., ... & Pech, P. (2007). Probabilistic analysis of recent snow avalanche activity and weather in the French Alps. *Cold Regions Science and Technology*, 47(1-2), 180-192.
- Kattelmann, R. (1984). Wet slab instability. In *Proceedings International Snow Science Workshop, Aspen, Colorado, USA* (pp. 24-27).
- Katz, R. W., Parlange, M. B., & Naveau, P. (2002). Statistics of extremes in hydrology. *Advances in water resources*, 25(8-12), 1287-1304.
- Kaufmann, A., 2014. Snow avalanche hazard prediction and warning procedure in the Arctic environment U. på Svalbard & É. polytechnique fédérale de Lausanne, eds.
- Kesel, R. H. (1985). Tropical fluvial geomorphology. *Themes in Geomorphology. Croom Helm, London*, 102-121.
- Kopec, B. G., Feng, X., Michel, F. A., & Posmentier, E. S. (2016). Influence of sea ice on Arctic precipitation. *Proceedings of the National Academy of Sciences*, 113(1), 46-51.
- Kottek, M., J. Grieser, C. Beck, B. Rudolf, and F. Rubel (2006), World map of the Köppen-Geiger climate classification updated, *Meteorologische Zeitschrift*, 15(3), 259- 263.
- Krautblatter, M., & Dikau, R. (2007). Towards a uniform concept for the comparison and extrapolation of rockwall retreat and rockfall supply. *Geografiska Annaler: Series A, Physical Geography*, 89(1), 21-40.

- Kristiansen, M.A., 2014. Spatial variability of snow and avalanche conditions along a climatic gradient in Central Spitsbergen, Svalbard Spatial variability of snow and avalanche conditions along a climatic gradient in Central Spitsbergen, Svalbard (Master's thesis).
- Kumar, A., Perlwitz, J., Eischeid, J., Quan, X., Xu, T., Zhang, T., Hoerling, M., Jha, B., and Wang, W., 2010: Contribution of sea ice loss to arctic amplification. *Geophysical Research Letters*, 37(21)
- L. Rubensdotter, A. Romundset, W.R. Farnsworth and H.H. Christiansen, 2015: Landforms and sediments in, Bjørndalen-Vestpynten. Svalbard. Quaternary geological map, 1:10 000. Geological survey of Norway. ISBN 978-82-7385-158-1
- LaChapelle, E. R. (1966). *Avalanche forecasting-a modern syn* (Doctoral dissertation, thesis. International Association of Hydrological Sciences Publication, 69: 350-356).
- LaChapelle, E. R. (1969). Field guide to snow crystals.
- LaChapelle, E. R., & Armstrong, R. L. (1977). *Temperature Patterns in an Alpine Snow Cover and Their Influence on Snow Metamorphism*. COLORADO UNIV BOULDER INST OF ARCTIC AND ALPINE RESEARCH.
- Lacka, M., Zajączkowski, M., Forwick, M., & Szczuciński, W. (2014). Late Weichselian and Holocene paleoceanography of Storfjordrenna, southern Svalbard. *Clim Past Discuss*, 10, 3053-3095.
- Landrø, M., Mikkelsen, O.-A., Jaedicke, C., 2017. Gjennomgang og evaluering av skredhendelsen i Longyearbyen 21.02.2017. Oslo, Norway
- Larsen, E., Lyså, A., Rubensdotter, L., Farnsworth, W. R., Jensen, M., Nadeau, M. J., & Ottesen, D. (2018). Lateglacial and Holocene glacier activity in the Van Mijenfjorden area, western Svalbard. *arktos*, 4(1), 9.
- Larsson, S. (1982), Geomorphological effects on the slopes of Longyear valley, Spitsbergen, after a heavy rainstorm in July 1972, *Geografiska Annaler. Series A. Physical Geography*, 105-125.
- Laskar, J., Correia, A. C. M., Gastineau, M., Joutel, F., Levrard, B., & Robutel, P. (2004). Long term evolution and chaotic diffusion of the insolation quantities of Mars. *Icarus*, 170(2), 343-364.
- Laternser, M., & Schneebeli, M. (2002). Temporal trend and spatial distribution of avalanche activity during the last 50 years in Switzerland. *Natural Hazards*, 27(3), 201-230.
- Lawrence, D. M., Slater, A. G., Tomas, R. A., Holland, M. M., & Deser, C. (2008). Accelerated Arctic land warming and permafrost degradation during rapid sea ice loss. *Geophysical Research Letters*, 35(11).
- Lefsky, M. A., Cohen, W. B., Parker, G. G., & Harding, D. J. (2002). Lidar remote sensing for ecosystem studies: Lidar, an emerging remote sensing technology that directly measures the three-dimensional distribution of plant canopies, can accurately estimate vegetation structural attributes and should be of particular interest to forest, landscape, and global ecologists. *BioScience*, 52(1), 19-30.
- Legates, D. R., & Willmott, C. J. (1990). Mean seasonal and spatial variability in gauge-corrected, global precipitation. *International Journal of Climatology*, 10(2), 111-127.
- Lehning, M., Löwe, H., Ryser, M., & Raderschall, N. (2008). Inhomogeneous precipitation distribution and snow transport in steep terrain. *Water Resources Research*, 44(7).
- Li, L., & Pomeroy, J. W. (1997). Estimates of threshold wind speeds for snow transport using meteorological data. *Journal of Applied Meteorology*, 36(3), 205-213.
- Libbrecht, K. G. (2005). The physics of snow crystals. *Reports on progress in physics*, 68(4), 855.
- Luckman, B. H. (1977). The geomorphic activity of snow avalanches. *Geografiska Annaler: Series A, Physical Geography*, 59(1-2), 31-48.
- Luckman, B. H. (1992). Debris flows and snow avalanche landforms in the Lairig Ghru, Cairngorm Mountains, Scotland. *Geografiska Annaler: Series A, Physical Geography*, 74(2-3), 109-121.

- Luckman, BH, 1978. Geomorphic work of snow avalanches in the Canadian Rocky Mountains. *Arctic and Alpine Research*, 10(2), 261-276.
- Luckman, BH, 1988. Debris accumulation patterns on talus slopes in Surprise Valley, Alberta. *Geographie physique et Quaternaire*, 42(3), 247-278.
- Maggioni, M., Bovet, E., Dreier, L., Buehler, Y., Godone, D. F., Bartelt, P., ... & Segor, V. (2013). Influence of summer and winter surface topography on numerical avalanche simulations. In *International Snow Science Workshop* (pp. 591-598). ISSW Committee.
- Maggioni, M., Freppaz, M., Christen, M., Bartelt, P., & Zanini, E. (2012, September). Back-calculation of small avalanches with the 2D avalanche dynamics model RAMMS: four events artificially triggered at the Seehore test site in Aosta Valley (NW-Italy). In *Proceedings of the International Snow Science Workshop, 16–21 September 2012, Anchorage, Alaska*.
- Maggioni, M., Gruber, U., & Stoffel, A. (2002). Definition and characterisation of potential avalanche release areas. In *Proceedings of the ESRI Conference, San Diego*.
- Major, H., Haremo, P, Dallmann, WK, Andresen, A, Salvigsen, O (2001), Geological map of Svalbard 1: 100,000, sheet C9G Adventdalen, Norsk Polarinstitut.
- Mangerud, J., & Svendsen, J. I. (2017). The holocene thermal maximum around Svalbard, Arctic North Atlantic; molluscs show early and exceptional warmth. *The Holocene*, 28(1), 65-83.
- Mangerud, J., Bolstad, M., Elgersma, A., Helliksen, D., Landvik, J. Y., Lønne, I., ... & Svendsen, J. I. (1992). The last glacial maximum on Spitsbergen, Svalbard. *Quaternary Research*, 38(1), 1-31.
- Marbouty, D. (1980). An experimental study of temperature-gradient metamorphism. *Journal of Glaciology*, 26(94), 303-312.
- Marienthal, A., Hendrikx, J., Chabot, D., Maleski, P., & Birkeland, K. (2012, September). Depth hoar, avalanches, and wet slabs: a case study of the historic March, 2012 wet slab avalanche cycle at Bridger Bowl, Montana. In *Proceedings of the 2012 International Snow Science Workshop, Anchorage, AK* (pp. 62-68).
- McCarroll, D. (1993). Modelling late-Holocene snow-avalanche activity: incorporating a new approach to lichenometry. *Earth Surface Processes and Landforms*, 18(6), 527-539.
- McCarroll, D., Matthews, J. A., & Shakesby, R. A. (1995). Late-holocene snow-avalanche activity in southern Norway: Interpreting lichen size–frequency distributions using an alternative to simulation modelling. *Earth Surface Processes and Landforms*, 20(5), 465-471.
- McClung, D. M. (1979). Shear fracture precipitated by strain softening as a mechanism of dry slab avalanche release. *Journal of Geophysical Research: Solid Earth*, 84(B7), 3519-3526.
- McClung, DM, Schaerer, P, 2006. The Avalanche Handbook. 3rd edition. The Mountaineers, Seattle. pp. 342.
- Miller, D. A., Adams, E. E., & Brown, R. L. (2003). A microstructural approach to predict dry snow metamorphism in generalized thermal conditions. *Cold regions science and technology*, 37(3), 213-226.
- Miller, G. H., Geirsdóttir, Á., Zhong, Y., Larsen, D. J., Otto-Bliesner, B. L., Holland, M. M., ... & Anderson, C. (2012). Abrupt onset of the Little Ice Age triggered by volcanism and sustained by sea-ice/ocean feedbacks. *Geophysical Research Letters*, 39(2).
- Mock, C. J., & Birkeland, K. W. (2000). Snow avalanche climatology of the western United States mountain ranges. *Bulletin of the American Meteorological Society*, 81(10), 2367-2392.
- Montagne, J., J. McPartland, A. Super, and H. Townes (1968), The Nature and control of snow cornices on the Bridger Range, Southwestern Montana, Alta Avalanche Study Center Rep., Miscellaneous Report.
- Müller, J., & Stein, R. (2014). High-resolution record of late glacial and deglacial sea ice changes in Fram Strait corroborates ice–ocean interactions during abrupt climate shifts. *Earth and Planetary Science Letters*, 403, 446-455.

- Müller, J., Werner, K., Stein, R., Fahl, K., Moros, M., & Jansen, E. (2012). Holocene cooling culminates in sea ice oscillations in Fram Strait. *Quaternary Science Reviews*, 47, 1-14.
- Nemec, W., & Postma, G. (1993). Quaternary alluvial fans in southwestern Crete: sedimentation processes and geomorphic evolution. In *Alluvial sedimentation* (Vol. 17, pp. 235-276). Oxford: International Association of Sedimentologists.
- Nesje, A., & Kvamme, M. (1991). Holocene glacier and climate variations in western Norway: evidence for early Holocene glacier demise and multiple Neoglacial events. *Geology*, 19(6), 610-612.
- Nesje, A., Bakke, J., Dahl, S. O., Lie, Ø., & Bøe, A. G. (2007). A continuous, high-resolution 8500-yr snow-avalanche record from western Norway. *The Holocene*, 17(2), 269-277.
- Nesje, A., Dahl, S. O., Thun, T., & Nordli, Ø. (2008). The 'Little Ice Age' glacial expansion in western Scandinavia: summer temperature or winter precipitation?. *Climate dynamics*, 30(7-8), 789-801.
- Nordli, Ø., Przybylak, R., Ogilvie, A. E., & Isaksen, K. (2014). Long-term temperature trends and variability on Spitsbergen: the extended Svalbard Airport temperature series, 1898–2012. *Polar research*, 33(1), 213-49.
- Norges vassdrags og energidirektorat. (2014). Naturfareprosjektet: Delprosjekt 3.1. Hvordan beregne ekstremverdier for gitte gjentakintervaller? Manual for å beregne returverdier av nedbør for ulike gjentakintervaller (for ikke-statistiker). (NVE rapport nr 22/2014). Collected from: http://publikasjoner.nve.no/rapport/2014/rapport2014_22.pdf
- Norges vassdrags og energidirektorat. (2018). Skredrapport Sukkertoppen (NVE rapport nr 80/2018). Collected from: http://publikasjoner.nve.no/rapport/2018/rapport2018_80.pdf
- Nowak, A., & Hodson, A. (2013). Hydrological response of a High-Arctic catchment to changing climate over the past 35 years: a case study of Bayelva watershed, Svalbard. *Polar Research*, 32(1), 196-91.
- Pellaud, C., 2014. Snow avalanche hazard prediction for Longyear valley, based on avalanche run-out models and taking in account the prognoses for climate change U. på Svalbard & E. polytechnique de Lausanne, eds.
- Perla, R. (1977). Slab avalanche measurements. *Canadian Geotechnical Journal*, 14(2), 206-213.
- Perla, R. I., & Martinelli, M. (1976). *Avalanche handbook* (No. 489). US Department of Agriculture, Forest Service.
- Pielmeier, C., & Schneebeli, M. (2003). Developments in the stratigraphy of snow. *Surveys in geophysics*, 24(5-6), 389-416.
- Pinzer, B. R., Schneebeli, M., & Kaempfer, T. U. (2012). Vapor flux and recrystallization during dry snow metamorphism under a steady temperature gradient as observed by time-lapse micro-tomography. *The Cryosphere*, 6(5), 1141.
- Pomeroy, J. W. (1989). A process-based model of snow drifting. *Annals of Glaciology*, 13, 237-240.
- Pomeroy, J. W., and D. M. Gray (1990), Saltation of snow, *Water Resources Research*, 26(7), 1583-1594.
- Pomeroy, J. W., D. Gray, and P. Landine (1993), The prairie blowing snow model: characteristics, validation, operation, *Journal of Hydrology*, 144(1-4), 165-192.
- Pomeroy, J. W., P. Marsh, and D. Gray (1997), Application of a distributed blowing snow model to the Arctic, *Hydrological processes*, 11(11), 1451-1464.
- Prokop, A. (2008). Assessing the applicability of terrestrial laser scanning for spatial snow depth measurements. *Cold Regions Science and Technology*, 54(3), 155-163.
- Prokop, A. (2009, September). Terrestrial laser scanning for snow depth observations: An update on technical developments and applications. In *International snow science workshop* (Vol. 27, pp. 192-196).
- Prokop, A., Hancock, H., Praz, M., & Jahn, E. (2018). Slope scale avalanche forecasting in the arctic (Svalbard). In *International Snow Science Workshop, Innsbruck, Austria* (pp. 1035-1039).

- Prokop, A., Schirmer, M., Rub, M., Lehning, M., & Stocker, M. (2008). A comparison of measurement methods: terrestrial laser scanning, tachymetry and snow probing for the determination of the spatial snow-depth distribution on slopes. *Annals of glaciology*, 49, 210-216.
- Prokop, A., Schön, P., Singer, F., Pulfer, G., Naaim, M., Thibert, E., & Soruco, A. (2015). Merging terrestrial laser scanning technology with photogrammetric and total station data for the determination of avalanche modeling parameters. *Cold Regions Science and Technology*, 110, 223-230.
- Rapp, A (Ed.), 1985. Extreme rainfall and rapid snowmelt as causes of mass movements in high latitude mountains. Field and Theory. University of British Columbia Press.
- Rapp, A. (1959). Avalanche boulder tongues in Lappland: Descriptions of little-known forms of periglacial debris accumulations. *Geografiska Annaler*, 41(1), 34-48.
- Rapp, A. (1960a). Recent development of mountain slopes in Kärkevagge and surroundings, northern Scandinavia. *Geografiska Annaler*, 42(2-3), 65-200.
- Rapp, A. (1960b). Talus slopes and mountain walls at Tempelfjorden, Spitsbergen: a geomorphological study of the denudation of slopes in an arctic locality.
- Rapp, A. (1995). Case studies of geoprocesses and environmental change in mountains of northern Sweden. *Geografiska Annaler: Series A, Physical Geography*, 77(4), 189-198.
- Reardon, B. A., Pederson, G. T., Caruso, C. J., & Fagre, D. B. (2008). Spatial reconstructions and comparisons of historic snow avalanche frequency and extent using tree rings in Glacier National Park, Montana, USA. *Arctic, Antarctic, and Alpine Research*, 40(1), 148-160.
- Rees, W. G. (2005). *Remote sensing of snow and ice*. CRC press.
- Ritter, J. B., Miller, J. R., Enzel, Y., & Wells, S. G. (1995). Reconciling the roles of tectonism and climate in Quaternary alluvial fan evolution. *Geology*, 23(3), 245-248.
- Roch, A. (1949). *Report on Snow and Avalanches Conditions in the USA Western Ski Resorts from January 1st to April 24th, 1949*. Swiss Snow and Avalanches Research Institute.
- Rockström, J., Steffen, W., Noone, K., Persson, Å., Chapin, F. S., Lambin, E. F., ... & Nykvist, B. (2009). A safe operating space for humanity. *nature*, 461(7263), 472-475.
- Rogers, J. C., L. Yang, and L. Li (2005), The role of Fram Strait winter cyclones on sea ice flux and on Spitsbergen air temperatures, *Geophysical Research Letters*, 32(6).
- Røthe, T. O., Bakke, J., Støren, E. W., & Bradley, R. S. (2018). Reconstructing Holocene glacier and climate fluctuations from lake sediments in Vårfluesjøen, northern Spitsbergen. *Frontiers in Earth Science*, 6, 91.
- Rubensdotter, L., Stalsberg, K., Christiansen, H.H., Eckerstorfer, M. and Trøyen, P. (2015) Landforms and sediments in Todalen and upper Gangdalen and Bødalen. Quaternary geological map, 1:25,000. Geological Survey of Norway.
- Salm, B. (1993). Flow, flow transition and runout distances of flowing avalanches. *Annals of Glaciology*, 18, 221-226.
- Salm, B., Burkard, A., Gubler, H., 1990. Berechnung von Fliesslawinen: eine Anleitung für Praktiker mit Beispielen. Mitteilung 47, Eidg. Institut für Schnee- und Lawinenforschung SLF.
- Salvigsen, O., Forman, S. L., & Miller, G. H. (1992). Thermophilous molluscs on Svalbard during the Holocene and their paleoclimatic implications. *Polar Research*, 11(1), 1-10.
- Sass, O., Heel, M., Hoinkis, R., & Wetzler, K. F. (2010). A six-year record of debris transport by avalanches on a wildfire slope (Arnspitze, Tyrol). *Zeitschrift für Geomorphologie*, 54(2), 181-193.
- Scherer, D., Gude, M., Gempeler, M., & Parlow, E. (1998). Atmospheric and hydrological boundary conditions for slushflow initiation due to snowmelt. *Annals of glaciology*, 26, 377-380.

- Schmid, U. G., & Sardemann, S. (2003). High-frequency avalanches: release area characteristics and run-out distances. *Cold regions science and technology*, 37(3), 439-451.
- Schön, P., Prokop, A., Vionnet, V., Guyomarc'h, G., Naaim-Bouvet, F., & Heiser, M. (2015). Improving a terrain-based parameter for the assessment of snow depths with TLS data in the Col du Lac Blanc area. *Cold Regions Science and Technology*, 114, 15-26.
- Schweizer, J. (1999). Review of dry snow slab avalanche release. *Cold Regions Science and Technology*, 30(1-3), 43-57.
- Schweizer, J. (2017). On recent advances in avalanche research. *Cold Reg. Sci. Technol.* 30 (1-3), 43-57
- Schweizer, J., & Jamieson, J. B. (2001). Snow cover properties for skier triggering of avalanches. *Cold Regions Science and Technology*, 33(2-3), 207-221.
- Schweizer, J., & Kronholm, K. (2007). Snow cover spatial variability at multiple scales: Characteristics of a layer of buried surface hoar. *Cold Regions Science and Technology*, 47(3), 207-223.
- Schweizer, J., & Lütschg, M. (2001). Characteristics of human-triggered avalanches. *Cold Regions Science and Technology*, 33(2-3), 147-162.
- Schweizer, J., Bruce Jamieson, J., & Schneebeli, M. (2003). Snow avalanche formation. *Reviews of Geophysics*, 41(4).
- Schweizer, J., Kronholm, K., Jamieson, J. B., & Birkeland, K. W. (2008). Review of spatial variability of snowpack properties and its importance for avalanche formation. *Cold Regions Science and Technology*, 51(2-3), 253-272.
- Seierstad, J., Nesje, A., Dahl, S. O., & Simonsen, J. R. (2002). Holocene glacier fluctuations of Grovabreen and Holocene snow-avalanche activity reconstructed from lake sediments in Grningstlsvatnet, western Norway. *The holocene*, 12(2), 211-222.
- Seligman, G. (1936), *Snow Structure and Ski Fields*, International Glaciology Society, Cambridge, U.K.
- Senderak, K., Kondracka, M., & Gądek, B. (2017). Talus slope evolution under the influence of glaciers with the example of slopes near the Hans Glacier, SW Spitsbergen, Norway. *Geomorphology*, 285, 225-234.
- Sessford, E. G., Strzelecki, M. C., & Hormes, A. (2015). Reconstruction of Holocene patterns of change in a High Arctic coastal landscape, Southern Sassenfjorden, Svalbard. *Geomorphology*, 234, 98-107.
- Siewert, M. B., Krautblatter, M., Christiansen, H. H., & Eckerstorfer, M. (2012). Arctic rockwall retreat rates estimated using laboratory-calibrated ERT measurements of talus cones in Longyeardalen, Svalbard. *Earth Surface Processes and Landforms*, 37(14), 1542-1555.
- Skirbekk, K., Kristensen, D. K., Rasmussen, T. L., Koç, N., & Forwick, M. (2010). Holocene climate variations at the entrance to a warm Arctic fjord: evidence from Kongsfjorden trough, Svalbard. *Geological Society, London, Special Publications*, 344(1), 289-304.
- Sommerfeld, R. A., & LaChapelle, E. (1970). The classification of snow metamorphism. *Journal of Glaciology*, 9(55), 3-18.
- Sorbel, L., Tolgensbakk, J., Hagen, J.O., Hogvard, K., 2001. Geomorphological and quaternary geological map of Svalbard. 1:100,000. C9G Adventdalen. Norsk Polarinst. Temakart 31/32.
- Sovilla, B., Bartelt, P., 2002. Observations and modelling of snow avalanche entrainment. *Nat. Hazards Earth Syst. Sci.* 2, 169–179
- Sovilla, B., Margreth, S., & Bartelt, P. (2007). On snow entrainment in avalanche dynamics calculations. *Cold Regions Science and Technology*, 47(1-2), 69-79.
- Steffensen, J. P., Andersen, K. K., Bigler, M., Clausen, H. B., Dahl-Jensen, D., Fischer, H., ... & Masson-Delmotte, V. (2008). High-resolution Greenland ice core data show abrupt climate change happens in few years. *Science*, 321(5889), 680-684.

- Stethem, C., & Perla, R. (1980). Snow-slab studies at Whistler mountain, British Columbia, Canada. *Journal of Glaciology*, 26(94), 85-91.
- Stoffel, M., Bollschweiler, M., & Hassler, G. R. (2006). Differentiating past events on a cone influenced by debris-flow and snow avalanche activity—a dendrogeomorphological approach. *Earth Surface Processes and Landforms: The Journal of the British Geomorphological Research Group*, 31(11), 1424-1437.
- Sturm, M., & Benson, C. S. (1997). Vapor transport, grain growth and depth-hoar development in the subarctic snow. *Journal of Glaciology*, 43(143), 42-59.
- Sturm, M., Holmgren, J., & Liston, G. E. (1995). A seasonal snow cover classification system for local to global applications. *Journal of Climate*, 8(5), 1261-1283.
- Svendsen, JI, Mangerud, J, 1997. Holocene glacial and climatic variations on Spitsbergen, Svalbard. *The Holocene*, 7(1), 45-57. doi: 10.1177/095968369700700105.
- Takeuchi, M. (1980), Vertical profile and horizontal increase of drift-snow transport, *J Glaciol*, 26, 481-492.
- Thiedig, F., & Lehmann, U. (1973). Die Entstehung von Muren als säkulares Ereignis auf Spitzbergen (Svalbard) und ihre Bedeutung für die Denudation in der Frostschuttzone. *Mitteilungen aus dem Geologisch-Paläontologischen Institut der Universität Hamburg*, 42, 71-80.
- Thiedig, V. F., & Kresling, A. (1973). Meteorologische und geologische Bedingungen bei der Entstehung von Muren im Juli 1972 auf Spitzbergen. *Polarforschung*, 43(1/2), 40-49.
- Thumlert, S., & Jamieson, B. (2014). Stress measurements in the snow cover below localized dynamic loads. *Cold regions science and technology*, 106, 28-35.
- Tolgensbakk J, Sørbel L, Høgvard K. 2001. *Geomorphological and Quaternary Geological map of Svalbard, 1; 100,000 Sheet C9Q Adventdalen. Map*. Temakart no 31/32, Norwegian Polar Institute: Oslo; 78 pp.
- Tomczyk, A. M., & Ewertowski, M. W. (2017). Surface morphological types and spatial distribution of fan-shaped landforms in the periglacial high-Arctic environment of central Spitsbergen, Svalbard. *Journal of Maps*, 13(2), 239-251.
- Tomczyk, A. M., Ewertowski, M. W., Stawska, M., & Rachlewicz, G. (2019). Detailed alluvial fan geomorphology in a high-arctic periglacial environment, Svalbard: application of unmanned aerial vehicle (UAV) surveys. *Journal of Maps*, 15(2), 460-473.
- van der Bilt, W. G., D'Andrea, W. J., Bakke, J., Balascio, N. L., Werner, J. P., Gjerde, M., & Bradley, R. S. (2018). Alkenone-based reconstructions reveal four-phase Holocene temperature evolution for High Arctic Svalbard. *Quaternary Science Reviews*, 183, 204-213.
- van Herwijnen, A., & Fierz, C. (2014). Monitoring snow cornice development using timelapse photography. In *Proceedings of the International Snow Science Workshop* (pp. 865-869).
- Van Herwijnen, A., & Jamieson, B. (2005). High-speed photography of fractures in weak snowpack layers. *Cold Regions Science and Technology*, 43(1-2), 71-82.
- Vasskog, K., Nesje, A., Støren, E. N., Waldmann, N., Chapron, E., & Ariztegui, D. (2011). A Holocene record of snow-avalanche and flood activity reconstructed from a lacustrine sedimentary sequence in Oldevatnet, western Norway. *The Holocene*, 21(4), 597-614.
- Veitinger, J., & Sovilla, B. (2016). Linking snow depth to avalanche release area size: measurements from the Vallée de la Sionne field site. *Natural Hazards & Earth System Sciences*, 16(8).
- Veitinger, J., Purves, R. S., & Sovilla, B. (2016). Potential slab avalanche release area identification from estimated winter terrain: a multi-scale, fuzzy logic approach. *Natural Hazards and Earth System Sciences*, 16(10), 2211.

- Vikhamar-Schuler, D., Isaksen, K., Haugen, J. E., Tømmervik, H., Luks, B., Schuler, T. V., and Bjerke, J. W.: Changes in winter warming events in the Nordic Arctic region, *J. Climate*, 29, 6223–6244, <https://doi.org/10.1175/jcli-d-15-0763.1>, 2016
- Vionnet, V., Martin, E., Masson, V., Guyomarc'h, G., Bouvet, F. N., Prokop, A., ... & Lac, C. (2014). Simulation of wind-induced snow transport and sublimation in alpine terrain using a fully coupled snowpack/atmosphere model.
- Vogel, S. C. E. W. (2010). *Cornice accretion, cracking and failure along with their meteorological controls at Gruvefjellet, Central Svalbard* (Master's thesis). Available at: <https://www.duo.uio.no/handle/10852/12668>
- Vogel, S., Eckerstorfer, M., & Christiansen, H. H. (2012). Cornice dynamics and meteorological control at Gruvefjellet, Central Svalbard. *The Cryosphere*, 6(1), 157.
- Walczowski, W., & Piechura, J. (2011). Influence of the West Spitsbergen Current on the local climate. *International journal of climatology*, 31(7), 1088-1093.
- Wanner, H., Solomina, O., Grosjean, M., Ritz, S. P., & Jetel, M. (2011). Structure and origin of Holocene cold events. *Quaternary Science Reviews*, 30(21-22), 3109-3123.
- Werner, A. (1990). Lichen growth rates for the northwest coast of Spitsbergen, Svalbard. *Arctic and Alpine Research*, 22(2), 129-140.
- Werner, K., Spielhagen, R. F., Bauch, D., Hass, H. C., & Kandiano, E. (2013). Atlantic Water advection versus sea-ice advances in the eastern Fram Strait during the last 9 ka: Multiproxy evidence for a two-phase Holocene. *Paleoceanography*, 28(2), 283-295.
- Whittecar, G. R., & Ryter, D. W. (1992). Boulder streams, debris fans, and Pleistocene climate change in the Blue Ridge Mountains of central Virginia. *The Journal of Geology*, 100(4), 487-494.
- Winther, J. G., Bruland, O., Sand, K., Gerland, S., Marechal, D., Ivanov, B., ... & König, M. (2003). Snow research in Svalbard—an overview. *Polar research*, 22(2), 125-144.
- Yosida, Z., Oura, H., Kuroiwa, D., Huzioka, T., Kojima, K., & KINOSHITA, S. (1956). Physical Studies on Deposited Snow. .; Mechanical Properties.(1). *Contributions from the Institute of Low Temperature Science*, 9, 1-81.
- Zhang, Y., Renssen, H., & Seppä, H. (2016). Effects of melting ice sheets and orbital forcing on the early Holocene warming in the extratropical Northern Hemisphere. *Climate of the Past*.

